Scalable Flat-Panel Nanoparticle MEMS/NEMS Propulsion Technology for Space Exploration in the 21st Century

Thomas Liu, Louis Musinski, Graduate Students
Prof. Alec Gallimore, Prof. Brian Gilchrist, Dr. Michael Keidar
University of Michigan

(NIAC Phase I Study)

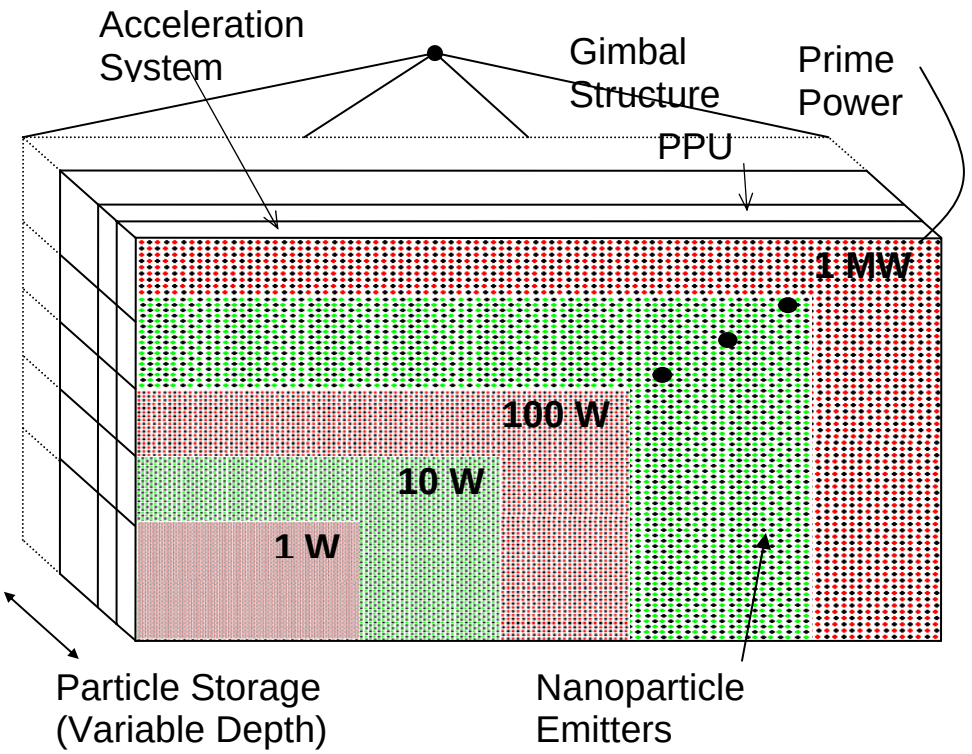

Table of Contents

Scalable Flat-Panel Nanoparticle MEMS/NEMS Propulsion Technology for Space Exploration in the 21st Century

Final Report (Phase I)
Thomas Liu, Louis Musinski, Graduate Students
Prof. Alec Gallimore, Prof. Brian Gilchrist, Dr. Michael Keidar
University of Michigan

Summary

The research in Phase I concerns the following two major areas:

i. assessment of the significance of the paradigm shift the *nanoFET* concept represents;
ii. fundamental questions regarding operation and application of *nanoFET* for in-space propulsion.

As a part of assessing the significance of the *nanoFET* paradigm shift, we have further analyzed the possible specific impulse range using the nanoparticle mode exclusively without the need for liquid indium ion emission at high specific impulse. We have determined that it may be possible to extend the operating range from 100 s up to 10,000 s using just three different sized particles while keeping the efficiency greater than 90% over the entire range. As a part of addressing fundamental questions regarding *nanoFET* operation, we have demonstrated the transportation of conducting particles through an insulating liquid by way of an electric field. In addition we have achieved particle extraction from a liquid prior to the onset of liquid surface instability, which is a significant step towards proving the fundamental feasibility of *nanoFET*.

1. Concept Overview

Figure 1 is a simplified systems sketch of the flat-panel MEMS/NEMS based thruster concept that uses nanoparticle propellant. Figure 2 shows a present-day ion thruster block-diagram for comparison. The ion thruster must create plasma using a gas (e.g., Xe) in a discharge chamber and allow the ions to escape across an accelerating grid structure. There are several practical limitations: (1) the ionization process represents an important life-limiting factor, (2) an important fraction of the propellant is never ionized, and (3) the plasma interacts with the walls and the grid, thus generating waste heat and limiting lifetime[5].

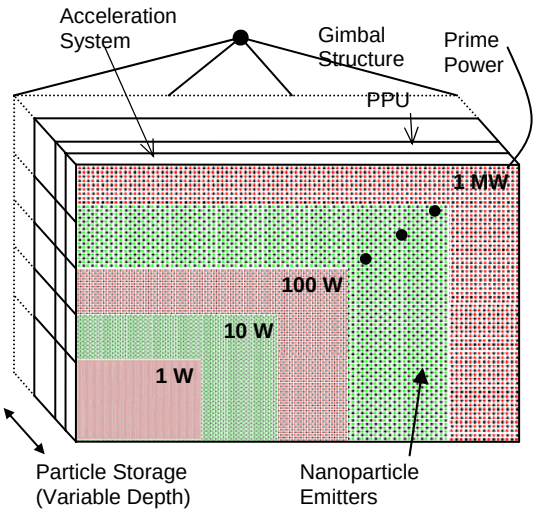

Figure 1: Concept sketch of a flat-panel nanoparticle and ion MEMS/NEMS thruster.

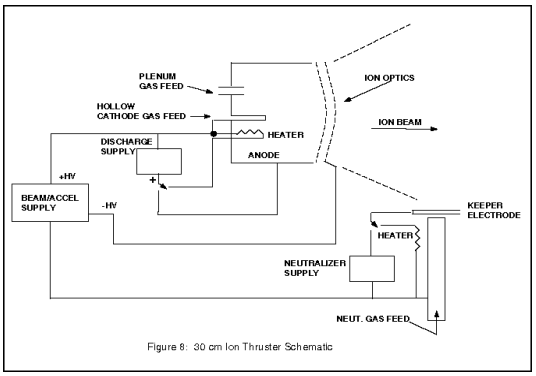

Figure 2: Block diagram of a present-day ion thruster system.[14]

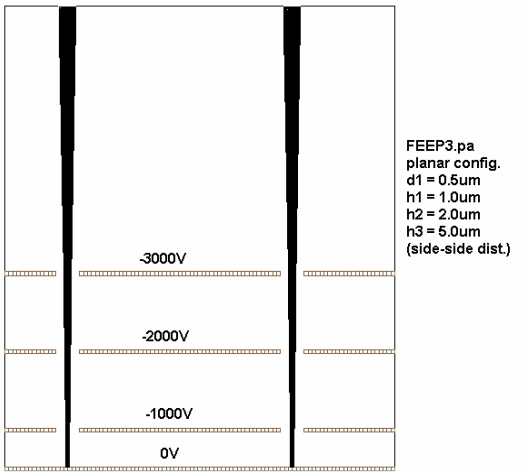

Figure 3: Two small vias shown extracting and accelerating nanoparticles.[5]

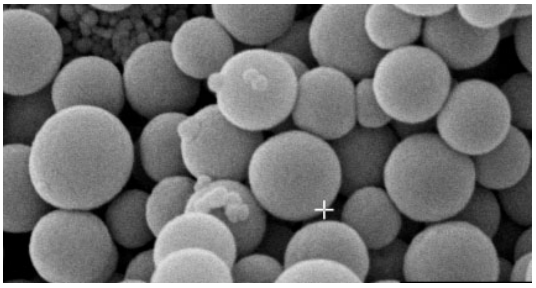

Figure 4: Example of a collection of unsorted nanoparticles in the 100-nm diameter range[1].

In contrast at the core of the flat-panel thruster, we will use millions of MEMS/NEMS-based micron-size vias, similar to what is shown in Figure 3, that have a multi-layer grid to establish critical electric-fields to extract and accelerate charged conducting nanoparticles (shown in Figure 4) from the surface of either an insulating or mildly conducting liquid used to transport these particles. These nanoparticles will range in size from below a 1 nm to over 100 nm.

The concept of utilizing field emission and electrostatic acceleration of ions is well known as Field Emission Electric Propulsion (FEEP). FEEP thrusters can produce specific impulses above 10,000 seconds at electrical efficiencies exceeding 90% using melted metal liquid propellant such as indium[3,13]. However, FEEPs use needle-like emitters that require footprints many times wider than the needle tips. Thus, their potential for being scaled-up to multi-kW power levels is doubtful. Our concept will use highly scalable MEMS/NEMS technologies applied to nanoparticle propulsion and is referred to as the nanoparticle Field Emission Thruster (nanoFET).

As will be shown more quantitatively in a later section, the use of nanoparticles in *nanoFET* will allow for the ability to continuously tune the specific impulse and thrust over a very broad range at high efficiency. The specific impulse range will be principally limited by the size, shape, and density of the particles, as well as the potential that they fall through. It is expected that with the use of just three separate particle types, nanoFET will cover a specific impulse range from 100 s to 10,000 s while maintaining efficiencies greater than 90%.

The use of nanoparticles should be contrasted with the formation of small droplets (colloid thruster). It is known that with the right emission current and temperature, charge extraction in FEEPs can produce instabilities that sometimes result in the formation of charged microscopic droplets (colloids)[3]. While these droplets could, in principle, be

used to accomplish the same goal as our nanoparticles, it is difficult to control their size and a distribution is expected. *Our nanoFET propulsion concept avoids the conditions that generate colloids and allows us to tune the nanoparticle size independently of other factors.* Other benefits of our nanoFET approach include the use of multiple grids for high-finesse control of nanoparticle extraction and acceleration processes, robust material selection for field emission surfaces to ensure long life, and the use of various nanoparticles to span the 100-10,000 s specific impulse range. The multiple-grid design ensures that a large accelerating potential can be applied without exceeding the breakdown potential between adjacent grids. A two-dimensional ion trajectory simulation through multiple nanoFET grids (Figure 3) shows that nanoparticles experience steady acceleration through each grid and that the use of multiple grids helps to collimate the beam, thus minimizing spreading due to space-charge effects. Thus, by reducing beam divergence and by better coupling the grid potentials to the charged particles, the multi-grid approach improves the efficiency and lifetime over the entire specific impulse range.

Unlike colloid thrusters, nanoFET emits charged conducting nanoparticles of well-defined size and charge-to-mass ratios. Figure 5 depicts a model of a single emitter from the nanoparticle thruster using an insulating liquid reservoir. These nano-spheres and cylinders would be transported to a liquid-filled reservoir by a liquid flow transport system and subjected to intense electric fields created by the acceleration grids. Particles that come into contact with the bottom conducting plate would become charged and pulled to the liquid surface by the electric field. If the electrostatic Coulomb force can cause charged nanoparticles to break through the surface tension, field focusing would allow the particles to lift out of the liquid. Once extracted, the charged nanoparticles would be accelerated by the electric field and ejected. It is also possible to consider with the same configuration a slightly conducting liquid where nanoparticles arrive at the surface and are preferentially charged relative to the surrounding surface, thus resulting in extraction.

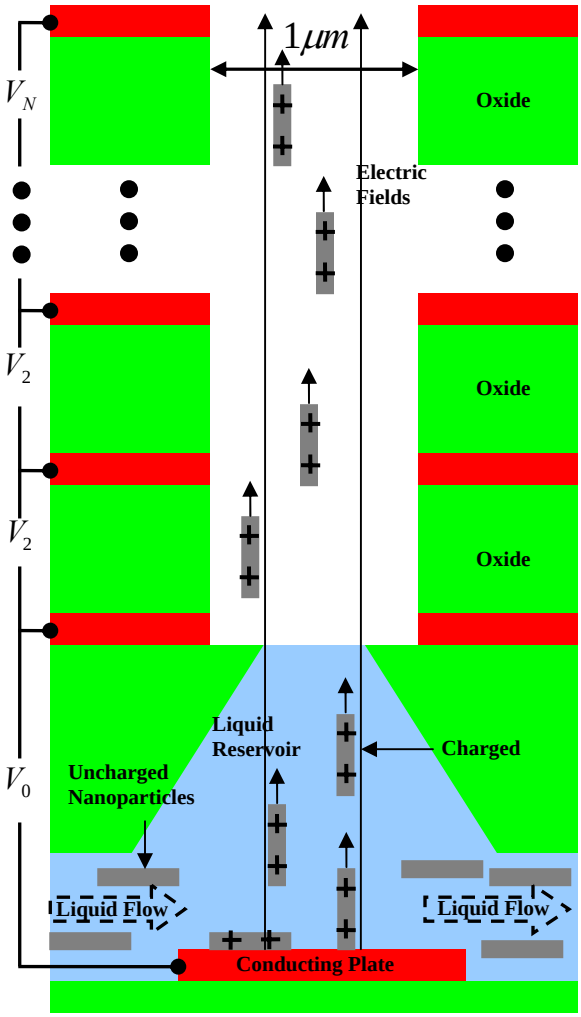

Figure 5: Structure of a single emitter, multi-grid nanoparticle thruster using an insulating liquid.

Note that neutralization of the charged particles is required. However,

the concept of using MEMS-based technology to manufacture arrays of small vias with biased grids (just like nanoFET) to extract electrons is well known[5,15,16]. These are called FEACs - Field Emission Array Cathodes. A more attractive option is the possibility of biasing separate sections of the grid with opposite polarity to emit both positive and negatively charged particles.

2. Electric Propulsion Background

Without getting into the details of extraction and acceleration of nanoparticles, it is possible to understand how particle charge and mass both affect thruster performance. It is interesting to recast well-known propulsion equations to show the dependence on both the particle's mass and charge. First, thrust can be derived as

$$T = 2nqV_o A, \qquad (1)$$

where n is the number density of particles, q is the charge of the nanoparticle, V_o is the potential difference applied across the accelerating grid(s), and A is the thruster area. The power is governed by

$$P = nA\left(\frac{2}{m}\right)^{\frac{1}{2}}\left(qV_o\right)^{\frac{3}{2}}, \qquad (2)$$

where m is the mass of the particle. Now, dividing the thrust by the power, the specific thrust is given as

$$\frac{T}{P} = \left(\frac{2m}{qV_o}\right)^{\frac{1}{2}}. \qquad (3)$$

The specific impulse is

$$I_{sp} = \frac{1}{g}\left(\frac{2qV_o}{m}\right)^{\frac{1}{2}}, \qquad (4)$$

where g is the Earth's gravitational constant.

Note that the I_{sp} is *directly proportional* to the square root of the charge-to-mass ratio of the particle while the thrust-to-power ratio is *inversely proportional* to the same square root quantity. The importance of the charge-to-mass ratio and the ability of nanoFET to tune it over a very large range lies at the foundation of many critical advantages of nanoparticle propulsion over other electrical propulsion systems and will be discussed in a later section.

3. Mission Analysis

The nanoFET concept derives its benefits from the (1) the ability to operate at very high efficiency, (2) near continuous variation of specific impulse over a large range (100-10,000 s), (3) scalability over a large power or thrust range, and (4) minimization of life-limiting factors.

Charging nanoparticles versus ionizing atoms means that the charge-to-mass ratio can be efficiently and precisely adjusted over a huge range even within a single mission and with a low expenditure of energy. In addition, the improved collimation of the particle beam reduces beam divergence and gate impingement.

The use of near continuously variable I_{sp} increases mission flexibility. For example, nanoFET would be able to accomplish an orbit transfer with different thrusting times dependent on I_{sp} level, while a constant I_{sp} thruster can only perform the same transfer with a

single thrusting time. If it is important to achieve the transfer in a short time, nanoFET can operate at a low I_{sp} and high thrust mode. On the other hand, if thrusting time is not important, then nanoFET can operate at a high I_{sp} and conserve propellant. A highly variable I_{sp} system will provide many more options to rescue an emergency situation than a constant I_{sp} system. This added security will be important in many cases, especially manned missions.

The use of flat panel MEMS technology enables a single thruster type, which can be straightforwardly scaled, to span a broad thrust range. This *plug-and-play* technology decouples thruster design from spacecraft design. As such, by providing better overall performance and a wider range of operating parameters, thus enabling a broader set of mission modes, nanoFET is both mission enhancing and mission enabling.

4. How nanoFET Works

In nanoFET, nanoparticles of well characterized dimensions and charge states are suspended in a low vapor pressure liquid. The use of nanoparticles provides tremendous flexibility in controlling the charge-to-mass ratio for tuning of propulsion performance, and they may be kept segregated by type in storage reservoirs. The nanoparticle solution is circulated and transported to charging and extraction zones through microfluidic channels. These extraction zones lay beneath arrays of stacked MEMS gridded structures, which contain millions of micron-sized vias. Biasing the grid layers produces the electric fields needed to charge and extract the nanoparticles from the liquid surface, as well as to accelerate them to the desired thruster exhaust velocity. Larger scale proof-of-concept tests have already demonstrated operational regimes in which particles may be charged and extracted without causing liquid surface instability.

5. Advantages of nanoFET

Significant operational and performance advantages may be achieved with nanoFET over other electric propulsion technologies. These advantages include:

- *Highly integrated system*: The use of MEMS technology enables a “flat panel” thruster design that incorporates power processing as well as nanoparticle manufacture, storage, feed, extraction, and acceleration. Such compact design simplifies propulsion system integration and lowers thruster specific mass. Because different regions of nanoFET can emit particles of opposite polarity, neutralizer requirements are simplified as nanoFET is a self-neutralizing thruster.
- *Geometrically scalable*: A “flat panel” design allows the nanoFET array size to be scalable with power, thus permitting a single ground-qualified engine type to be used in applications ranging from nanosatellites operating at a few watts to space tugs or space stations in the hundreds of kilowatts range. Such “plug-and-play” functionality provides greater spacecraft design flexibility and significant cost savings.
- *Longer operational lifetime*: Charging of the nanoparticles is accomplished without ionization,

meaning greater reliability and the absence of cathodes and charge-exchange collisions that are the principal lifetime limiters of current electric propulsion systems. Propellant charging, as opposed to propellant ionizing, also accounts for part of the efficiency gains nanoFET affords.

- *Better controllability*: Charge-to-mass ratio is much better regulated for nanoparticles than for colloids, resulting in better controllability for nanoFET versus colloidal thrusters.
- *Higher thrust density*: Whereas state-of-the-art ion thrusters operate substantially below the space charge limit to ensure proper ion optics operation, nanoFET can operate much closer to the space charge limit since the charges will be contained in a fewer number of particles. Thus, thruster specific mass is reduced.
- *Enormous specific impulse range at high thrust efficiency*: The ability to tune propulsion characteristics via different nanoparticle dimensions and charge states permits thrust efficiencies over 90% for a specific impulse range of 100 s to 10,000 s. Such high efficiencies result in thrust-to-power ratios, especially at low specific impulse, that are orders of magnitude greater than state-of-the-art ion and Hall thrusters. Consequently, nanoFET can operate at high specific impulse in cruise mode and yet switch to a high thrust and low I_{sp} mode when needed. This flexibility provides a wider margin for mission designers to accommodate off-nominal mission scenarios as well as dynamic retasking of space assets to take advantage of in-flight opportunities.

For example, by using just three types of nanoparticles, the nanoFET system can span an I_{sp} range from 100 s to 10,000 s. Three possible carbon nanotube particles are listed in Table 1.

Diameter [nm]	Height [nm]	Isp range [s]
5	100	100-500
1	100	500-2000
1	3500	2000-10000

Table 1: Carbon nanotube particles enabling nanoFET to span 100-10,000-s Isp range.

Note that the entire I_{sp} range is covered with over 90% thrust efficiency using just the three particle types as shown in Figure 6. No existing electric propulsion technologies can cover this large of an I_{sp} range at such high efficiencies. Such performance can be obtained at reasonable voltages between 800 to 10,000 V due to the MEMS gated structures that provide the extraction and acceleration electric fields. Note that in the nanoFET system, efficiency losses may be due to viscous drag in the liquid, charge loss to the liquid, particle impingement on the gates, and beam defocusing. As research and development work continues on nanoFET, the system will be optimized to further reduce efficiency losses.

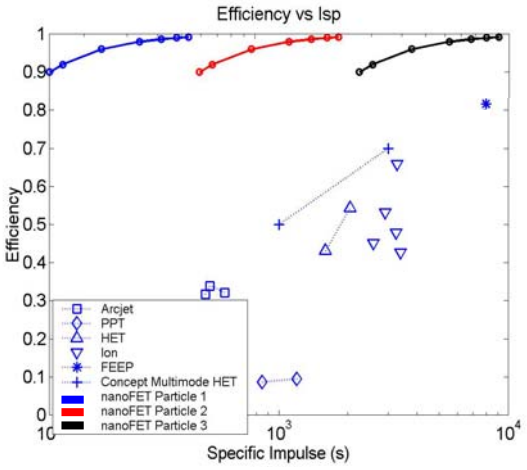

Figure 6: Very high efficiency of nanoFET for entire specific impulse range compared with other electric propulsion systems. The nanoparticles are specified in Table 1.

NanoFET's superior thrust-to-power ratios over state-of-the-art thrusters (shown in Figure 7) provide mission designers with the flexibility to engage a high thrust mode to climb out of gravity wells, perform abort scenarios or emergency maneuvers, and reduce trip times.

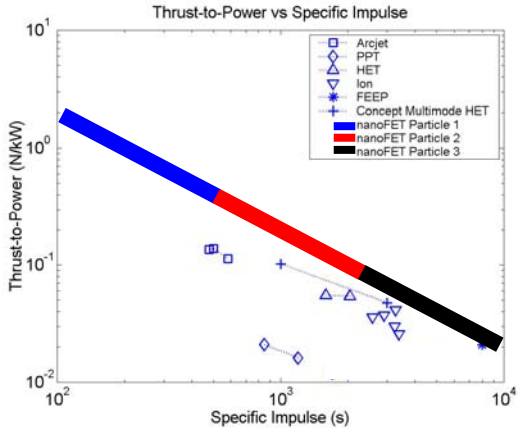

Figure 7: High thrust-to-power ratio for nanoFET compared to other electric propulsion systems. The nanoparticles are specified in Table 1. The thick blue-red-black line represents 100% to 90% efficiency.

6. Experimental and Theoretical Study of *nanoFET*

The nanoFET system charges conductive particles in contact with an electrode that is immersed in a dielectric liquid. When the particle acquires sufficient charge, it is lifted off the electrode by an imposed electric field and transported to the liquid surface. There, the electrostatic force acting on the particle must overcome the surface tension force to extract the particle from the liquid. Following extraction, the particle is accelerated by the imposed electric field to provide thrust. To understand nanoFET's governing physics, the following aspects must be understood:

- imposed electric field
- particle charging and lift-off
- particle dynamics within liquid
- particle extraction through liquid surface
- post-extraction particle acceleration

6.1. Electric Fields

The nanoFET system can be modeled as follows with a set of biased electrodes separated by a dielectric liquid layer of height d_ℓ and a vacuum gap (Figure 8). Within the vacuum gap, the electric field E_0 is given by

$$E_0 = \frac{V}{d + \left(\frac{\varepsilon_0}{\varepsilon_\ell} - 1\right) d_\ell}, \qquad (5)$$

where V is the bias voltage, d is the total electrode gap, and ε_0 and ε_ℓ are the permittivities of free space and the liquid, respectively. Within the dielectric liquid, the electric field is

$$E_\ell = \frac{\varepsilon_0}{\varepsilon_\ell} E_0 = \frac{V}{\frac{\varepsilon_\ell}{\varepsilon_0} d + \left(1 - \frac{\varepsilon_\ell}{\varepsilon_0}\right) d_\ell}. \qquad (6)$$

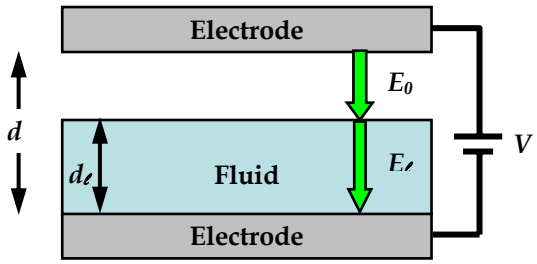

Figure 8: Simplified model of nanoFET to understand electric fields.

6.2. Particle Lift-Off

The forces experienced by a particle in contact with a charging electrode are shown in Figure 9. For the charged particle to lift off the electrode,

the electrostatic and buoyant forces on it must exceed the gravitational, image charge, and adhesion forces restraining it. In a zero-g space environment, the gravitational and buoyant forces should be neglected.

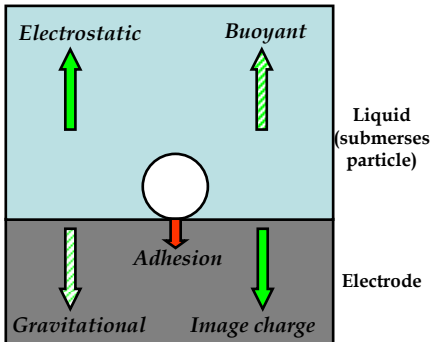

Figure 9: The forces experienced by a particle in contact with a charging electrode.

For a conductive spherical particle in contact with an electrode and immersed in a fluid medium, Félici[17,18] gives the acquired particle charge as

$$q_{0,\mathrm{sp}} = \frac{2\pi^3}{3} r^2 \varepsilon_\ell E_\ell , \qquad (7)$$

where r is the particle radius. In a gravitational environment, the minimum electric field in the fluid needed for lift-off is

$$E_{\mathrm{lift,sp}} = 0.494 \left[\frac{r(\rho_p - \rho_\ell) g}{\varepsilon_\ell} \right]^{\frac{1}{2}}, \qquad (8)$$

where ρ_p and ρ_ℓ are the particle and liquid mass densities, respectively, and g is the gravitational constant.

For horizontally orientated cylinders, the acquired charge is

$$q_{0,\mathrm{cy-h}} = 2\pi r l \varepsilon_\ell E_\ell , \qquad (9)$$

where l is the particle length. The associated minimum lift-off field in the fluid is

$$E_{\mathrm{lift,cy\text{-}h}} = 0.836 \left[\frac{r(\rho_p - \rho_\ell) g}{\varepsilon_\ell} \right]^{\frac{1}{2}}. \qquad (10)$$

Proof-of-concept tests have shown that field focusing on the particle's tips leads to a moment that rotates the cylinder from a horizontal to a vertical position prior to lift-off. The acquired charge for a vertically orientated cylinder is

$$q_{0,\mathrm{cy\text{-}v}} = \pi \frac{l^2}{\ln\left(\frac{2l}{r}\right) - 1} \varepsilon_\ell E_\ell , \qquad (11)$$

and the associated minimum lift-off electric field in the fluid is

$$E_{\mathrm{lift,cy\text{-}v}} = \frac{\ln\left(\frac{2l}{r}\right) - 1}{\left[\ln\left(\frac{l}{r}\right) - \frac{1}{2}\right]^{\frac{1}{2}}} \left[\frac{r(\rho_p - \rho_\ell) g}{\left(\frac{l}{r}\right)\varepsilon_\ell} \right]^{\frac{1}{2}}. \qquad (12)$$

Figure 10 shows the charge, minimum lift-off electric field, and electrostatic lift-off force ratio between vertical and horizontal cylinders as a function of the particle's aspect ratio. As the cylinder rotates from a horizontal to a vertical orientation, it acquires a larger charge and a greater electrostatic lifting force for a given electric field. Consequently, the minimum required electric field for lift-off decreases as the particle becomes vertical.

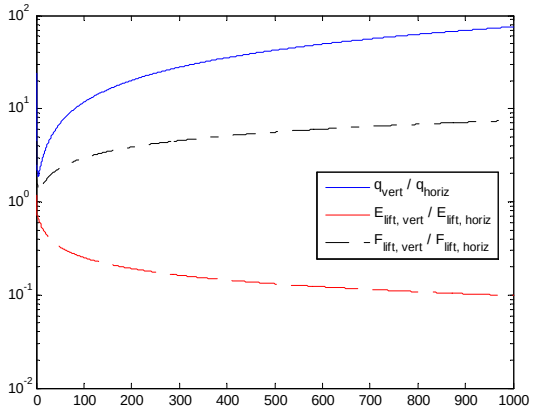

Figure 10: Charge, minimum lift-off electric field, and electrostatic lift-off force ratio between vertical and horizontal cylinders as a function of the particle's aspect ratio.

The equations above have assumed a negligible adhesion force between the particle and the electrode. This assumption is no longer valid for particle sizes on the order of the electrode surface roughness. Part of the proposed Phase II work will address this issue for nanoparticles.

6.3. Particle Dynamics in Liquid

Once the particle leaves the electrode surface, the adhesion and electric image force rapidly vanishes, and a fluid drag force now acts to counteract particle motion through the liquid. For the viscous flow regime, the Reynolds number is less than unity and is given as

$$Re = \frac{\rho_p v(2r)}{\mu_\ell} < 1, \qquad (13)$$

where v is the particle velocity and μ_ℓ is the dynamic viscosity coefficient of the liquid. In the viscous flow regime, the drag force on a sphere is

$$D = 6\pi\mu_\ell r v. \qquad (14)$$

A cylindrical particle can be modeled as an elongated rod moving parallel to its axis. Tobazeon[17] gives the fluid drag as

$$D = \frac{2\pi\mu_\ell l v}{\ln\left(\frac{l}{2r}\right) + 0.193}. \qquad (15)$$

As the particle moves through the fluid, charge on the conductive particle is gradually lost to the fluid medium. The particle charge is reduced with time according to

$$q(t) = q_0 \exp\left(-\frac{t}{\tau}\right), \qquad (16)$$

where q_0 is the particle charge acquired at the electrode. The charge loss time constant is given as

$$\tau \equiv \frac{\varepsilon_\ell}{\sigma_\ell}, \qquad (17)$$

where σ_ℓ is the electrical conductivity of the liquid.

The particle's inertial force must account for the "added mass" of the liquid that is accelerated along with the particle. This inertial force is given by

$$F_{\text{inertial}} = \left(m_p + K m_\ell\right)\frac{dv}{dt}, \qquad (18)$$

where m_p is the particle mass, and m_ℓ is the fluid mass displaced by the particle. The coefficient K is dependent on the particle geometry. For spheres, this coefficient is equal $K = 0.5$. For cylinders, they can be modeled as prolate ellipsoids moving parallel to its axis; the "added mass" becomes negligible at high aspect ratios as

$$\frac{l}{r} > 5 \Rightarrow K < 0.1. \qquad (19)$$

Assuming that particle motions are independent of other particles, the equation of motion for a particle in the fluid is

$$\left(m_p + Km_\ell\right)\frac{dv}{dt} = q(t)E_\ell + F_{\text{buoyant}} - W - D, \quad (20)$$

where F_{buoyant} is the buoyant force and W is the particle weight. In zero-g, these last two gravitational forces vanish.

Figure 11 shows the expected dynamical behavior in the fluid of the millimeter-sized particles used in the proof-of-concept experiments. The particle quickly reaches terminal velocity in the low-Re flow and traverses the liquid layer fast enough that charge loss to the liquid is negligible.

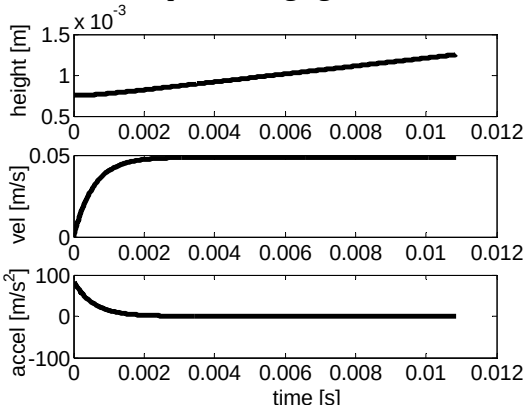

Figure 11: Expected dynamical behavior in the liquid of the millimeter-sized particles used in the proof-of-concept experiments.

Figure 12 indicates the relative magnitudes of the forces acting on the particle while it is in the liquid. Note that even in the lab environment, the electrostatic and drag forces easily dominate the gravitational forces. As smaller particles are used, the gravitational forces become even less significant.

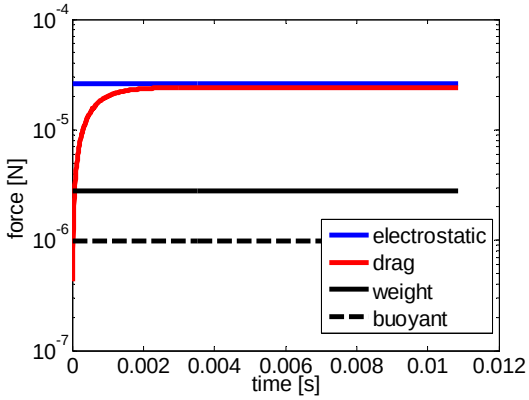

Figure 12: Relative magnitudes of the forces acting on the particle while it is in the liquid.

6.4. Particle Oscillation Experiment

We have experimentally demonstrated the ability to charge and transport conducting particles submersed in an insulating liquid with intense electric fields. Figure 13 shows a diagram of our experimental setup. The setup includes a liquid-filled electrode gap with conducting particles initially resting on the bottom electrode and a high voltage power supply used to generate electric fields in the gap between the electrodes.

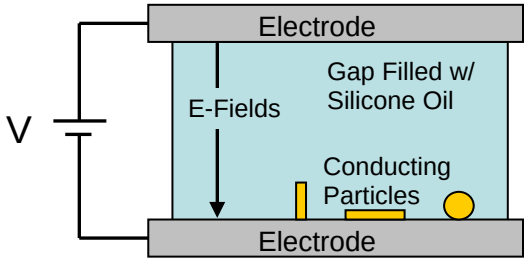

Figure 13: Experimental setup for particle oscillation.

The electrodes are made from stainless steel and are circular with a four inch diameter. We used silicone oil as our liquid because of its low conductivity, high breakdown potential, and very low vapor pressure. Silicone oil has a density of 965 kg/m^3, a viscosity of 100 cSt, and a conductivity of 3.33x10^{-13} S/m. The particles (Figure

14) were mostly millimeter-sized spheres and cylinders made from aluminum because of its high conductivity and low density.

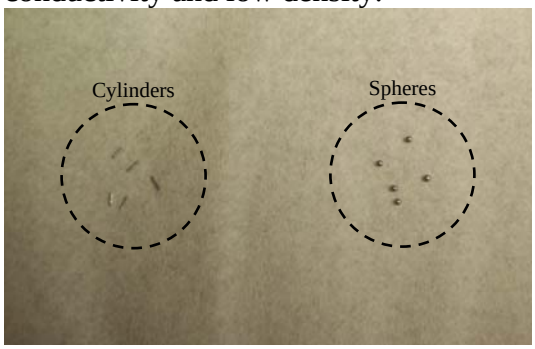

Figure 14: Picture of millimeter-sized aluminum spherical and cylindrical particles used in experiments. Spheres have an 800-µm diameter. Cylinders have a 300-µm diameter and 2.5-mm length.

To begin the experiment, the voltage between the electrodes was zeroed with the positive lead connected to the upper electrode and the ground connected the bottom electrode. The particles were placed at rest on the bottom electrode. As the voltage was increased to generate uniform electric fields in the gap, the conducting particles in contact with the bottom electrode began to charge negatively. Once the electric force on the charged particles was great enough, they were lifted from the bottom electrode and transported to the upper electrode. Once reaching and coming into contact with the upper electrode, the particles underwent a charge exchange, becoming positively charged with the same magnitude as when they were charged on the bottom electrode. The particles were then transported back down through the liquid to the bottom electrode. The resulting particle oscillation is depicted in Figure 15.

From our experiments, we found that we could put both spherical and cylindrical particles into oscillation at predictable electric fields. As expected, cylindrical particles were able to oscillate at much lower electric fields than the spherical particles due to the greater field focusing at the tips. Also, increasing the aspect ratio of the cylindrical particles lowered the required electric field for the same reason.

Most of the experiments were performed with aluminum cylindrical particles with diameters of 300 µm and lengths ranging from 1 mm to 2.5 mm initially placed horizontally on the bottom electrode. When the voltage between the electrodes was increased, the horizontal cylinders were pulled into a vertical position before oscillating. Once the particles were lifted from the electrode and set into motion, they reached terminal velocity very quickly, where the terminal velocity could be controlled readily by adjusting the potential applied between the electrodes.

Figure 16 shows a picture of two particles in mid-oscillation between the electrodes. This experiment used 300-

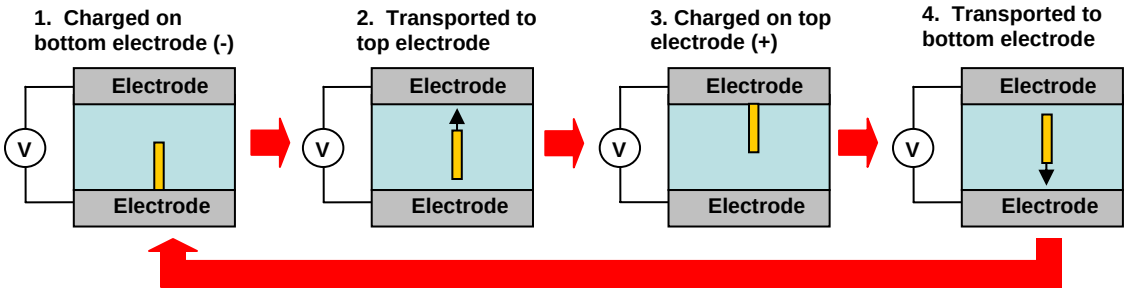

Figure 15: Stages of particle oscillation.

μm by 2-mm aluminum cylindrical particles, a 12-mm gap between the electrodes, and silicone oil filling the gap.

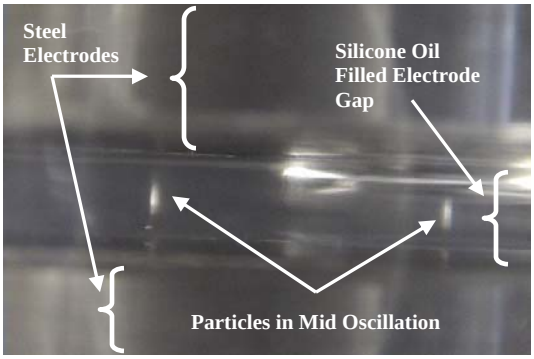

Figure 16: Two cylindrical particle in oscillation. The particles are aluminum with dimensions: d = 300 μm, l = 2 mm. Electrode gap is 12 mm.

From the particle oscillation experiment, we learned that we can accurately charge and transport conducting particles that are submersed in an insulating liquid by controlling the electric field around the particles.

6.5. Particle Extraction

At the liquid surface, the particle must overcome surface tension forces in order to be extracted. The surface tension force is given as

$$F_{\text{surface}} = 2\pi r\gamma, \qquad (21)$$

where γ is the surface tension coefficient. Field focusing on the particle leads to an increase in the electrostatic force extracting the particle at the liquid surface. As a first-order estimate, the field enhancement factor is assumed to be

$$\beta \approx \sqrt{1+\frac{l}{r}}, \qquad (22)$$

which is a scaling typically used for carbon nanotube field emitters[21]. By making simplifying assumptions that the liquid wets the particle completely for the maximum surface tension force and that particle extraction does not take place until a full particle length above the unperturbed fluid surface, the equations of motion can be iterated to determine the particle dynamics during the extraction process. Figure 17 shows the typical dynamical behavior of the millimeter-sized particles used in the proof-of-concept experiments. As in the case of particle motion in the fluid, the gravitational forces are negligible compared to the electrostatic, drag, and surface tension forces.

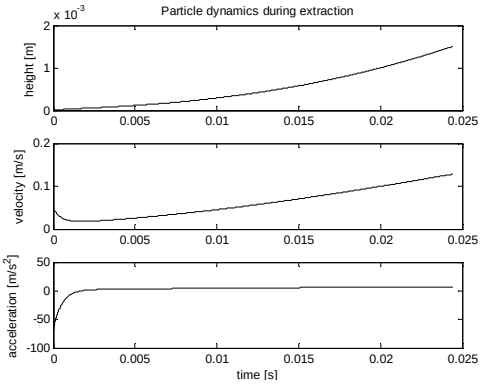

Figure 17: Expected dynamical behavior of the millimeter-sized particles used in the proof-of-concept experiments during extraction process.

6.6. Post-Extraction Particle Acceleration

After extraction from the liquid, the particle emerges in the vacuum gap. Neglecting the insignificant gravitational force, the particle undergoes constant accelerated motion due to the vacuum electric field before being expelled as thrust.

6.7. Particle Extraction Experiments

The next step after experimenting with particle charging and transport is to prove the feasibility of extracting

particles through a liquid surface. Figure 18 shows the experimental setup used for the particle extraction experiment. This setup is very similar to the particle oscillation setup, but now the liquid only partially fills the electrode gap, leaving the upper section of the gap air-filled.

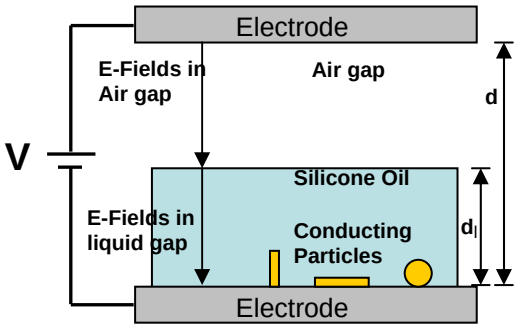

Figure 18: Experimental setup for particle extraction.

This experiment was run in a very similar manner as the particle oscillation experiment. The voltage between the electrodes was initially zeroed with the positive lead connected to the upper electrode and the ground connected the bottom electrode. The cylindrical or spherical particles were placed at rest on the bottom electrode. When the voltage was increased, generating an electric field in the gap, the conducting particles were charged. The electric force on the charged particles lifted and transported them to the liquid-air interface. If the electric force on the particles was strong enough, they would break through the surface tension and particle extraction would be achieved. After being extracted, they would travel through the air gap and contact the upper electrode, where they underwent a charge exchange and were accelerated back into the liquid and down to the bottom electrode. The resulting particle oscillation is depicted in Figure 19.

From our experiment, we proved the feasibility of extracting particles from a liquid into air. In addition, we also measured the minimum required electric fields to extract particles of various sizes and shapes for different liquid heights and found very good agreement with our theoretical predictions. Just as in the oscillation experiment, the cylindrical particles were extracted at much lower electric fields than the spherical particles due to the greater field focusing at the tips. And, increasing the aspect ratio of the cylindrical particles lowered the required electric field for the same reason.

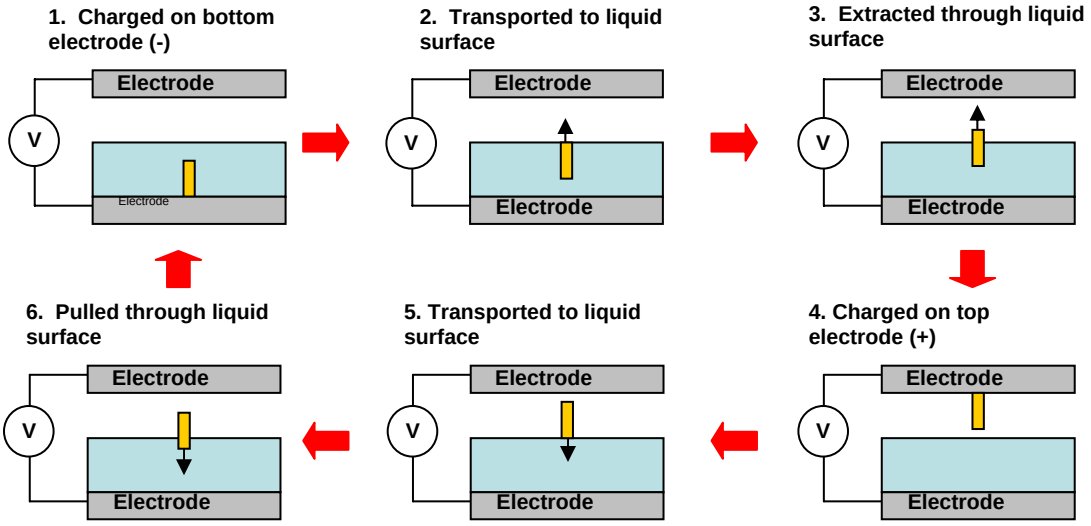

Figure 19: Stages of particle extraction

Results from these experiments are discussed in section 6.9.

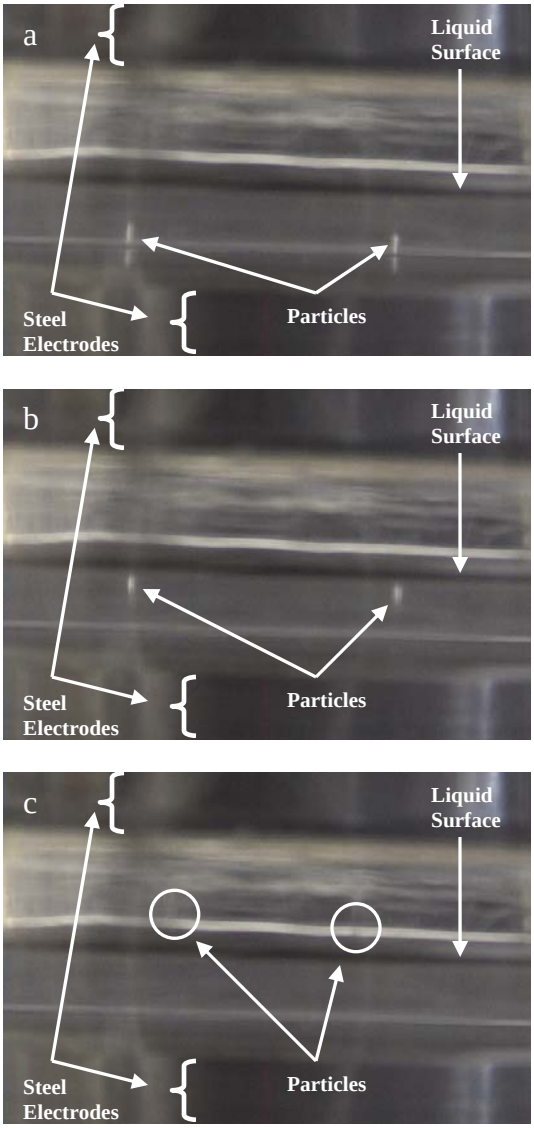

Figure 20: Two cylindrical particle being extracted. The particles are aluminum with dimensions: d = 300 µm, l = 2 mm. Electrode gap is 12 mm.

a) particles are on bottom electrode
b) particles pulled to liquid surface
c) particles extracted and in air gap (difficult to see particles because of high velocities)

Figure 20 shows a series of pictures of two particles being extracted. This experiment used 300-µm by 2-mm aluminum cylindrical particles, a 12-mm gap between the electrodes, and silicone oil filling the gap up to 6 mm. Picture a) shows the two particles on the bottom electrode oriented vertically. Next, the particles are pulled to the liquid surface as seen in picture b). Finally the particles are extracted through the liquid surface and are in the air gap in picture c). It is difficult to see the particles in the final picture because they are moving very quickly.

From the particle extraction experiment, we proved that it is feasible to extract particles from liquid using electric fields, an important step to demonstrating nanoFET's feasibility.

6.8. Surface Instability

The presence of a vacuum (air) electric field at the fluid interface can lead to surface instabilities. These instabilities are undesirable for nanoFET because they grow to form Taylor cones that can eject fluid droplets. These colloids, with poorly defined charge-to-mass ratios, would reduce the overall nanoFET performance.

At equilibrium, the fluid achieves a balance between electric pressure, hydrostatic pressure, and surface tension. Using a corrected version of Tonks's[20] formula adapted for dielectric liquids, the minimum vacuum (air) gap electric field that would cause a perturbed fluid surface to become unstable is given as

$$E_{0,\min} = \left(\frac{4g\gamma\rho_\ell}{\varepsilon_0^{\,2}} \right)^{\frac{1}{4}} \left[1 + \left(\frac{\varepsilon_0}{\varepsilon_\ell} \right)^2 \right]^{-\frac{1}{2}} . \quad (23)$$

As gravitation effects vanish in zero-g, this simple model for the critical electric field must be modified to account for the presence of electrohydrodynamic waves. Part of the proposed Phase II work will address this

issue of liquid surface instability in zero-g.

6.9. Surface Instability and Taylor Cone Formation Experiments

While running the particle extraction experiments, we found that at very high electric fields, Taylor cones would form on the surface of the liquid. Taylor cones are a result of instabilities in the liquid surface and form when the electric field pulls on free charge caught at the liquid surface. At very high electric fields, small charged liquid droplets can be pulled off of the liquid surface just as in a colloid thruster. Figure 21 shows the stages of Taylor cone formation.

It is very important for nanoFET to be able to operate in a regime where Taylor cones do not form. In other words, we need to be sure that it is possible to extract particles through a liquid surface at electric field strengths below those that cause the liquid to become unstable.

This experiment was run in a very similar manner as the particle extraction experiment, but without the particles. The electric field in the gap was increased until Taylor cones began to form. The electric fields required to form the cones were measured as a function of the liquid height and compared extremely well with theory.

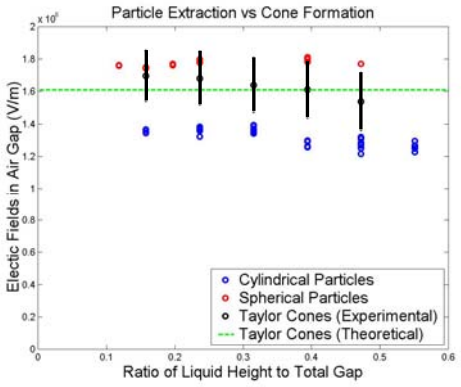

Figure 22: Required electric fields for particle extraction and Taylor cone formation.

Next, we compared the electric fields required to extract various particles through the liquid surface with the minimum fields at which cones begin to form. Figure 22 shows a plot of the required fields to extract different particles and the fields to form cones as a function of liquid height. The total electrode gap was 12.7 mm. The spherical particles were 800 μm in diameter and the cylindrical particles were 300 μm in diameter and 2 mm in length. Both particles were aluminum. We found that the average extraction electric field was 1.8E6 V/m for spherical particles and 1.3E6 V/m for cylindrical particles; these values are within 20% of the theoretical predictions using a preliminary particle extraction model. For Taylor cone formation, the measured formation electric field of

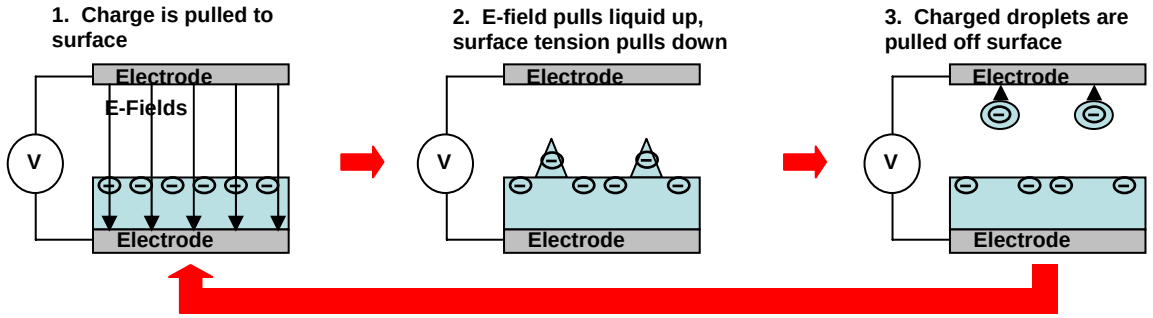

Figure 21: Stages of Taylor cone formation.

1.63E6 V/m agreed very well with Equation 23. The experiments indicate that a regime exists where particles may be extracted prior to the onset of liquid instability. It is also important to note that the presence of particles do not reduce the critical threshold for Taylor cone formation.

6.10. Feasible Design Space

The feasible design space for the proof-of-concept test configuration using cylindrical particles is shown in Figure 23. For nanoFET to be feasible, geometric configurations of the emitters must exist such that the electric fields in the liquid are greater than the minimum electric fields needed to lift off the particles from the electrode surface. At the same time, the corresponding vacuum electric fields must be greater than the minimum electric fields needed to extract the particle from the liquid surface while less than the minimum electric fields that would cause liquid surface instabilities.

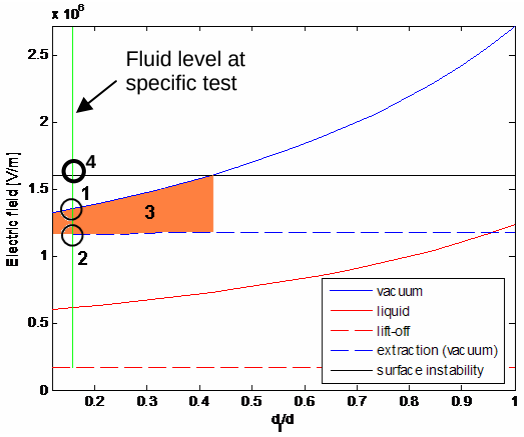

Figure 23: The feasible design space (3) for the proof-of-concept test configuration using cylindrical particles. Particle extraction threshold for experiment (1) and theory (2); Taylor cone formation threshold (4) for experiment and theory.

Note that the theory indicates the existence of operational regimes where particles may be extracted prior to Taylor cone formation, which was validated by experiment. Test data indicates excellent agreement between the predicted and measured electric field strength needed to cause liquid surface instability. Use of a simplified particle extraction model led to an underprediction of the extraction fields by about 20%. This discrepancy suggests the need to acquire a better understanding of the particle field enhancement effect at the liquid surface as well as the effects of surface tension on particle extraction, both of which will be investigated further in the Phase II work. Continued exploration of the feasible design space as particles are scaled down to the nano-scales will also be a focus of the Phase II work.

6.11. Particle Size Scaling

Preliminary analysis has indicated that as the particles are scaled down, spherical particles become less attractive. The initial particle charge scales with the square of the particle radius. As the particle travels through the liquid, the final particle charge after accounting for charge loss to the liquid can be determined by

$$\begin{aligned} q(t_{ex}) &= q_0 \exp\left(-\frac{t_{ex}}{\tau}\right) \\ \Rightarrow q(t_{ex}) &\propto r^2 \exp\left(-\frac{1}{r}\right) \end{aligned}, \qquad (24)$$

where the extraction time t_{ex} can be approximated as

$$\begin{aligned} t_{ex} &\approx \frac{d_\ell}{v_{term}} \\ &\propto \frac{1}{r} \end{aligned}, \qquad (25)$$

assuming that the particle reaches terminal velocity immediately after leaving the electrode and neglecting the interaction time with the liquid surface. The terminal velocity v_{term} can be approximated as

$$v_{\text{term}} = \frac{\pi^2}{9}\frac{\varepsilon_\ell E_\ell^{\,2}}{\mu} r, \qquad (26)$$
$$\propto r$$

assuming negligible gravitational forces and charge exchange with the liquid. Therefore, the final charge-to-mass ratio scales as

$$\frac{q(t_{\text{ex}})}{m} \propto \frac{1}{r}\exp\left(-\frac{1}{r}\right), \qquad (27)$$

which decreases with smaller particle sizes.

Results from simulations for small spherical particles are shown in Figure 24. Note that for a fixed emitter geometry, the required electric field to extract particles from the liquid surface increases with decreased particle size. As the particle size decreases, so does its terminal velocity in the liquid. Since the particle now takes longer to traverse the liquid layer, it loses more charge to the surrounding liquid before reaching the liquid surface. Consequently, a larger electric field is needed to extract the particle of reduced charge.

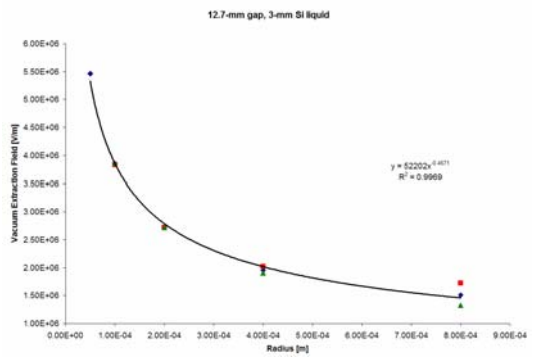

Figure 24: Results from extraction field simulations for small spherical particles. Note that the required extraction field increases with smaller radius.

To overcome this limitation, the liquid height must be scaled along with the particle size to reduce the liquid layer transit time. Otherwise, cylindrical particles are preferable, since its longer aspect ratio helps to offset this problem.

A similar analysis with cylindrical particles follows. As the particle travels through the liquid, the final particle charge after accounting for charge loss to the liquid can be determined by

$$q(t_{\text{ex}}) = q_0 \exp\left(-\frac{t_{\text{ex}}}{\tau}\right)$$
$$q(t_{\text{ex}}) \propto \frac{l^2}{\ln(4A)}\exp\left(-\frac{\ln(4A)}{l \ln A}\right), \qquad (28)$$

where the aspect ratio A is large and given as

$$A = \frac{l}{2r}. \qquad (29)$$

The extraction time t_{ex} can be approximated as

$$t_{\text{ex}} \approx \frac{d_\ell}{v_{\text{term}}}$$
$$\propto \frac{\ln(4A)}{l \ln A}, \qquad (30)$$

assuming that the particle reaches terminal velocity immediately after leaving the electrode and neglecting the interaction time with the liquid surface. The terminal velocity v_{term} can be approximated as

$$v_{\text{term}} \approx \frac{1}{2}\frac{\varepsilon_\ell E_\ell^{\,2}}{\mu}\frac{l\ln A}{\ln(4A)}, \quad (31)$$
$$\propto \frac{l\ln A}{\ln(4A)}$$

assuming negligible gravitational forces and charge exchange with the liquid. Therefore, the final charge-to-mass ratio scales as

$$\frac{q(t_{\text{ex}})}{m} \propto \frac{A^2}{l\ln(4A)}\exp\left(-\frac{\ln(4A)}{l\ln A}\right), \quad (32)$$

which decreases with shorter cylinders but increases with longer aspect ratios. Again, liquid height should be scaled down along with the particle length to reduce charge loss to the liquid during particle transport to the surface.

6.12. Particle Extraction through a Grid

The next step in the experimental process was to demonstrate the feasibility of extracting particles through a grid structure, since the nanoFET design calls for a multi-grid structure for particle extraction and acceleration. This experiment was another extension to the particle extraction experiment where a grid structure was inserted in the air gap as shown in Figure 25. The holes in the grid structure were designed to have a diameter approximately equal to the gap dimension in order to keep the electric fields uniform.

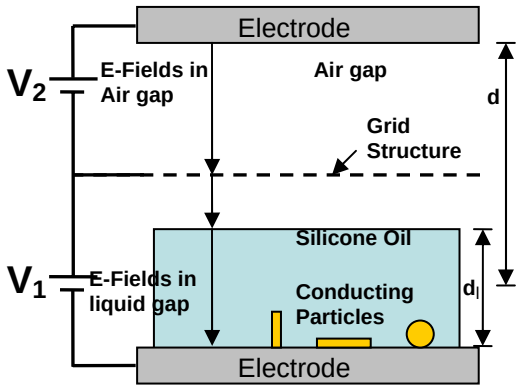

Figure 25: Experimental setup for particle extraction through a grid structure.

The power supply connected from the bottom electrode to the grid structure was responsible for particle charging, extraction, and acceleration through the grid. The power supply connected from the grid to the upper electrode would be responsible for continuing to accelerate the particles through additional grid structures, but since we were working with only a single grid, it was not necessary apply a bias from the grid to the upper electrode.

This experiment was performed several times with various particle shape and sizes, and it was experimentally proven that particle extraction through a grid structure is feasible. Figure 26 shows a series of pictures showing spherical particles being extracted through a grid structure. Picture a) shows nine particles resting on the bottom electrode before the electric field was increased, and picture b) shows the particles stuck to the upper electrode after being extracted through the grid structure.

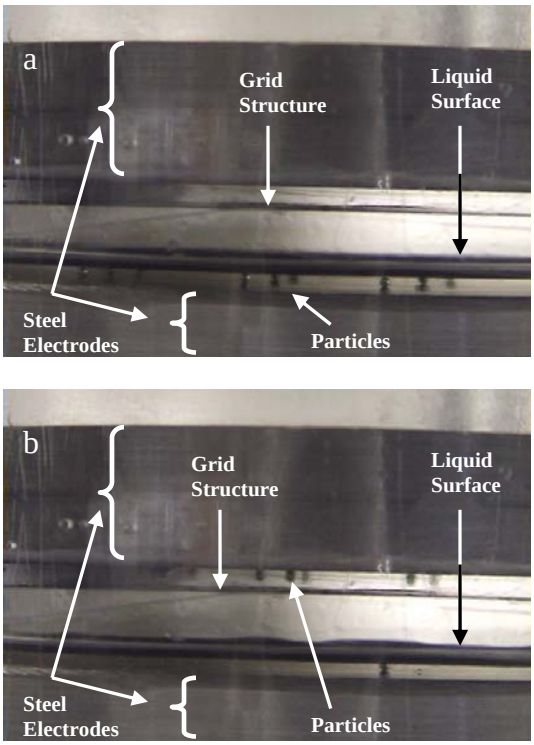

Figure 26: Spherical particle extraction through a grid structure.
a) Particles are on bottom electrode before electric field is turned on.
b) Particles are stuck to upper electrode after being extracted through grid structure.

6.13. Vacuum Experiments

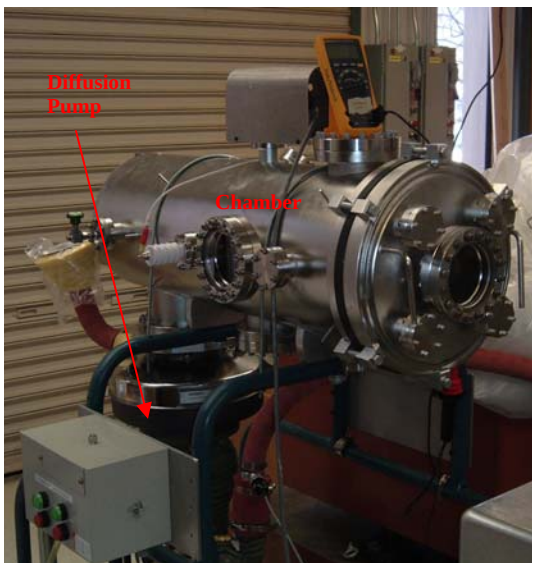

Figure 27: Vacuum Chamber

Since the nanoFET will be operating in space it is important to run the experiments discussed earlier in vacuum to be assured that particle extraction and cone formation still behave as expected. Figure 27 is a picture of our vacuum chamber which reaches an ultimate pressure of approximately 1E-6 Torr using a diffusion pump.

A series of experiments have been run within the vacuum chamber environment to demonstrate that the nanoFET concept works in vacuum conditions. Preliminary results suggest that particle extraction and the onset of liquid surface instability are not strongly dependent on the external pressure. We plan to continue these experiments in Phase II.

6.14. Experiments with Nanoparticle

To experimentally verify that nanoparticles can be charged and transported just like the millimeter-sized particles, we have begun experiments using various spherical nanoparticles ranging in size from 5 nm to 70 nm. The materials that we are currently working with are silver, nickel, and copper.

We have shown that the nanoparticles can be charged and transported when submersed in a liquid with electric fields just like the larger particles. We used the same experimental setup as in the particle oscillation experiment (Figure 13). Figure 28 shows a picture of a silver nanoparticle cloud put into oscillation within an electrode gap filled with silicone oil. It is important to note that the larger visible distinguishable particles are clumps of nano-spheres, since the individual nanoparticles are not visible with the naked eye.

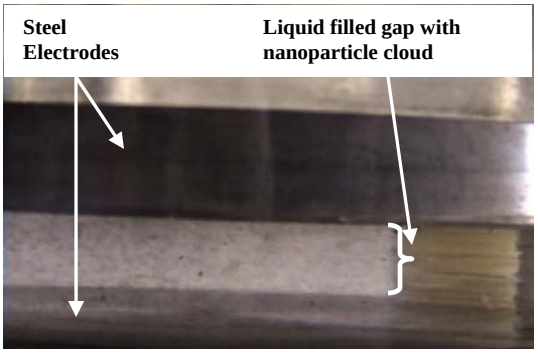

Figure 28: Silver nanoparticle cloud oscillating between electrodes when submersed in silicone oil.

6.15. Nanoparticle Properties

Through the experimental and modeling processes, we have learned a great deal about how the particle's shape and size affect various aspects of nanoFET, most importantly the charge-to-mass ratio. The charge-to-mass ratio of a spherical particle in contact with an electrode in the presence of an electric field is

$$\left(\frac{q}{m}\right)_{\text{sphere}} = \frac{\pi^2}{2}\frac{\varepsilon_\ell E_\ell}{\rho_p}\frac{1}{r}, \qquad (33)$$

where E_ℓ is the electric field in the liquid, r is the particle diameter, and ρ_p is the particle density. The charge-to-mass ratio for a vertically oriented cylindrical particle of radius r and length ℓ is

$$\left(\frac{q}{m}\right)_{\text{cylinder}} = \frac{\varepsilon_\ell E_\ell}{\rho_p}\frac{\ell}{r^2\left[\ln\left(\frac{2\ell}{r}\right)-1\right]}. \qquad (34)$$

The initial charge-to-mass ratio of both spherical and cylindrical particles can be increased by decreasing the particle radius. But the charge-to-mass ratio of the cylindrical particle increases faster as the radius is decreased. In addition, the cylindrical particle has one more degree of freedom in that its length can be changed as well. As the aspect ratio of the cylindrical particle is increased, its charge-to-mass ratio is also increased. For these two reasons, cylindrical particles are more attractive to nanoFET than spherical particles. Note that less dense particles result in larger charge-to-mass ratios and are more desirable.

In addition to particle size, shape, and density, another important characteristic is the conductivity. A high conductivity is preferred so that charging can occur very quickly when the particles briefly come into contact with the charging electrode.

6.16. Liquid Properties

Choosing the proper liquid for nanoFET requires a balance between many different liquid properties. The five main liquid properties of concern are vapor pressure, viscosity, permittivity, surface tension, and density.

The vapor pressure must be low enough so that the liquid does not evaporate when at very low pressures. The viscosity should be kept low so that dissipation during particle transport is minimized. A high permittivity would help to increase the charge-to-mass ratio and increase the minimum field strength that causes liquid surface instability.

The surface tension needs to be high enough to keep the liquid in the reservoir when in a zero-g environment, but it should be low enough to allow for particle extraction. In addition, increasing the surface tension increases the minimum electric field strength that causes the surface to become unstable. A liquid with a high density will also help to maintain liquid surface stability

in the laboratory environment, high densities would increase the total mass of the thruster.

The final choice of liquid will have to be a compromise of all the properties discussed above.

7. MEMS Gate Status

A fully realized nanoFET system requires a set of MEMS gated structures to provide the extraction and acceleration electric fields. At the University of Michigan, a second-generation MEMS gated structure prototype has been designed and fabricated. The fabrication process is outlined in Figure 29.

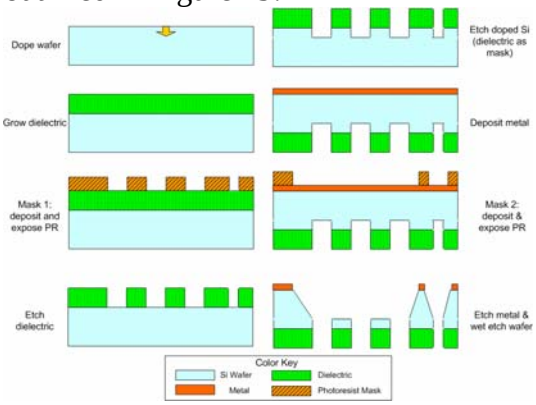

Figure 29: Fabrication process for MEMS gate structure.

Each MEMS gate consists of a conductive layer placed over an insulating spacer with channels arrayed throughout the structure to permit passage of charged particles. The gate layers are supported in a bulk silicon square with 1-cm sides. Viewing windows are etched in the bulk silicon to expose the emission channels, with each viewing window containing tens of thousands of emission channels. Thicker silicon between the windows provides structural stability. The top surface of the MEMS gate is a metal layer to facilitate electrical contact to the gate, and open regions are present that enable the gate to be clamped down upon the emission interface. Figure 30 shows the current MEMS gate design.

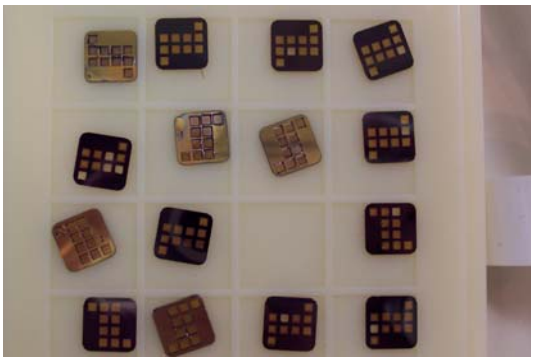

Figure 30: Current MEMS gate design. Each gate is 1-cm by 1-cm in size.

These gates are currently undergoing characterization and integrated testing with various field emission substrates, including cubic boron nitride and carbon nanotubes, to understand the performance of MEMS gated structures. An optimized future design iteration could be integrated for nanoFET.

8. Conclusions

During Phase 1, we have further assessed the significance of the *nanoFET* paradigm shift. While analyzing the possible specific impulse range using the nanoparticle mode exclusively, we have determined that it may be possible to extend the operating range from 100 s up to 10,000 s using just three differently sized particles while keeping the efficiency greater than 90% over the entire range.

We have also addressed fundamental questions regarding *nanoFET* operation. We have demonstrated the transport of conducting particles through an insulating liquid by way of an electric field and have achieved particle extraction from a liquid prior to the onset of liquid surface instability. These experimental results

have validated our theoretical models and represent a significant step towards proving the fundamental feasibility of *nanoFET*.

9. Publications

Phase I results were presented at IEPC and published in Conf. Proceedings

Musinski, L., Liu, T., Gilchrist, B., Gallimore, A., and Keidar, M., "*Scalable Flat-Panel Nano-Particle MEMS/NEMS Thruster*" IEPC-2005-176, 29th International Electric Propulsion Conference, Princeton, NJ, 31 October – 4 November 2005.

Additional results will be presented at AIAA Joint Propulsion Conference:

1. Musinski, Liu, Gilchrist, Keidar, Gallimore, *"Flat Panel Nanoparticle Electrostatic Thruster,"* AIAA-2006-4803, 42nd AIAA/ASME/SAE/ASEE Joint Propulsion Conference & Exhibit, Sacramento, CA, July 2006.

2. M. Keidar, L. Musinski, T. Liu, F. Saliki, B. Gilchrist and A. Gallimore, "*Theoretical Aspects on Nano- Particle Propulsion*", AIAA-2006-4335, 42nd AIAA/ASME/SAE/ASEE Joint Propulsion Conference & Exhibit, Sacramento, CA, July 2006.

References:

1. Behan, Niall, "Nanomedicin and Drug delivery at the University of Limerick," The University of Limerick. http://www.ul.ie/elements/Issue4/behan.htm
2. Calero, J. "The electrohydrostatics of a Conductive Liquid Meniscus," IEEE 1988, p 1547-1551.
3. Chesta, E., Nicolini, D., Robertson, D. and Saccoccia, G., "Experimental Studies Related to Field Emission Thruster Operation: Emission Impact On Solar Cell Performances And Neutralization Electron Backstreming Phenomena," IEPC-2003-102, Proceedings of the International Electric Propulsion Conference, Toulouse, France, March 17-20, 20033
4. Choi, Changrag. "Dynamic Motion of a Conductive Particle in Viscouse Fluid Under DC Electric Field," IEEE Transactions on industry Applications, vol 37, No 3, May/June 2001.
5. Gallimore, A. "Micro Electric Propulsion Proposal," The University of Michigan, November 2003.
6. J.R. Brophy, J.E. Polk, V.K. Rawlin, Ion engine service life validation by analysis and testing, AIAA Paper 96-2715, July 1996.
7. Khayari, A. "The Charge Acquired by a Spherical Ball Bouncing on an Electrode: Comparison Between Theory and Experiment;" 2000 Conference on Electrical Insulatoin and Dielectric Phenomena.
8. Marcuccio, S. "Attitude and Orbit Control of Small Satellites and Constellations with FEEP Thrusters," Electric Rocket Propulsion Society, 1997.
9. Marcuccio, S. "FEEP Microthruster Technology Status and Potential Applications," International Astronautical Federation, 1997.
10. Marcuccio, S. "FEEP Thrusters," Nov. 1998, http://www.centrospazio.cpr.it/Centrospazio6FEEP.html.
11. M. Fehringer, F. Ruedenauer, W. Steiger, ESTEC Contract 12376/97/NL/PA Tech. Note No. 2, 1997.
12. Najafi, Khalil. Personal Communications, University of Michigan, 2004.
13. Stark, John. "Micro-Fabrication and Operation Nano Emitters Suitable for a Colloid Thruster Array," University of London, UK, https://escies.org/public/mnt4/S9.1Stark.pdf
14. Chock, R. "Photovoltaic & Space Environment Branch," NASA Glenn Research Center, July 2002, http://powerweb.grc.nasa.gov/pvsee/publications/tropix/Paper/AppA.html
15. Morris, D.P., Gilchrist, B.E., Gallimore, A.D., "Application of Dual Grids to Cold Cathode/ Field Effect Electron

Emission, AIAA-2005-3669, 41st Joint Propulsion Conference, Tucson, AZ, July 10-13, 2005.

16. Goldberg, H., Encarnación, P., A., Morris, D., Gilchrist, B., Clarke, R., "Cold-Cathode Electron Field Emission of Boron Nitride Thin Film with a MEMS-Based Gate for Space Applications, AIAA-2004-3499, 40th Joint Propulsion Conference, Ft. Lauderdale, FL, July 11-14, 2004.
17. Tobazeon, R. "Behavior of Spherical and Cylindrical Particles in an Insulating Liquid Subjected to a DC Uniform Field." Laboratoire d'Electrostatique et de Materiaux Dielectriques. BP 166-38042 Grenoble Cedex 9 (France) pp. 415-420.
18. Felici, N. Rev. Gen. Elect., 75, pp. 1145-1160, 1966.
19. Wertz, Larson, "Space Mission Analysis and Design 3rd Ed." 1999
20. Tonks, L., "A Theory of Liquid Surface Rupture by a Uniform Electric Field," *Physical Review*, Vol. 48, 15 September 1935, pp. 562-8
21. Smith, R.C., Carey, J.D., Forrest, R.D., Silva, S.R.P., "Effect of aspect ratio and anode location on the field emission properties of a single tip based emitter," J. Vac. Sci. Technol. B 23(2), Mar/Apr 2005, pp. 632-5.

Appendix A

NIAC Phase I Final Presentation

UNIVERSITY OF MICHIGAN

Scalable Flat-Panel Nanoparticle Propulsion Technology for Space Exploration in the 21st Century

NIAC Phase 1

End-of-Project Presentation

Atlanta, GA

2006 March 7-8

Students: T. Liu†, L. Musinski*, P. Patel†† (and M. Forsyth)

Faculty: A. Gallimore§, B. Gilchrist‡, M. Keidar**

University of Michigan, Ann Arbor, MI 48109, USA

*Graduate Student, Electrical Engineering, louisdm@umich.edu

†Graduate Student, Aerospace Engineering, liutm@umich.edu

‡Professor, Electrical Engineering and Space Science, gilchrst@umich.edu

§Professor, Aerospace Engineering, rasta@umich.edu

**Research Professor, Aerospace Engineering, keidar@umich.edu

††Graduate Student, patelpr@umich.edu

Presentation Outline

- What is nanoparticle EP (nanoFET)?
- How does nanoFET work?
- What are the advantages offered by nanoparticle EP?
- What have we learned to-date in Phase 1?
- Looking to the future

What is **nanoFET**?
nanoparticle Field Emission Thruster

- Electrostatically *charges* and *accelerates* *nanoparticles* as propellant
  - Tremendous flexibility controlling charge/mass *(q/m)* ratio to tune propulsion performance

*Use **nanoparticles** of various geometries and material as **propellant***

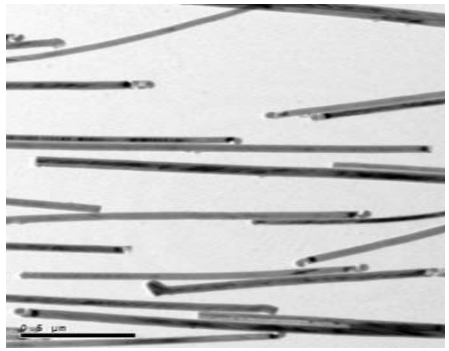

45 nm dia. x 500 nm long

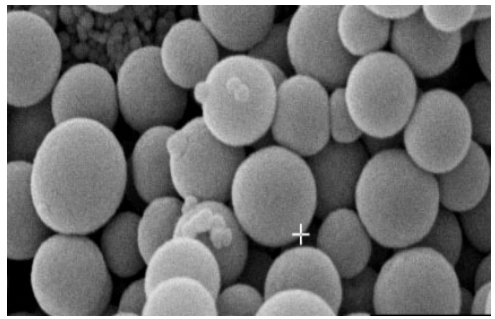

100 nm dia.

- Uses scalable array (*thousands* to many *millions*) micron-sized emitters
  - *Millions* of emitters per square cm feasible

*Use MEMS/NEMS structures for particle **feed**, **extraction**, and **acceleration***

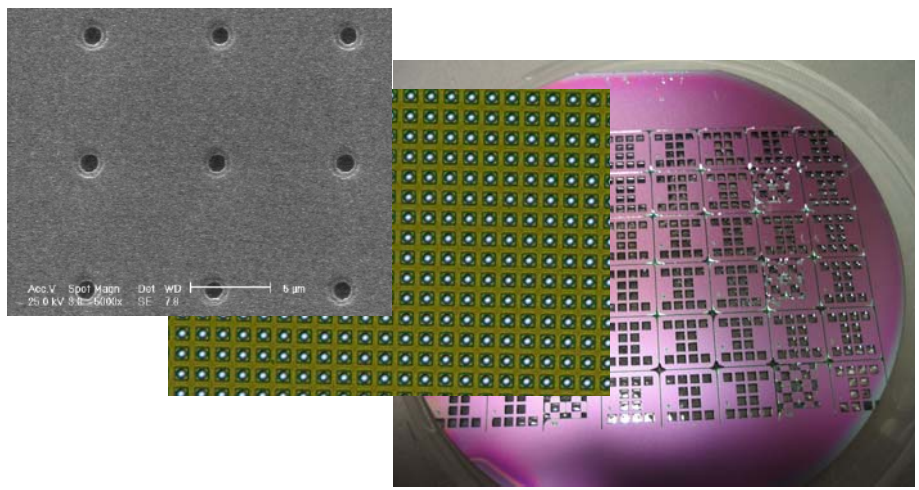

How Does nanoFET Work?

Single nanoparticle thruster emitter

(using insulating liquid)

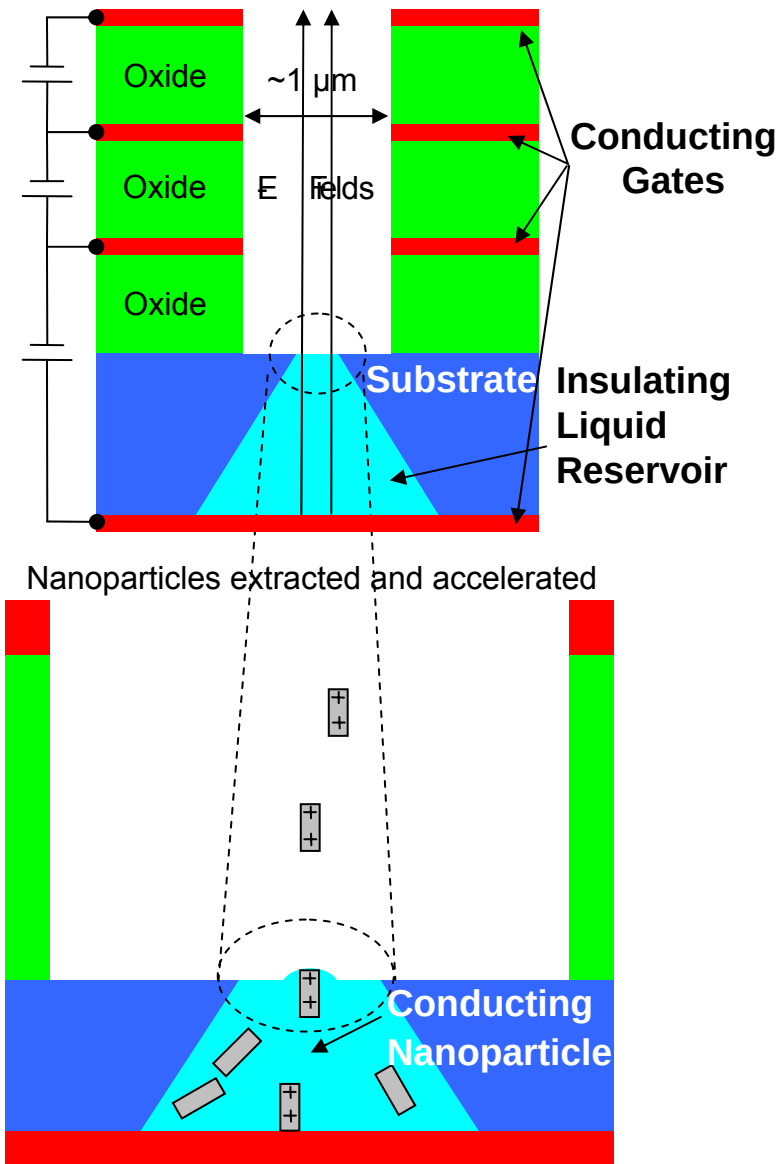

- Nanoparticles of specific size/shape immersed in low conductivity or insulating liquid carrier reservoir
- Electric field created by applying potential between extraction and accelerating electrodes
- Nanoparticles in contact with bottom electrode become charged
- Coulomb force transports charged particles to liquid surface, overcomes surface tension, extracts particles
- Extracted particles accelerated/ejected
- Note:
  - Specific charge of nanoparticles controlled by particle size, shape, and applied E- field
    - Different nanoparticles stored separately
  - Extraction with either polarity possible
    - *Neutralizer requirements simplified*

How Does nanoFET Work?

Single nanoparticle thruster emitter

(using conducting liquid)

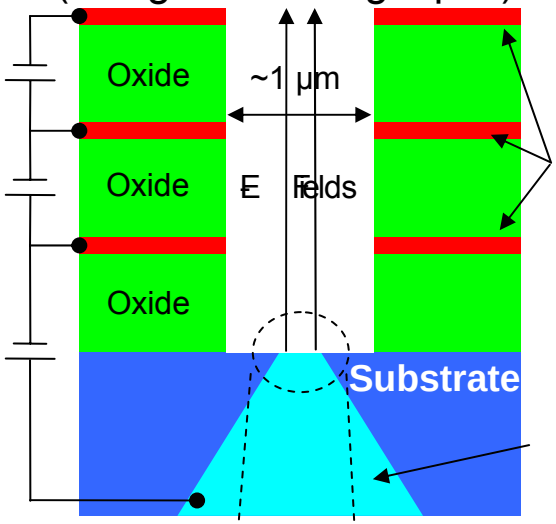

Nanoparticles extracted and accelerated

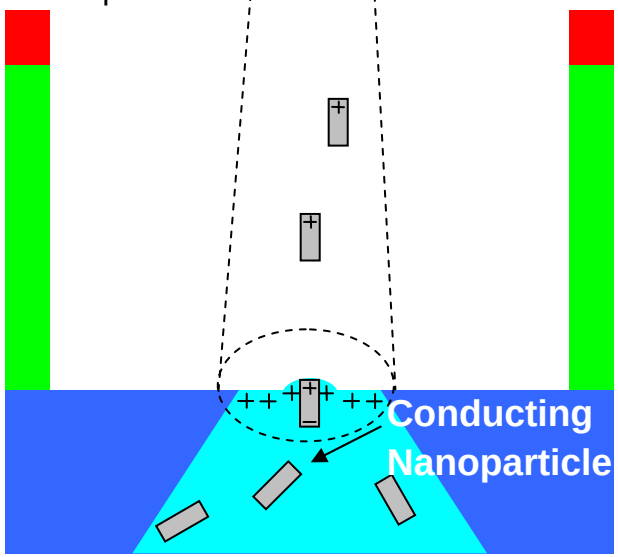

Conducting Liquid Option

- Electric fields do not exist in the liquid
- Nanoparticles reaching liquid surface experience strong polarization charging (>than surrounding liquid)
- Particles extracted and accelerated just like insulating case

No Liquid Option

- Looking at non-liquid option

Describing the Advantages of the nanoFET Concept - nanoparticle EP System Level Picture

Flat Panel MEMS/NEMS micro-Thruster using nanoparticles

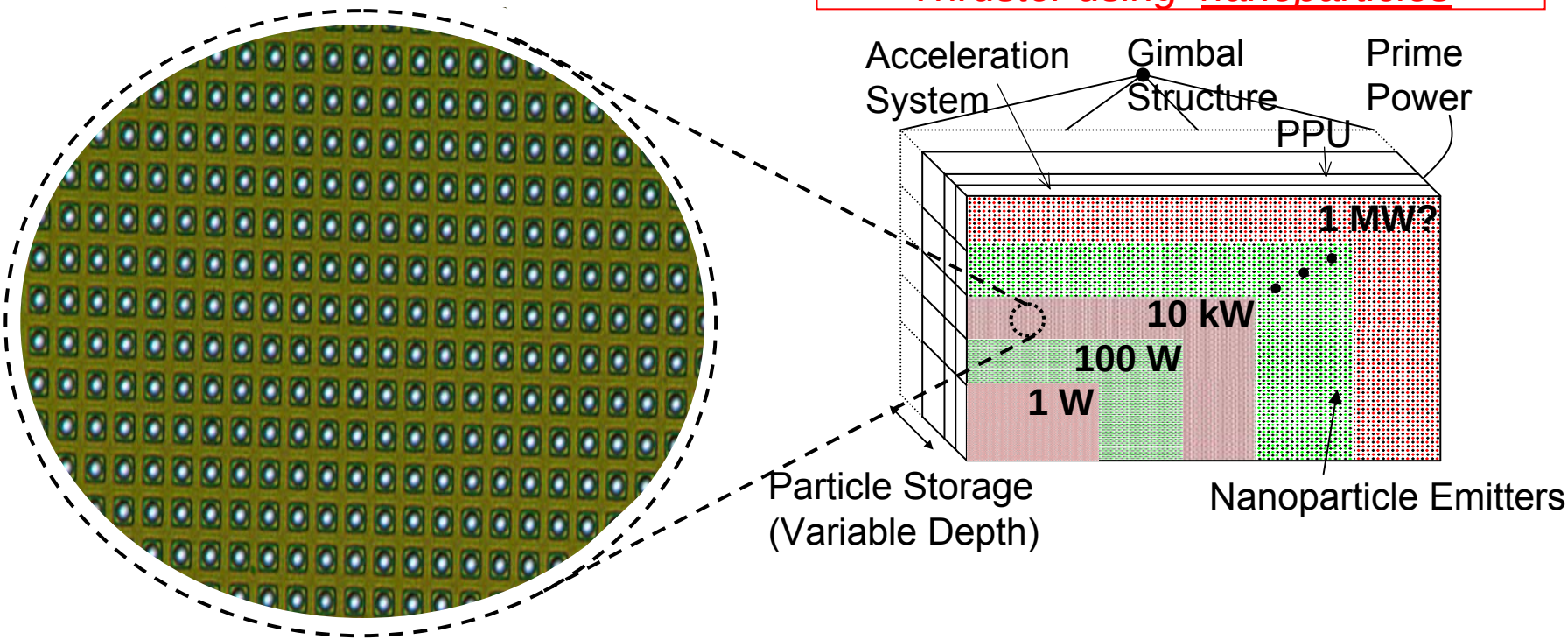

What are the advantages offered by nanoFET?

- *Affords much broader set of missions and mission phases with a single engine type*
- *Decoupling of propulsion system design from spacecraft design*
- *Propulsion system that is both mission enhancing and mission enabling*

Flat Panel MEMS/NEMS electrostatic thruster using nanoparticles

Notional Concept

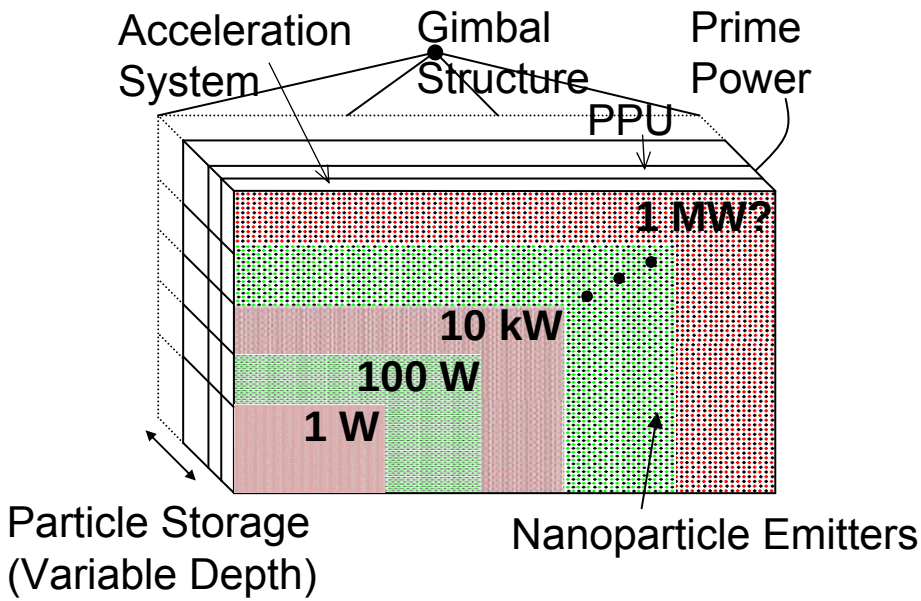

What are the advantages offered by nanoFET?

- *Affords much broader set of missions and mission phases with a single engine type*
  - Variable specific impulse over huge range (100 - 10,000 s)
  - High efficiency (~90%+) over entire specific impulse range
  - Unprecedented thrust-to-power ratios for EP due to high efficiency even at low specific impulse
- *Decoupling of propulsion system design from spacecraft design*
- *Propulsion system that is both mission enhancing and mission enabling*

Flat Panel MEMS/NEMS electrostatic thruster using nanoparticles

Notional Concept

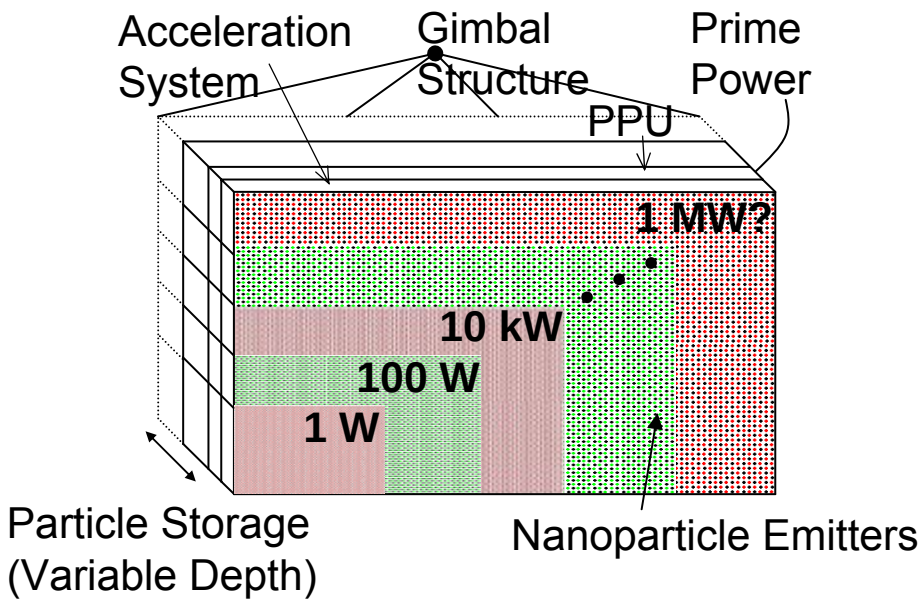

What are the advantages offered by nanoFET?

- *Affords much broader set of missions and mission phases with a single engine type*

- *Decoupling of propulsion system design from spacecraft design*
  - Scalable from watts to MWs with low thruster specific mass (kg/kW) by changing nano-accelerator array size
  - *"Plug & Play"* approach provides greater flexibility and significant cost savings to mission planners and spacecraft developers
- *Propulsion system that is both mission enhancing and mission enabling*

Flat Panel MEMS/NEMS electrostatic thruster using nanoparticles

Notional Concept

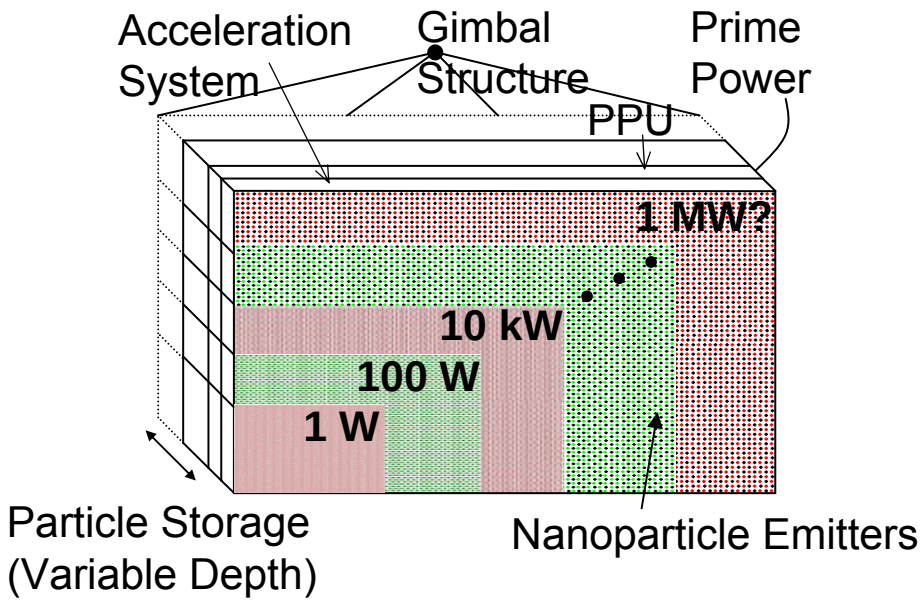

What are the advantages offered by nanoFET?

- *Affords much broader set of missions and mission phases with a single engine type*
- *Decoupling of propulsion system design from spacecraft design*
- *Propulsion system that is both mission enhancing and mission enabling*
  - Improved thrust density over ion and Hall thrusters lowers specific mass
  - Improved life span over ion and Hall thrusters improves reliability and also lowers specific mass

Flat Panel MEMS/NEMS electrostatic thruster using nanoparticles

Notional Concept

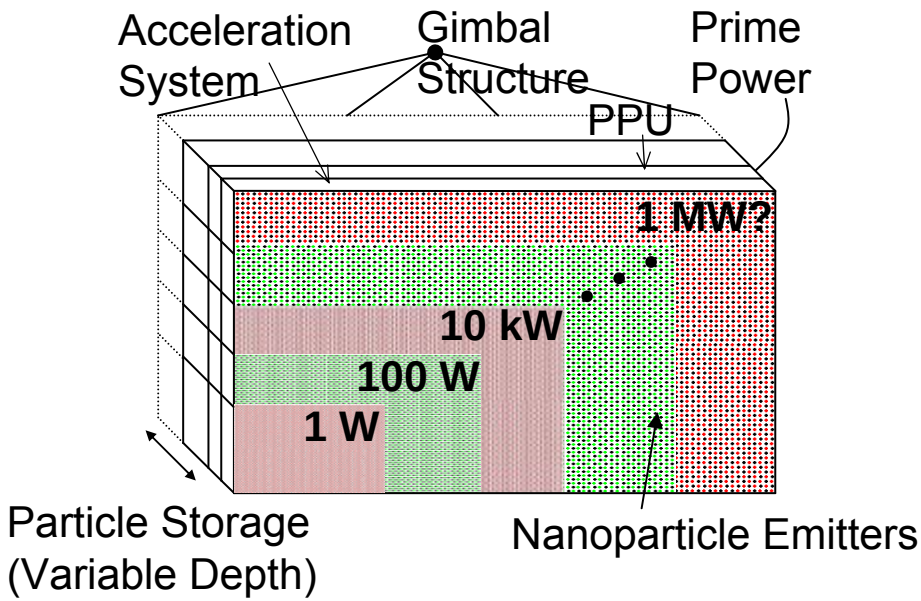

Nanoparticle Propulsion Compared

Highly Scalable ***Specific Impulse*** and ***Thrust-to-Power*** Using Nanoparticles (insulating liquid case)

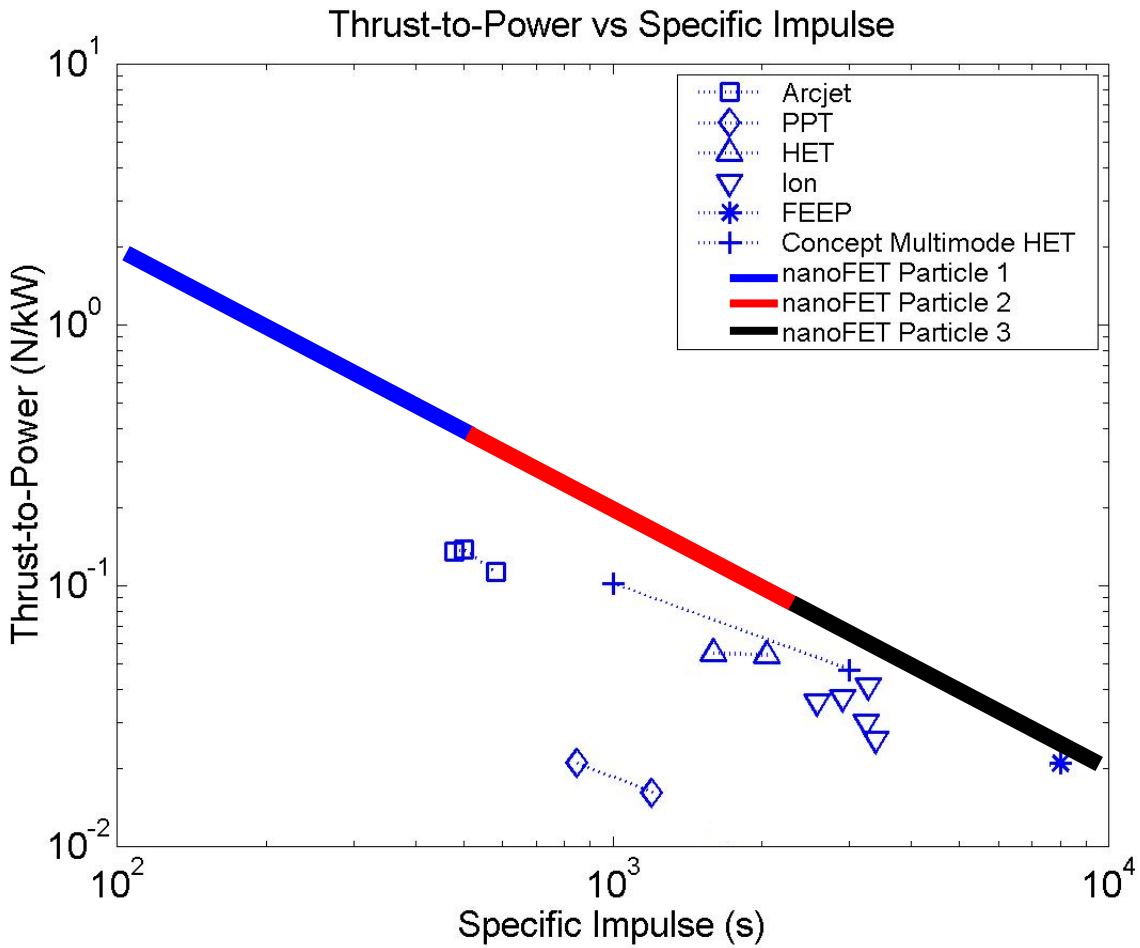

$$I_{sp} = \frac{1}{g}\left(2V_o \frac{q}{m}\right)^{\frac{1}{2}}$$

$$\frac{T}{P} = \left(\frac{2}{V_o}\frac{m}{q}\right)^{\frac{1}{2}}$$

Particle 1
- Diameter = 5 nm
- Length = 100 nm

Particle 2
- Diameter = 1 nm
- Length = 100 nm

Particle 3
- Diameter = 1 nm
- Length = 3.5 μm

Voltage Range
- 800 – 10,000 V

Source: Wertz and Larson, 3rd Ed.

Nanoparticle Propulsion Compared: Efficiency

- Particle 1
  - Diameter = 5 nm
  - Length = 100 nm
- Particle 2
  - Diameter = 1 nm
  - Length = 100 nm
- Particle 3
  - Diameter = 1 nm
  - Length = 3.5 μm
- Voltage Range
  - 800 – 10,000 V
- Sources of Losses
  - Viscous drag
  - Charge loss to liquid
  - Particle Impingemen on gates
  - Defocusing

Improved Efficiency for entire I_{sp} Range Using Nanoparticles (insulating liquid case)

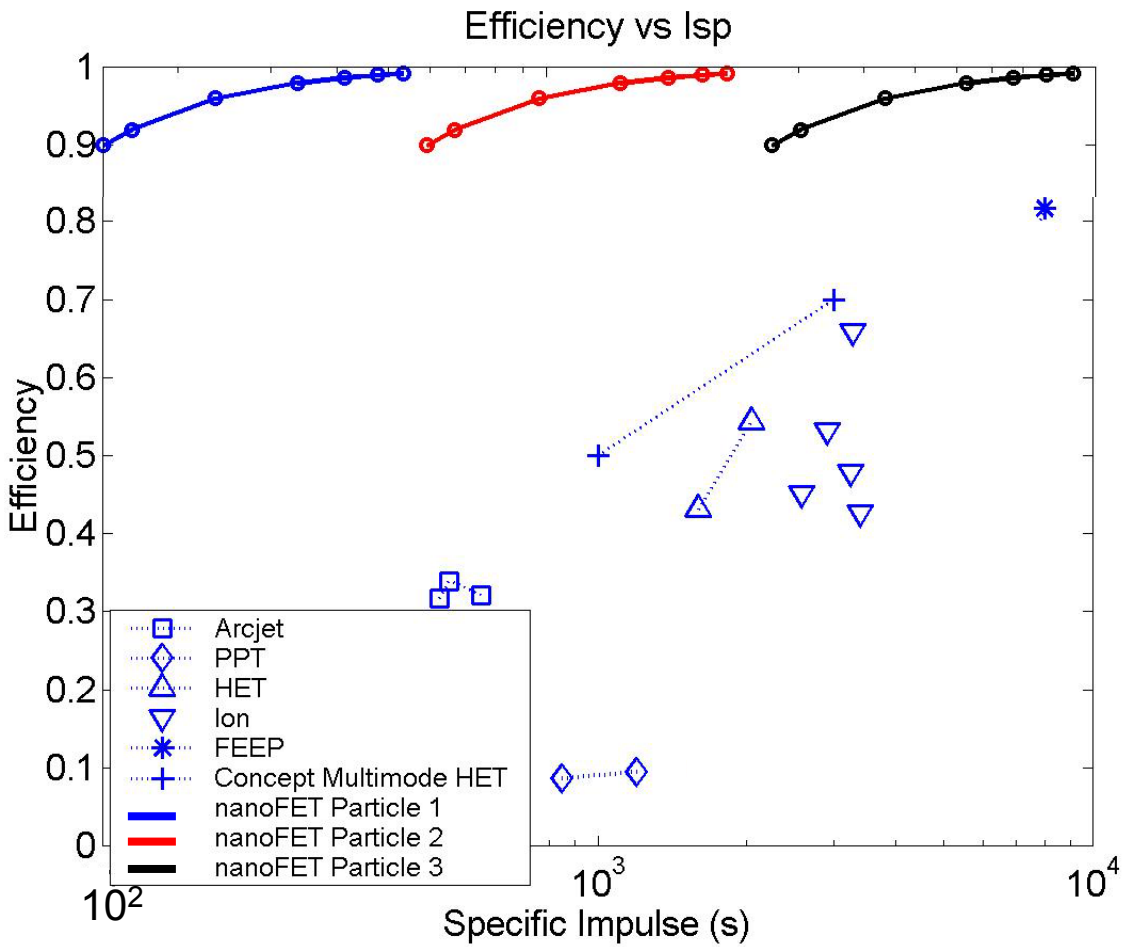

nanoFET advantages span huge range of activities

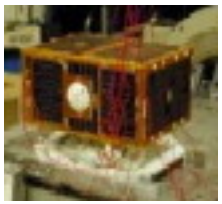
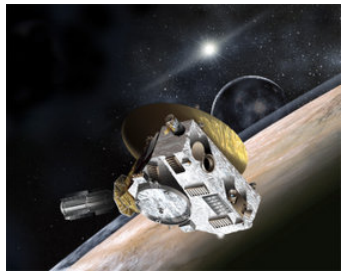
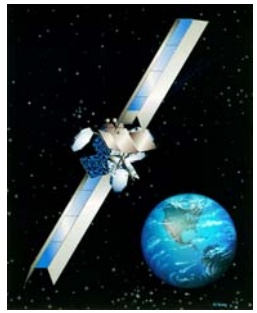
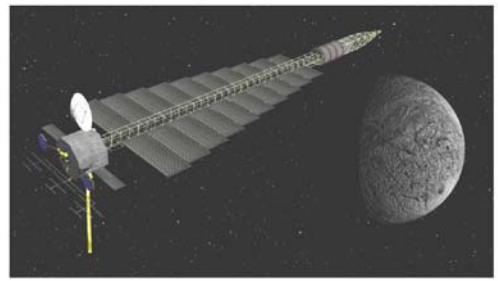
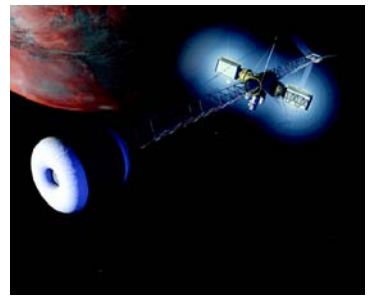

- nanoFET is geometrically scalable
  - Engine scales geometrically with power
  - Easier to ground-qualify system
- nanoFET offers wider margin for off-nominal mission scenarios
  - Example: JIMO craft enters unstable orbit around Europa and requires high emergency thrust
    - JIMO craft would be lost with ion/Hall thruster technology under extreme (but possible) scenario
    - Difference? nanoFET's ability to have T/P orders of magnitude higher than ion/Hall

- nanoFET Isp and T/P range ideal for piloted/resupply missions to Mars
  - Allows for short trip times with flexible abort scenarios
- nanoFET Isp and T/P range ideal for Earth orbit
  - Enables dynamical re-tasking of space assets
  - SINGLE engine type for most satellites (nanoSATs to very large space stations and space tugs)
    - Decouples propulsion and satellite design

Nanoparticles

- Pre-fabricated conducting nano-particles (wires or spheres)
- Different sizes and shapes used for different performance needs
- Particle sizes from ~1 nm to microns
- Potential particles today
  - Carbon nano-tubes (CNT)
  - Metal spheres and wires
  - Silicone wires fused with nickel
  - Fullerenes
- Considerations
  - Wettability
  - Variability in particle dimensions
  - Contamination
  - Quantum effects
  - Adhesion between nanoparticles and bulk surfaces

Nano-wires approximately 45 nm dia. [1]

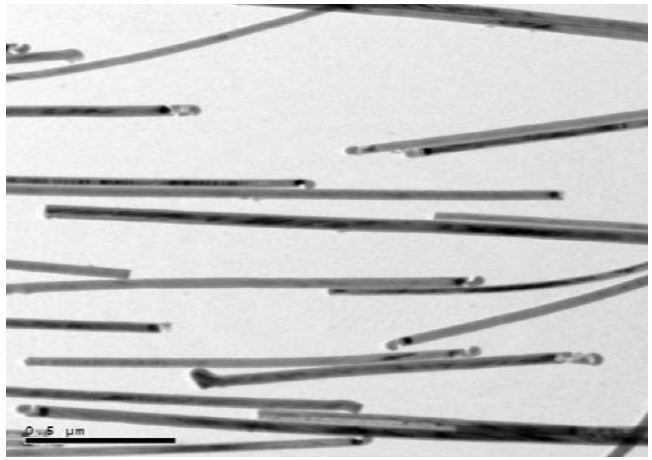

Nano-spheres in 100 nm dia. range [2]

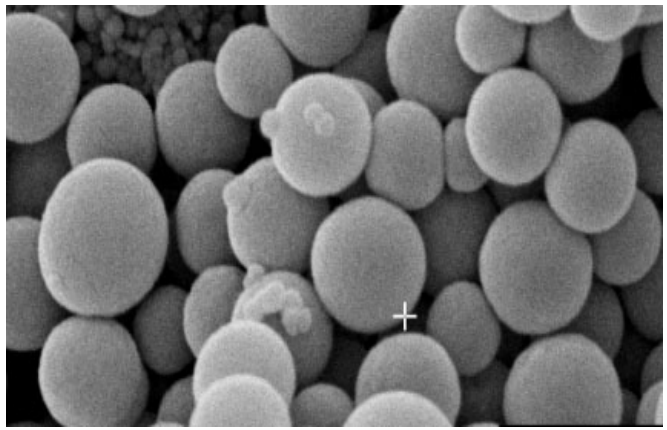

1. Koninklijke Philips Electronics. "www.research.philips.com/newscenter/pictures/ldm-nanotech.html
2. Behan, N. "Nanomedicine and Drug Delivery," www.ul.ie/elements/Issue4/behan.htm

Microfluidics & Nanoparticle Transport

- NanoFET needs
  - Nano-particles transport to extraction zone
  - Liquid recirculation
  - Conductive particles transport to liquid surface to be extracted
- Related research work
  - Bio-MEMS and miniaturized chemical reactors
  - No fundamental infeasibility issues
- Possible transport methods
  - Pressure gradients and peristalsis
  - Capillary effects
  - Electrokinetics
  - Lorentz forces
  - Acoustic streaming

Influenza genotyper chip (Burns, UM)

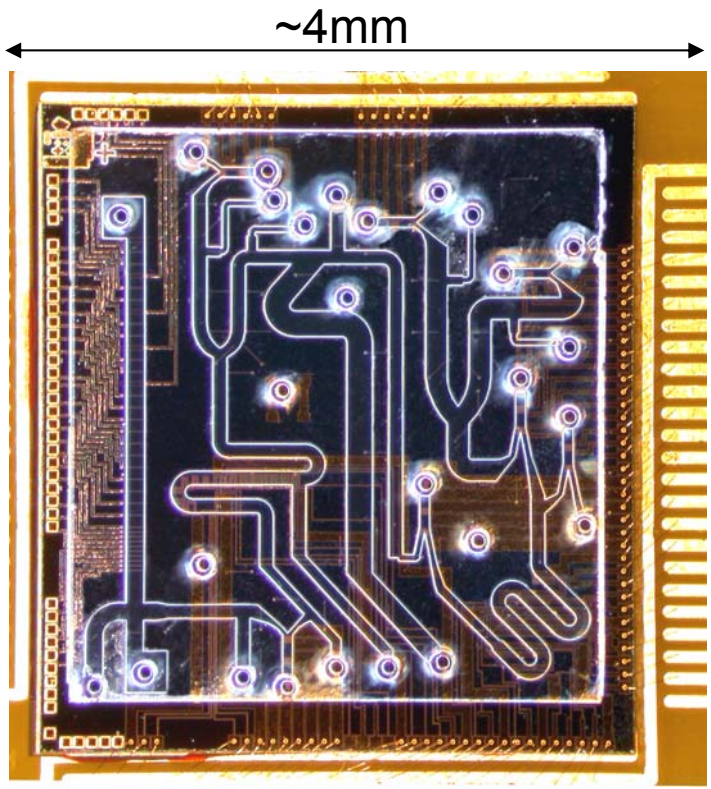

- Considerations
  - Minimize particle wetting upon extraction
  - Minimize wetting of gated structures

MEMS Gate Structure

- Gates provide electric field to extract and accelerate nanoparticles
- Stacked gate design permits decoupling of extraction and acceleration stages
- Different gated regions may be biased to opposite polarity to provide charge neutralization
- Current gate design: beta version
  - 2-micron dielectric thickness
  - 3.4E5 emission holes per 1-cm^2 device
  - 2-micron diameter emission holes spaced 5-microns center-to-center

MEMS gate array on 4-in diameter Si wafer

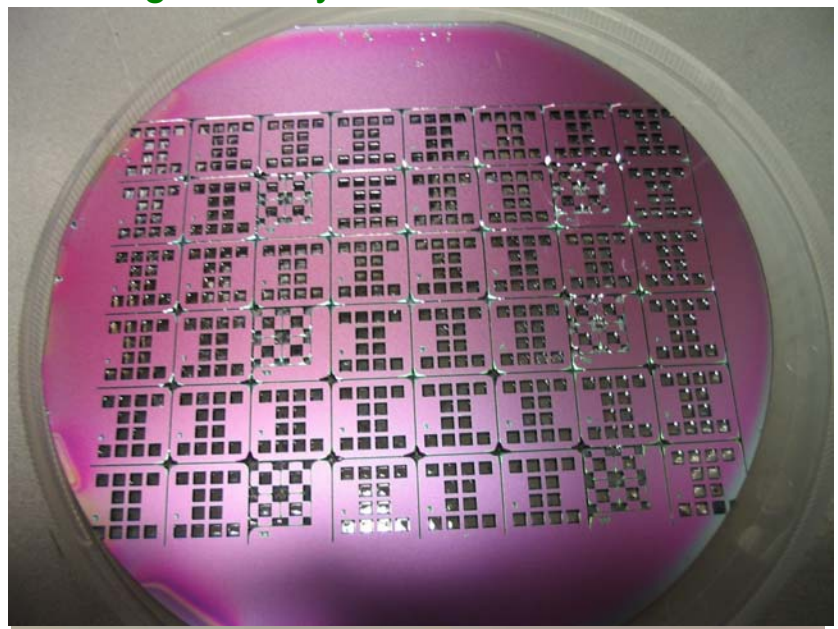

nanoFET Experiments

- Purpose of proof-of-concept experiments in insulating liquid
  - Understand how nanoFET concept works at *scaled-up* dimensions
  - Validate models of particle behavior and Taylor cone formation in large electric fields
- Experiments conducted
  - Particle lift-off and oscillation
  - Particle extraction
  - Taylor cone formation threshold
  - Vacuum operation
- Prove feasibility of particle extraction
  - Through liquid surface
  - Through grid structure
  - Prior to Taylor cone formation
  - In vacuum environment
- Planned future tests
  - Conductive liquid
  - Nanoparticles

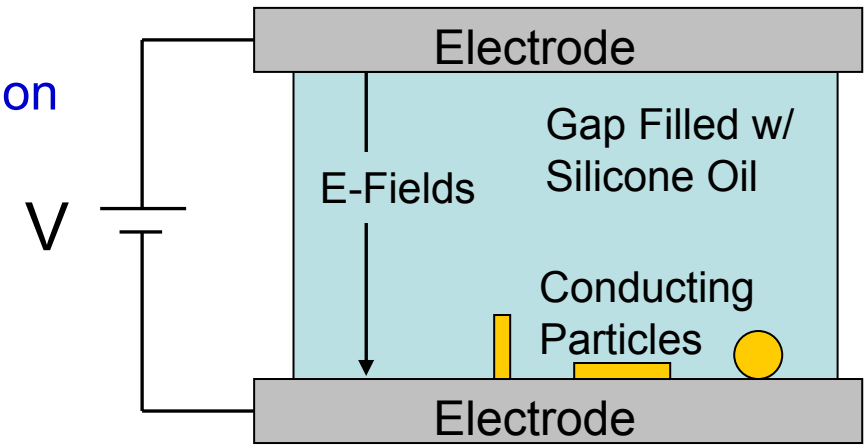

Particle Lift-Off

- Lift-off forces
  - electrostatic force in liquid
  - buoyant force
    - vanishes in zero-g
- Restraining forces
  - gravitational force
    - vanishes in zero-g
  - electric image force
    - reduces net electric field on particle
  - adhesion force between particle and electrode
    - significant for particle sizes on order of electrode surface roughness

$$q_{sph} = \frac{2\pi^3}{3} r^2 \varepsilon_\ell E_\ell, \qquad q_{cyl} = \frac{\pi \ell^2 \varepsilon_\ell E_\ell}{\ln\left(\frac{2\ell}{r}\right) - 1}$$

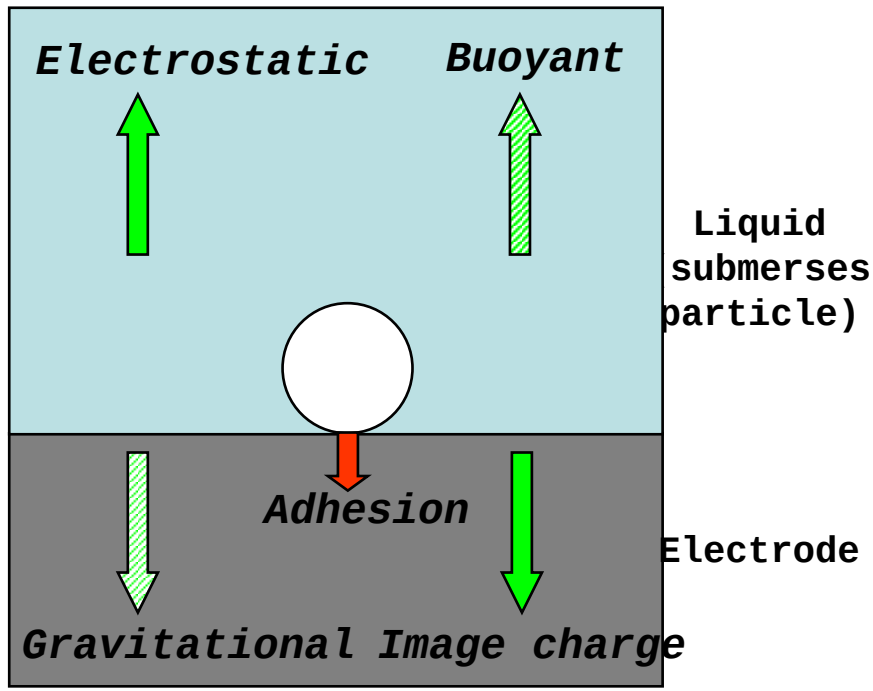

Particle Oscillation Experiments

- Demonstrate conductive particle lift-off and motion in insulating liquid due to E-fields
- Particles: aluminum
  - spheres (800-micron dia.)
  - cylinders (300-micron dia. by 1.5-mm length)
- Liquid: 100 cSt silicone oil

Experimental Setup: Liquid filled electrode gap with conducting particles

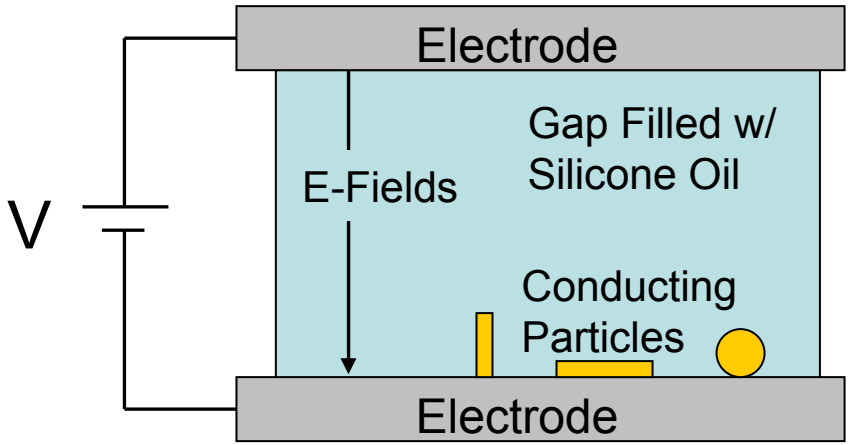

1. Charged on bottom electrode (-)
2. Transported to top electrode
3. Charged on top electrode (+)
4. Transported to bottom electrode

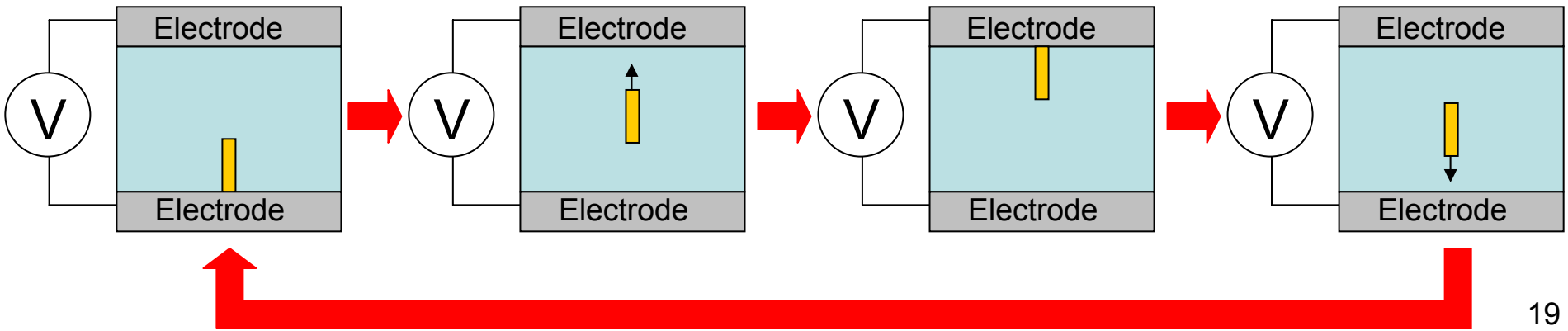

Particle Oscillation Video

- Cylindrical
  - diameter = 300 μm
  - length = 1.5 mm
  - gap = 6.35 mm
  - V ~ 5 kV

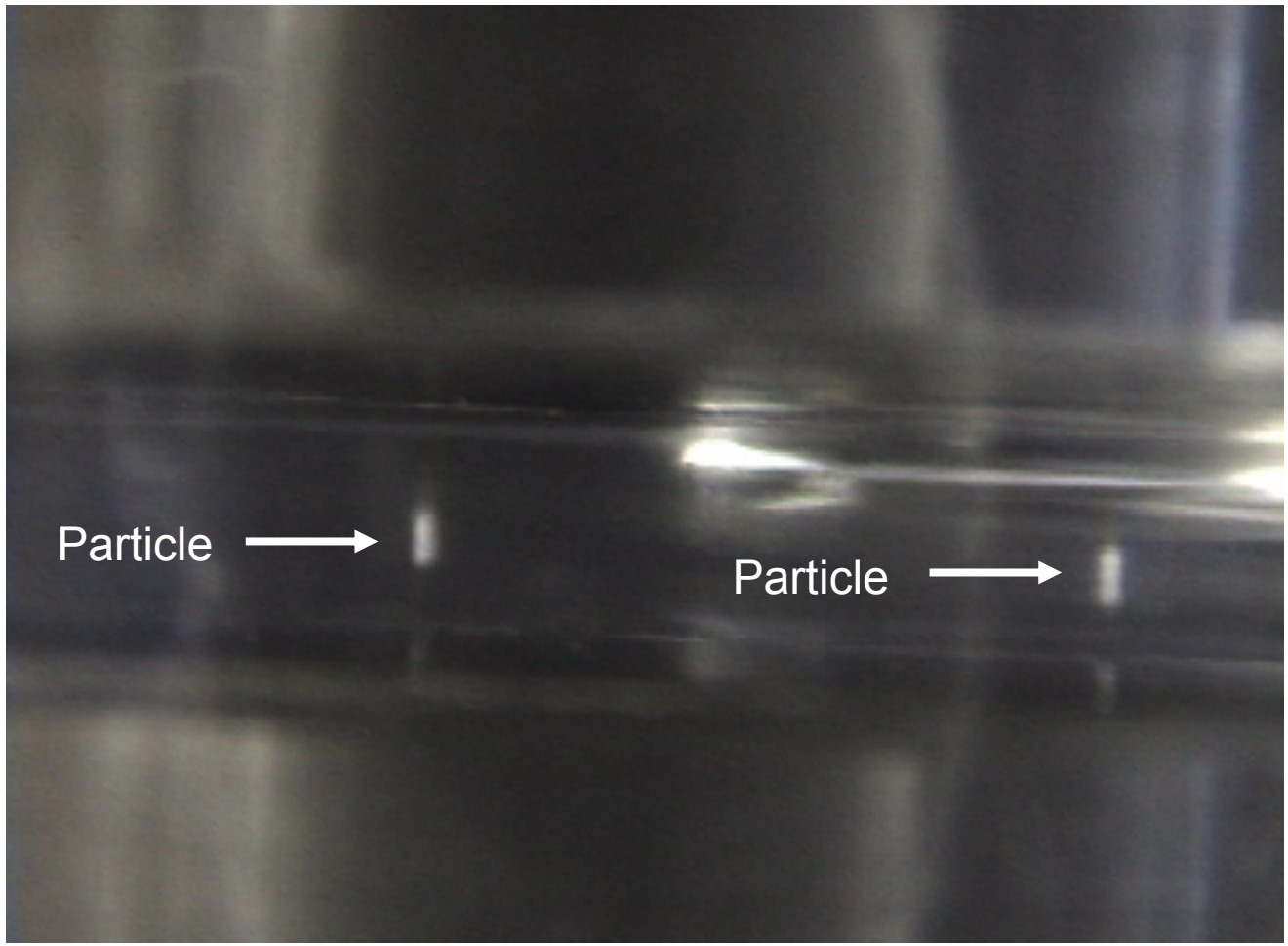

Particle Extraction Experiments (I)

- Experiments to demonstrate
  - conductive particle extraction through insulating liquid surface due to E- fields
  - feasibility of particle extraction prior to formation of Taylor cones
- Particles: aluminum
  - spheres (800-micron dia.)
  - cylinders (300-micron dia. by 1.5-mm length)
- Liquid: 100 cSt silicone oil
- Results: Particles of same kind extracted with approx same E-field strength independent of liquid height
  - Terminal velocity reached prior to extraction
  - Negligible charge loss in fluid

Experimental Setup: Partially liquid filled electrode gap with conducting particles

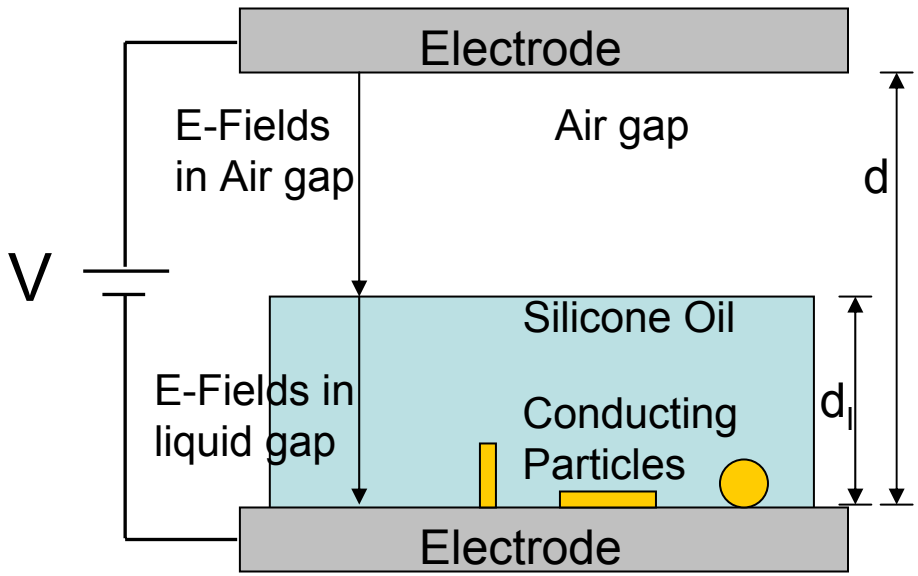

Particle Extraction Experiments (II)

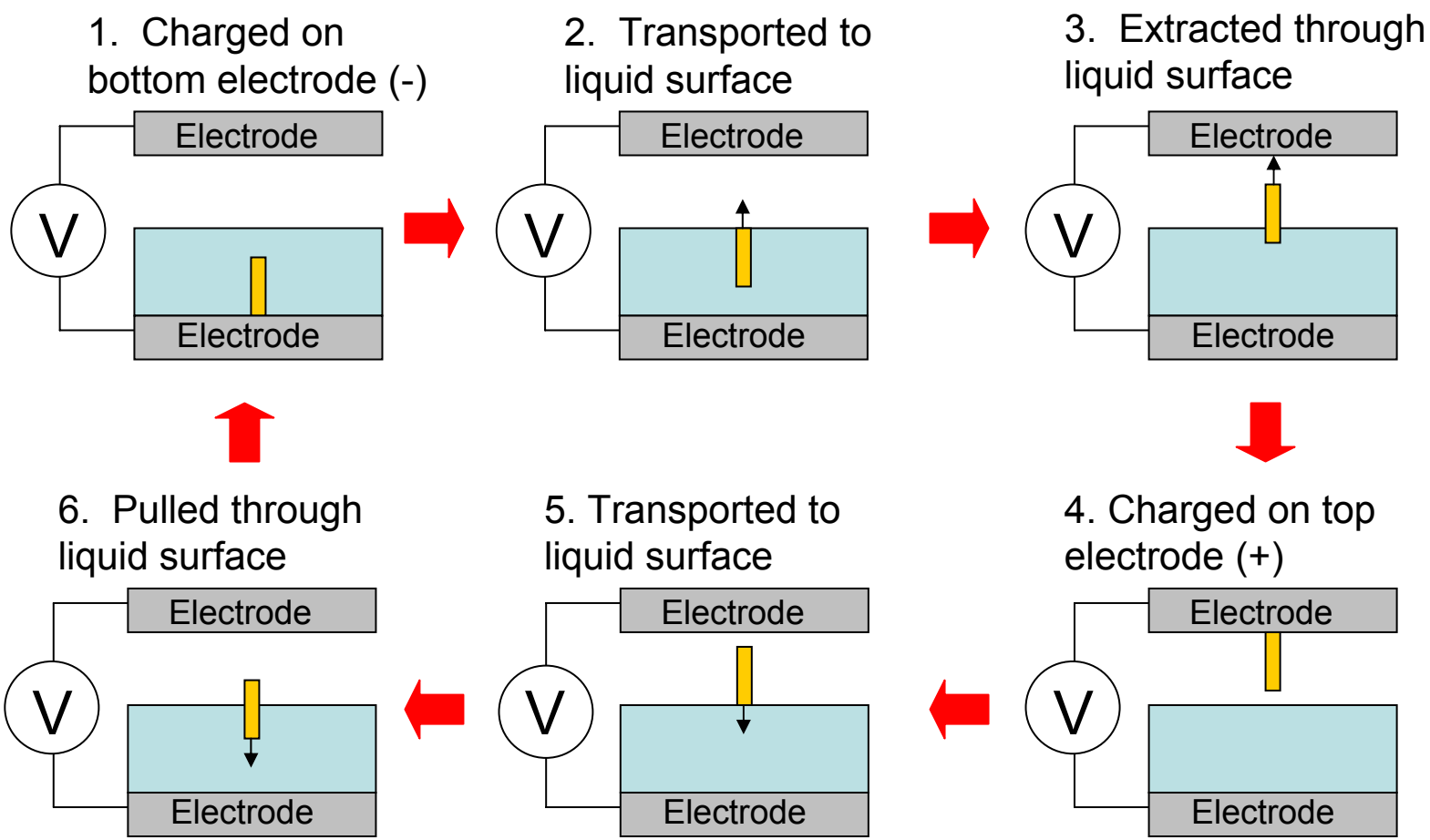

Particle Extraction Video

- Cylindrical Particle
  - diameter = 300 μm
  - length = 1.5 mm
  - gap = 12.7 mm
  - liquid thickness = 5 mm
  - V ~ 14 kV

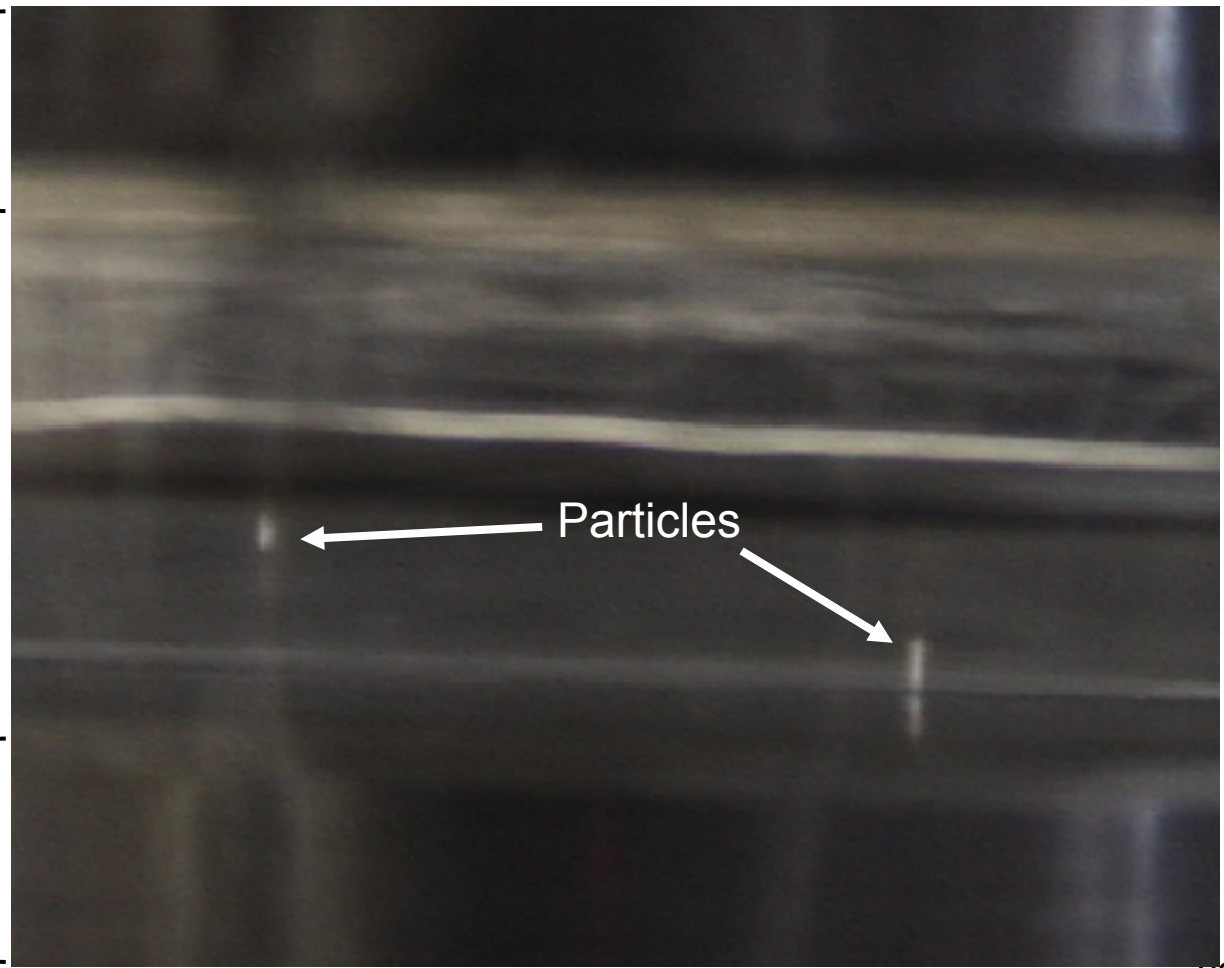

Taylor Cone Formation

- Electric field acts to pull free charges from the liquid
- Surface tension acts to keep charge within liquid
- Cones form as a result of balance of forces
- Strong enough E-field pulls cones to top electrode

$$E_{\min} = \left(\frac{4g\gamma\rho_\ell}{\varepsilon_0^{\,2}}\right)^{\frac{1}{4}}\left[1+\left(\frac{\varepsilon_0}{\varepsilon_\ell}\right)^2\right]^{-\frac{1}{2}}$$

1. Charge pulled to surface

2. E-field pulls liquid up, surface tension pull down

3. Charged droplets are pulled off surface

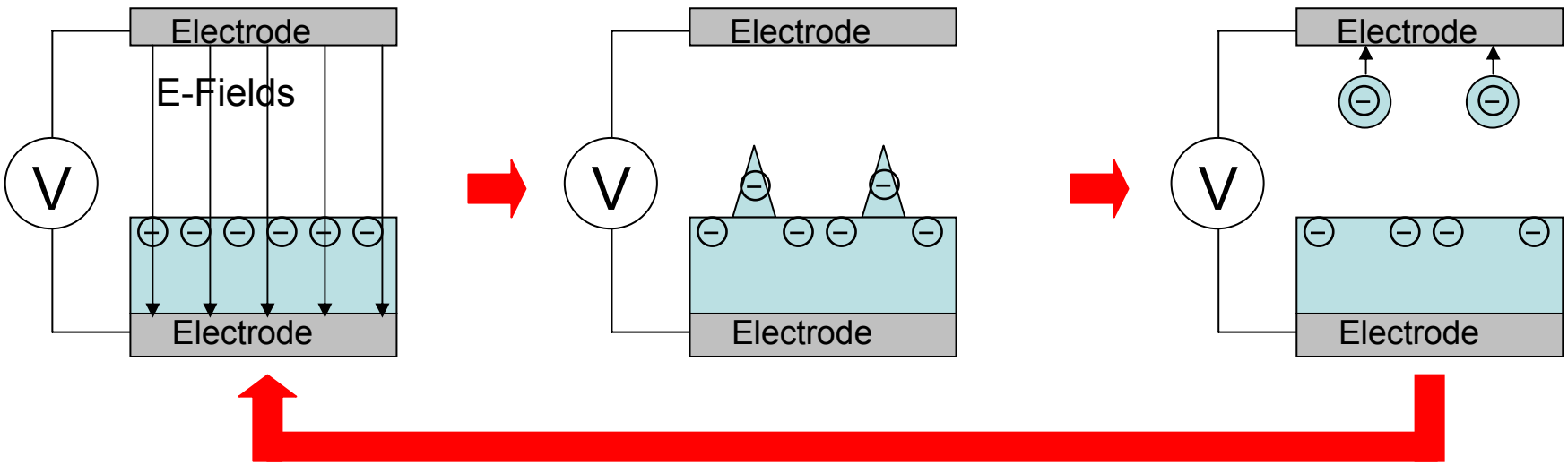

Video of Taylor Cone Formation

- gap = 12.7 mm
- liquid thickness = 5 mm
- V ~ 18 kV

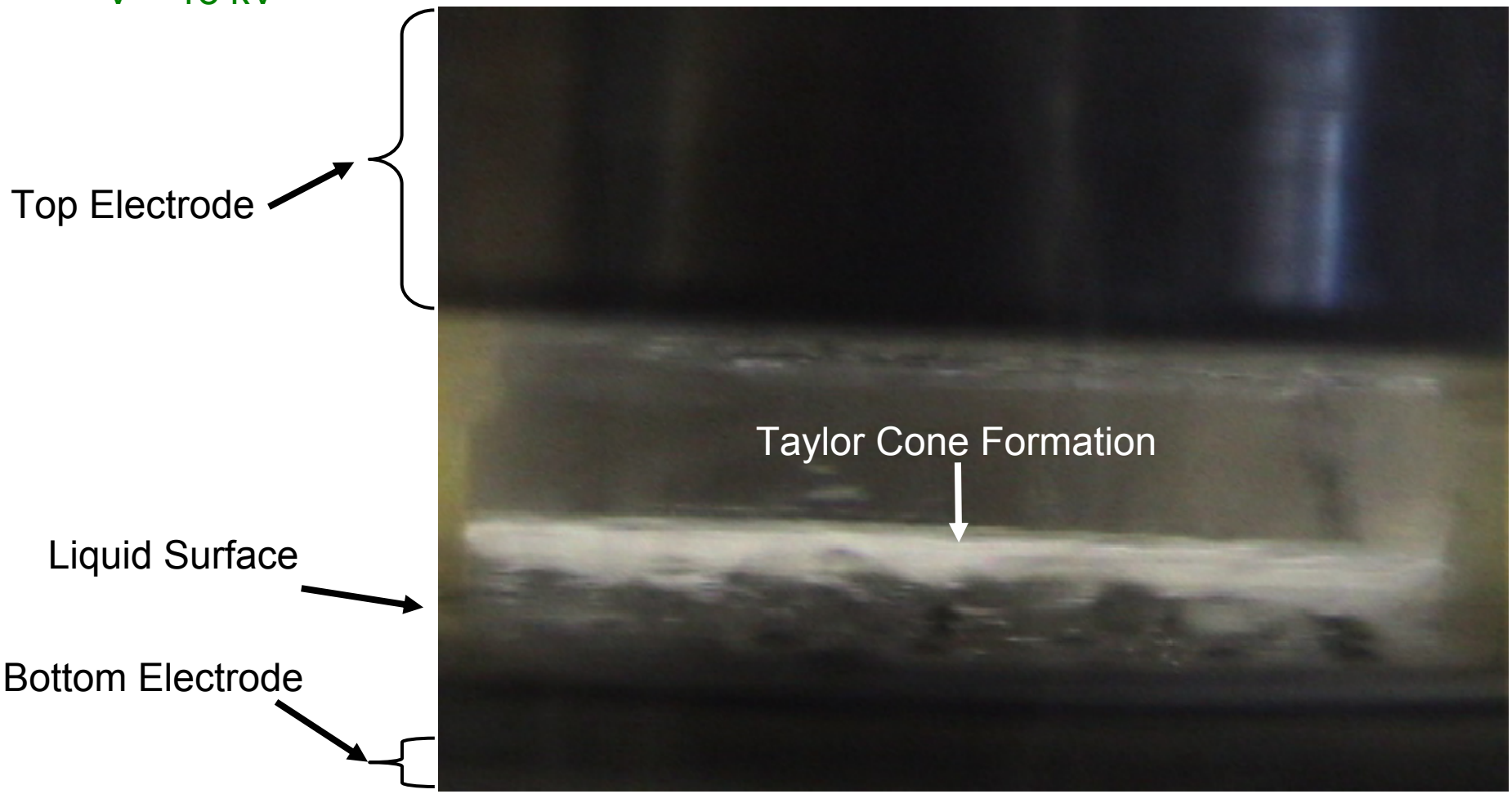

Taylor Cone Formation vs. Particle Extraction

- What do Taylor cones mean to nanoFET?
  - Formation of Taylor cones could mean problems for nanoFET because liquid could be emitted along with particles
  - Is there a regime where particles are extracted and cones do not form?...

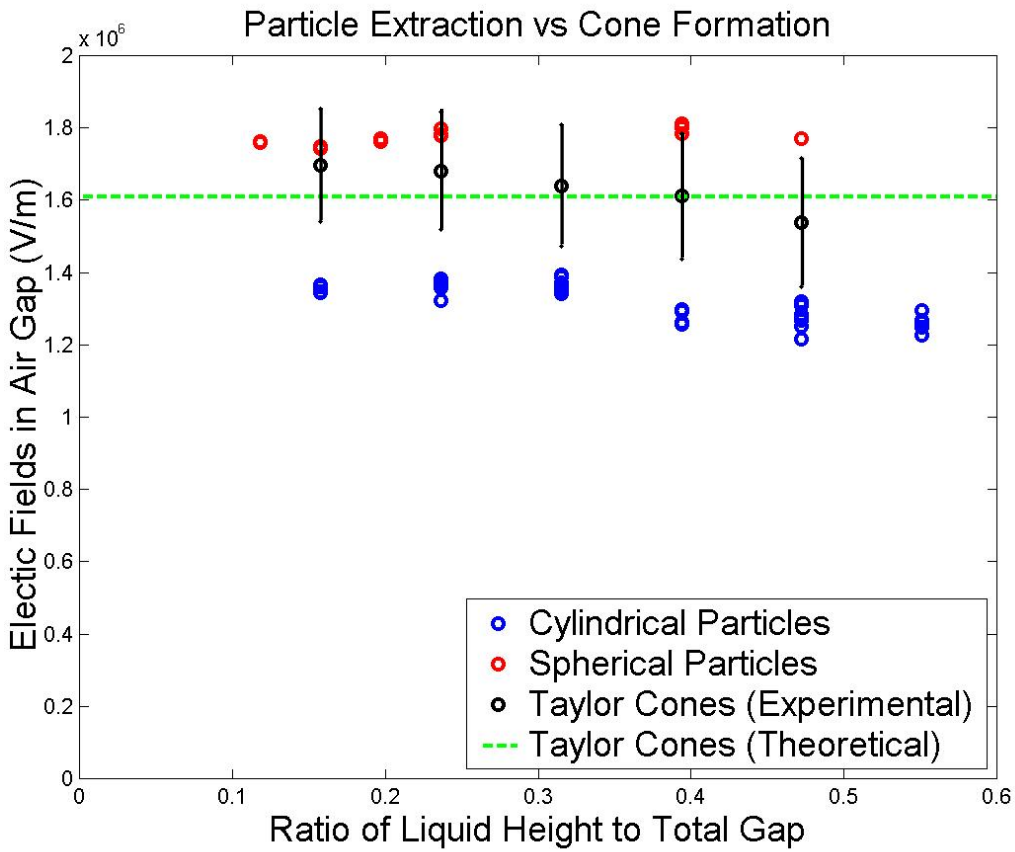

- Spherical Extraction
  - average extraction E-field = 1.78E6 V/m
- Cylindrical Extraction
  - average extraction E-field = 1.32E6 V/m
- Cone Formation
  - average cone formation E-fields = 1.63E6 V/m
- …Experimentally demonstrated a regime where particles can be extracted before cone formation begins!

Feasible Design Space

- Theory shows regimes exist for particle extraction *prior* to Taylor cone formation
- Excellent agreement between Taylor cone formation experiment and theory
- Preliminary model under predicts particle extraction field by 20%
  - Requires better understanding of particle field enhancement at liquid surface
  - Requires better understanding of surface tension effects on particle

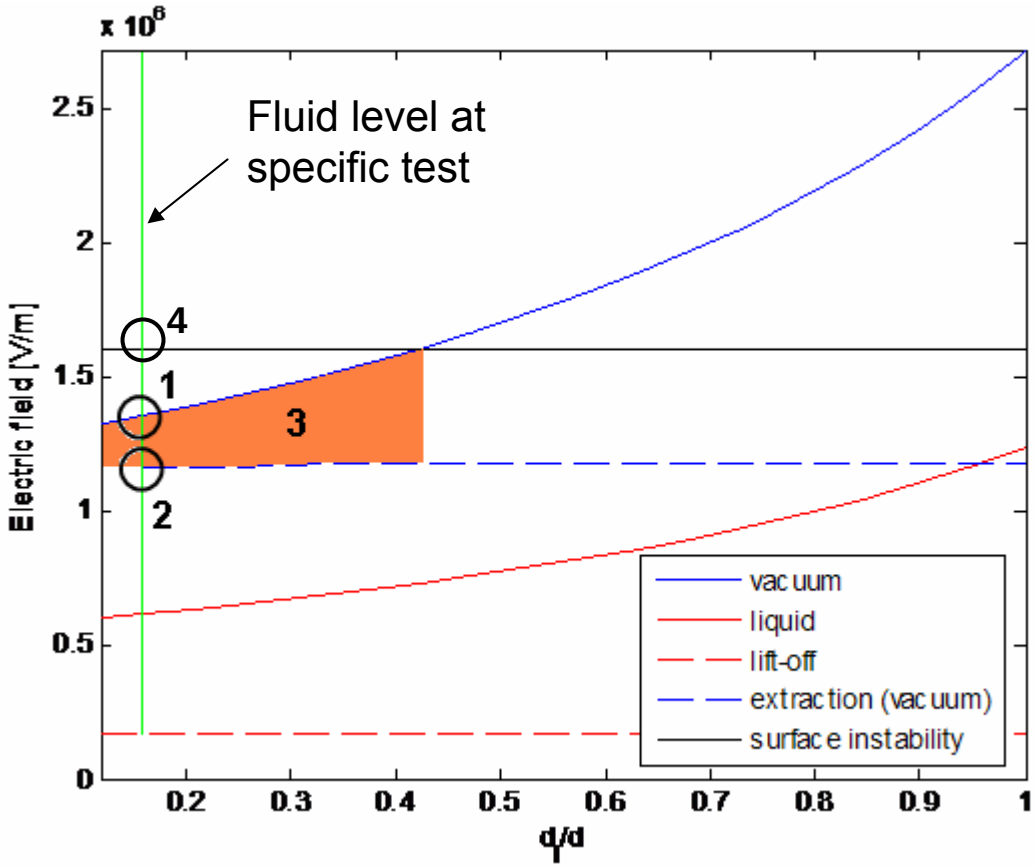

1. Particle extraction (experiment)
2. Particle extraction (theory)
3. Feasible design space (theory)
4. Taylor cone formation (experiment and theory)

Particle Extraction Through Grids

- Demonstrate extraction of conducting particles from insulating liquid by electric fields through a grid structure

Experimental Setup: Partially liquid filled electrode gap with conducting particles and grid

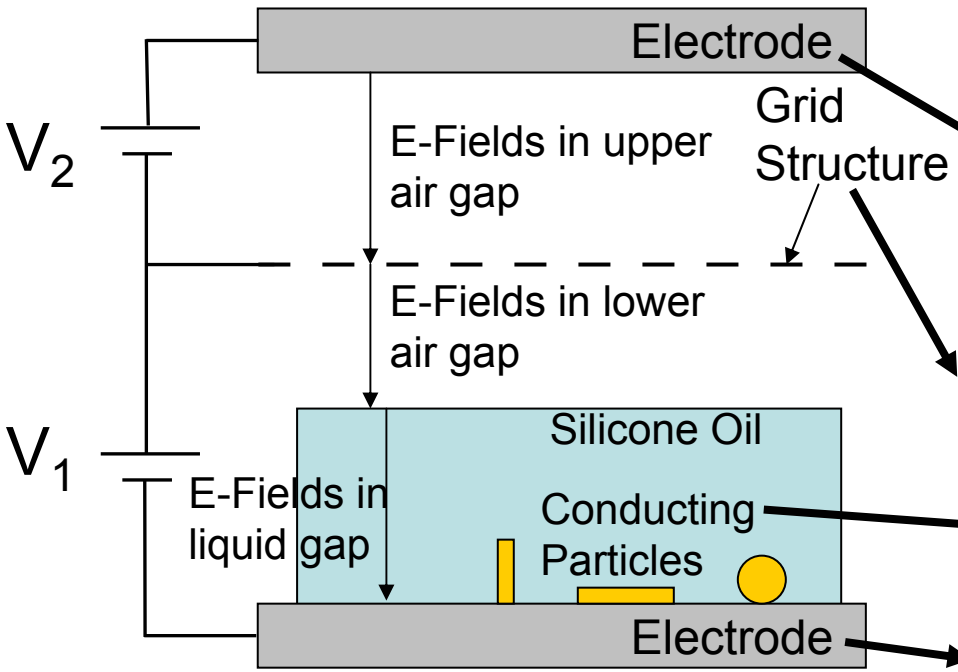

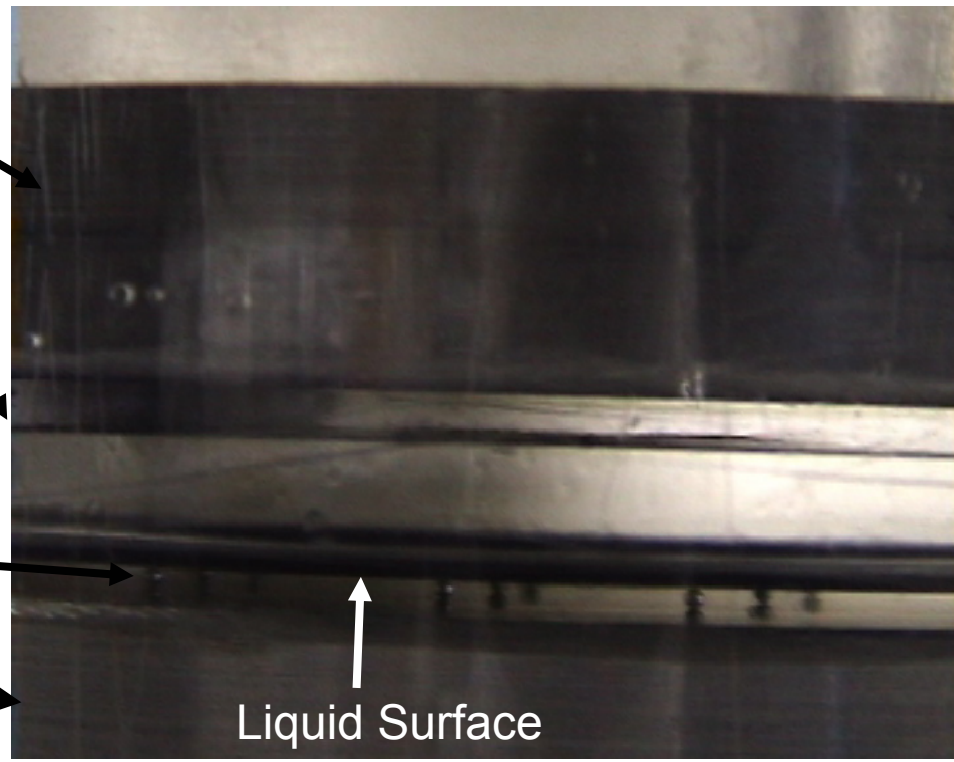

Particle Extraction in Vacuum (I)

- Our new vacuum chamber:
  - Pumps: Diffusion and Roughing
  - Ultimate Pressure ~ 10^{-7} Torr

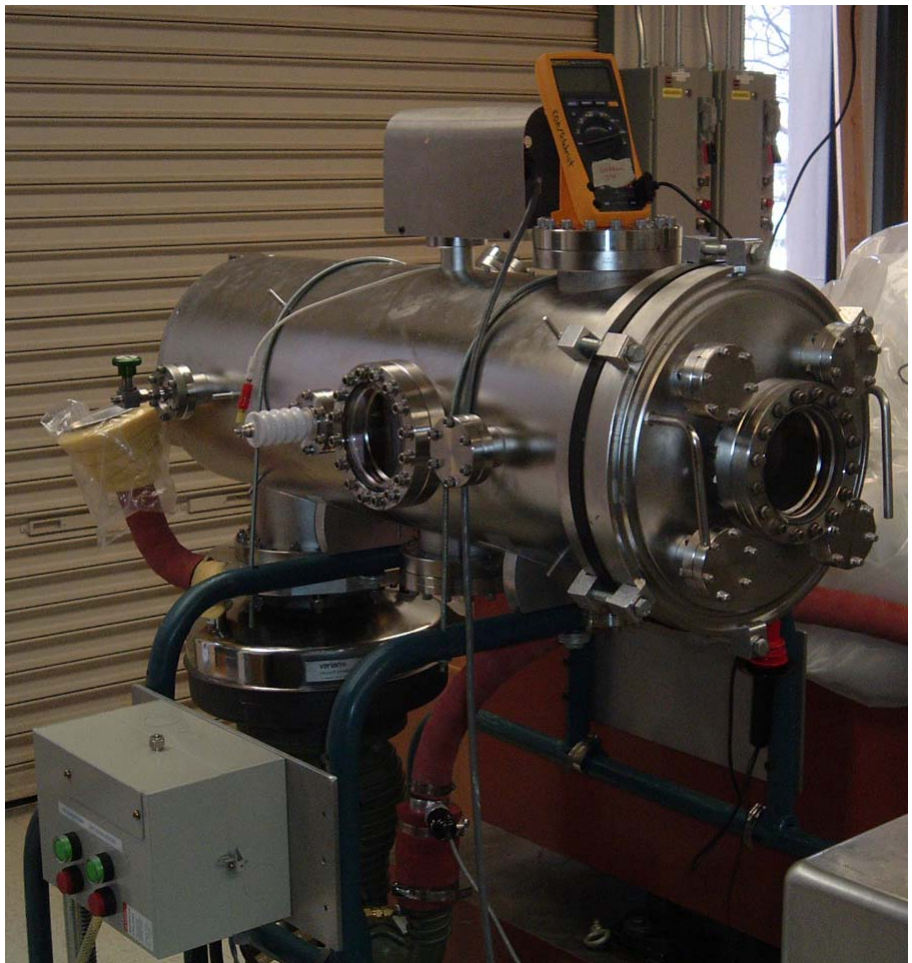

Particle Extraction in Vacuum (II)

- Expect E-fields required for particle extraction to be same when at atmosphere or in vacuum, but somewhat better in vacuum

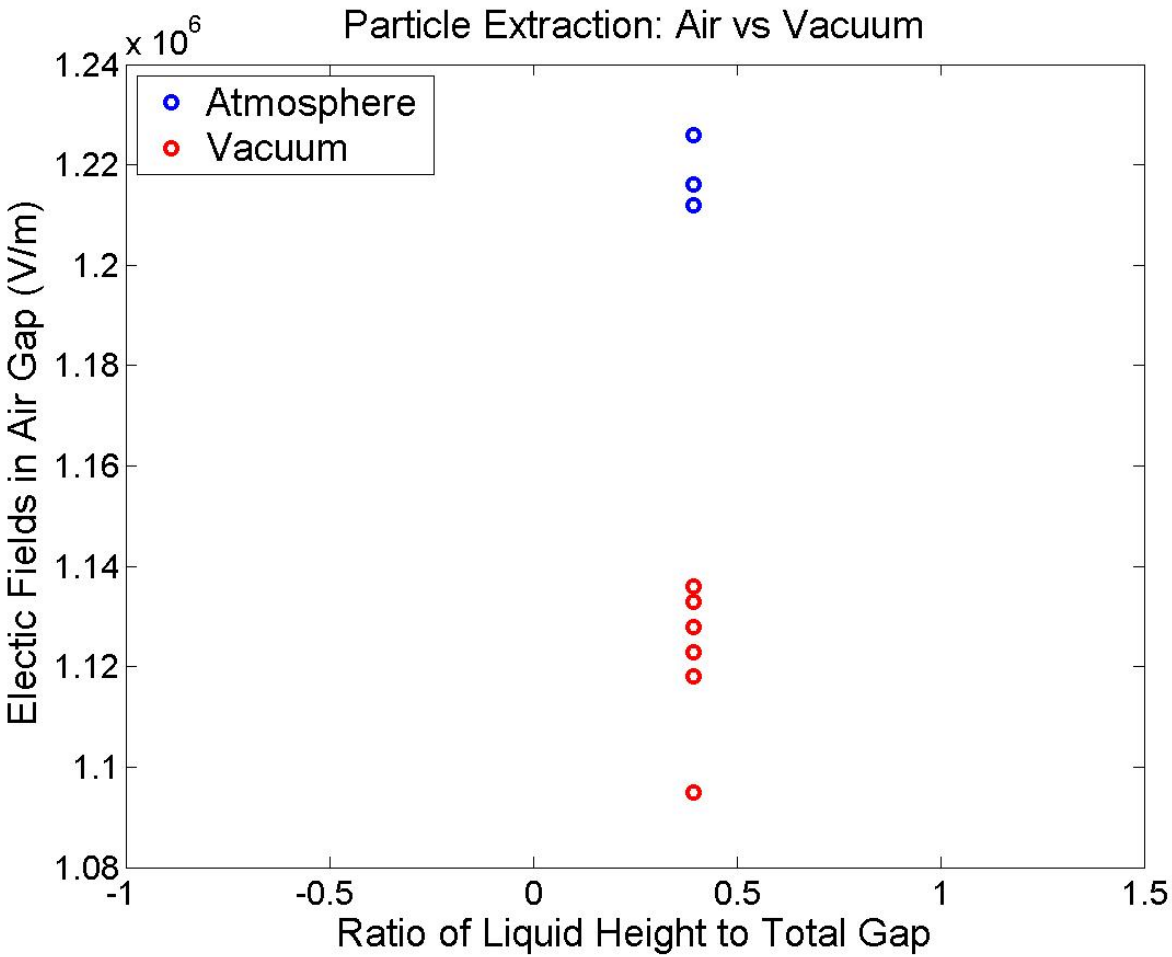

- Setup
  - Al Cylinders
    - d = 300 μm
    - l = 1.5 mm
  - Gap = 12.7 mm
  - Silicone Oil
    - 5.0 mm thick
- At atmosphere
  - P = 760 Torr
  - E_{av} = 1.22E6 V/m
- In Vacuum
  - P = 2.5E-5 Torr
  - E_{av} = 1.12E6 V/m

Looking to the Future

- Quantify vacuum environment performance (understand differences)
- Scale experiments to smaller dimensions
- Research full range of nanoparticle options
- Identify particle transport options
  - Micro-fluidic Bio-MEMS and Chemical analysis technology *synergism*
  - Non-fluid options
- MEMS/NEMS structures
- Refine a more complete integrated system concept
- More quantified assessment of mission scenarios

Nanoparticle EP Concept Appears Feasible

New Paradigm: High Efficiency over tremendous Isp and T/P

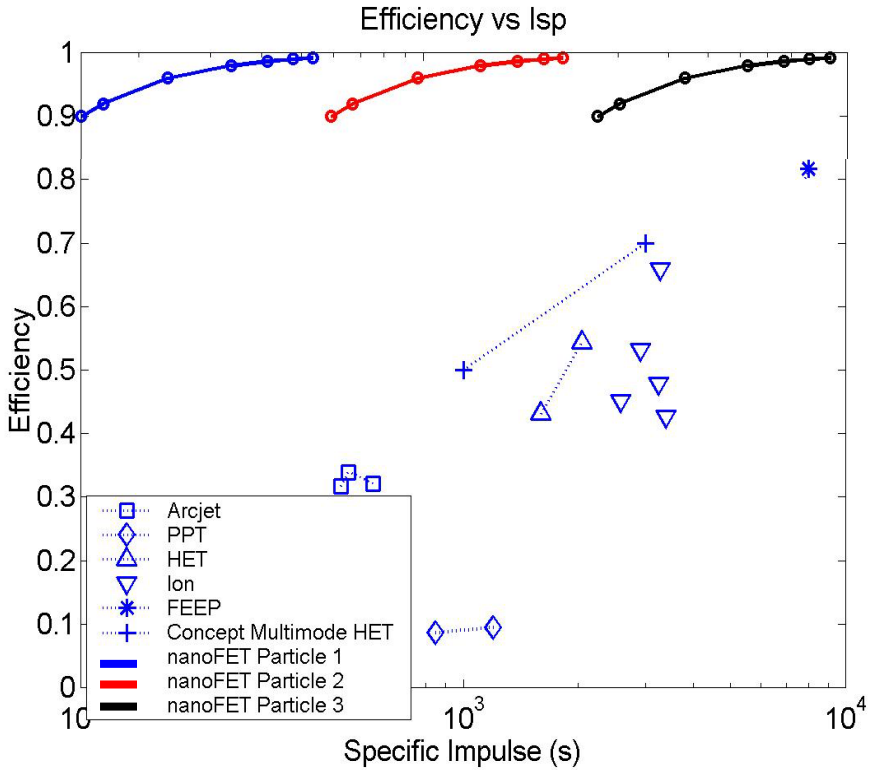

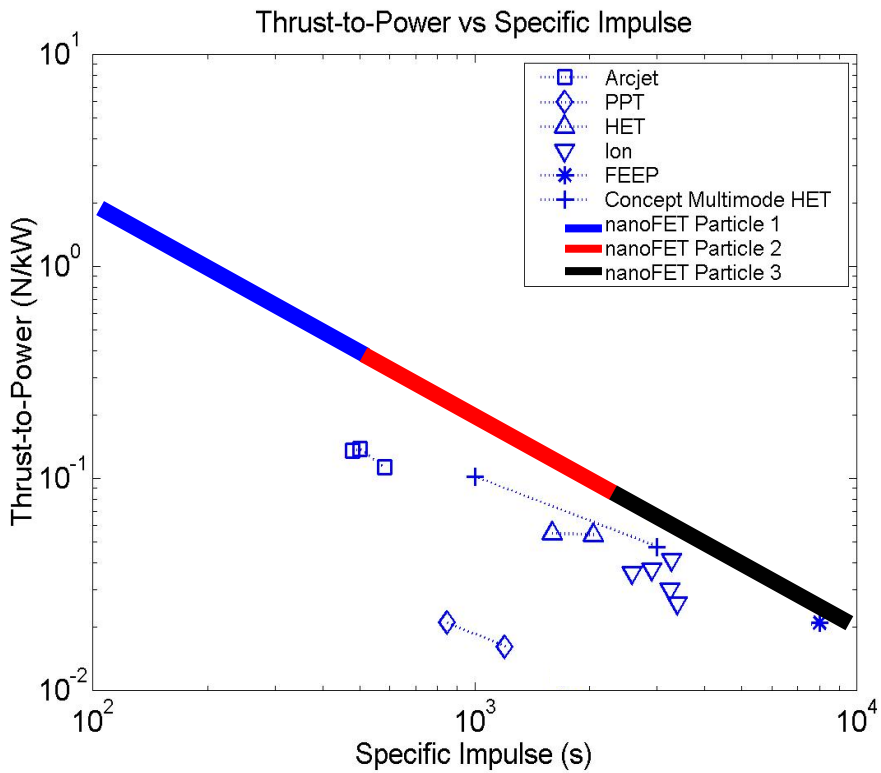

- *Broad set of missions - mission phases with single engine type*
- *Decouples propulsion system and spacecraft design*
- *nanoFET is both mission enhancing and mission enabling*

Appendix B

NIAC Phase I Status Report 1

Scalable Flat-Panel Nano-Particle MEMS/NEMS Propulsion Technology for Space Exploration in the 21st Century – *nanoFET*

Status Report 1 (3rd Month)

University of Michigan

Overview

The following is the 3rd month status report for exploration of the *nanoFET* (nano-particle Field-Emission Thruster) propulsion concept. In Phase I, we are especially focusing on:

a) More fully assessing the significance of the paradigm shift the *nanoFET* concept represents;
b) Addressing fundamental questions that could be viewed by some as "show stoppers" in the application of the *nanoFET* concept to in-space transportation.

To better understand the significance and possibly revolutionary aspects of the *nanoFET* concept for in-space propulsion, we are conducting mission analysis simulations and soliciting additional inputs from a variety of sources. The nano-particle and planar MEMS/NEMS structure enable a wide, variable range of I_{sp} operation, It also appears to dramatically increase mission flexibility and offer additional safety, especially for manned missions.

We are preparing three initial experiments to help us better understand the ideas and concepts behind nano-particle electrostatic propulsion. After completing these initial experiments, it is our hope to better understand the practicality of extracting and accelerating nano-particles through (sub)micron vias most likely from a liquid carrier.. There are several physical parameters of the liquid (conductivity, surface tension, wetting, vapor pressure) that may play an important role.

Mission Analysis

Any new paradigm shift often requires considerable effort to fully understand the implications, both positive and negative, of its impact. The nanoFET concept for in-space propulsion is no different. Our "going-in" assessment was that a propulsion system with very high efficiency, the ability to vary its specific impulse over a very wide range (from about 100 to possibly as high as 10,000 seconds), and ability to scale over large power ranges, would open new opportunities in space flight. We are continuing to assess these both qualitatively and quantitatively. Some specific points are as follows:

- The use of a variable I_{sp} thruster can increase mission flexibility. If a mission requires a certain change in velocity, Δv, a constant I_{sp} thruster can only accomplish this with one thrusting time, Δt, while burning Δm propellant. A variable I_{sp} thruster will be able to accomplish the Δv with many different thrusting times. If it is important to achieve the Δv in a short time period, the thruster can operate at a low I_{sp} and consume a larger amount of propellant. But, if the time to achieve Δv is not important, then the thruster can operate at a high I_{sp} and conserve propellant.
- It can widen the margins for response to emergency and off-nomianl situations. If an emergency occurs during a manned mission, a variable I_{sp} thruster will provide significantly more scenarios to get the spacecraft back safely than a fixed I_{sp} thruster.
- A scalable, variable I_{sp} thruster can potentially decouple the propulsion and

[1] Point of Contact: Prof. Brian Gilchrist, University of Michigan, 1301 Beal Ave, Ann Arbor, MI 48105-2122; Michigan team: A. Gallimore, B. Gilchrist, M. Keidar, T. Liu, L. Musinski, K. Najafi, P. Patel

satellite designs. Spacecraft designers may be able to design their spacecraft without the narrow constraints of available propulsion systems. A qualified thruster technology that can operate over a larger Isp range and which can be scaled over a large power range without concerns for requalification provides such a capability.

We are presently developing basic simulation models to provide a more quantitative assessment of mission examples.

Experiments

We are developing a series of initial experiments to better understand and prove the feasibility of nano-particle propulsion. The objectives of these initial experiments are to 1) determine the behavior of particles in an insulating liquid subjected to an electric field, 2) prove the feasibility of extracting particles from a liquid by way of electric field, and 3) identify appropriate liquid and nano-particle characteristics for in-space operation. To accomplish these objectives, the experiments are divided into three separate stages.

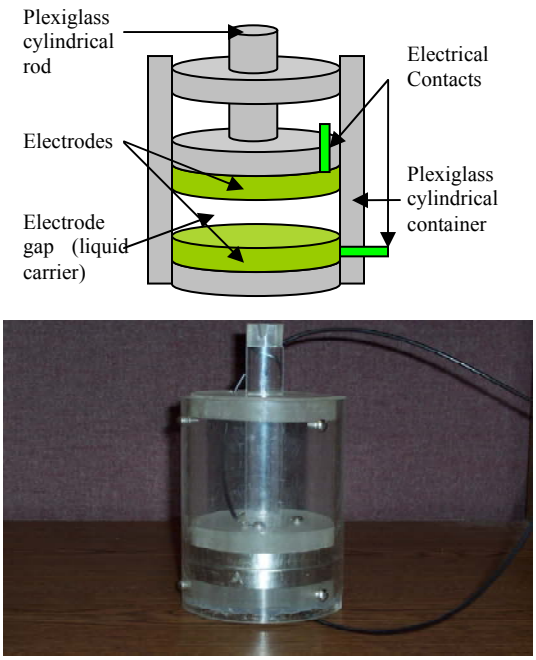

Figure 1: (a) Sketch of particle in liquid test vessel, (b) Picture of experimental apparatus.

The first stage is based on experiments previously performed by others[6,16] and will analyze the behavior of a conducting particle immersed in an insulating liquid subjected to an electric field. Figure 1 depicts the experimental apparatus, where two parallel electrodes are contained in an acrylic cylinder with the electrode gap filled with an insulating liquid, say silicone oil, and a conducting particle on the millimeter scale will be resting on the bottom electrode. Applying a potential difference between the electrodes will create uniform electric fields in the electrode gap and cause the conducting particle to become charged. The resulting charge acquired by the particle is expected to dependant on particle's size, shape, the electric field intensity, and the relative permittivity of the liquid. The expected charge acquired by spherical and cylindrical particles is given as follows[16].

$$q_{sph} = 4\pi r^2 \varepsilon_\ell \frac{\pi^2}{6} E \qquad (1)$$

$$q_{cyl} = \frac{\pi \ell^2 \varepsilon_\ell E}{\ln\left(\frac{2\ell}{r}\right) - 1} \qquad (2)$$

where r is nano sphere and cylinder radius, l is cylinder length, ε_l is the liquid dielectric constant, E is the electric field.

Once charged, the particle will experience an electrostatic force pulling the particle toward the upper electrode. To determine the behavior of the particle, it is important to look at all the forces acting on the particle, which are Coulomb's force

$$F_c = qE \qquad (3)$$

the drag force,

$$F_d = C_d \frac{\pi}{8} d^2 \rho_l v^2 \qquad (4)$$

the gravitational force

$$F_g = mg \qquad (5)$$

and the buoyancy force

$$F_b = m_l g \qquad (6)$$

The equation governing the particle's motion is obtained by applying Newton's force equation.

$$m\frac{d^2z}{dt^2} = F_c - F_d + F_b - F_g \qquad (7)$$

In the above equations, ρ_s is the particle density, ρ_l is the liquid density, v is the particle velocity, C_d is the coefficient of drag, d is the particle diameter, and m_l is the liquid mass with the same volume as the particle.

If a high enough potential is applied, the particle should be lifted from the bottom electrode and transported to the upper electrode. Once reaching the upper electrode, it will experience a charge exchange, acquiring charge of the opposite polarity, and will be transported back to the bottom electrode, where it will experience another charge exchange. The particle should continue to oscillate back and forth between the electrodes while bias is applied. It is important to note that the charge acquired by the particle at the electrodes can be dissipated slowly in the liquid depending on the conductivity of our insulating liquid. The charge will be dissipated as

$$q(t) = q_o e^{-t/\tau} \qquad (8)$$

where τ is the electrical relaxation time constant of the liquid.

We have developed a simulation to determine the particle's trajectory based on the parameters of the system. Figures 2 through 4 are plots of the particle's trajectory, charge, and velocity, respectively, as a particle is transported from the bottom electrode to the upper electrode using an 800 µm aluminum spherical particle, silicone oil, an electrode gap of 0.5 cm, and an applied potential difference of 2 kV.

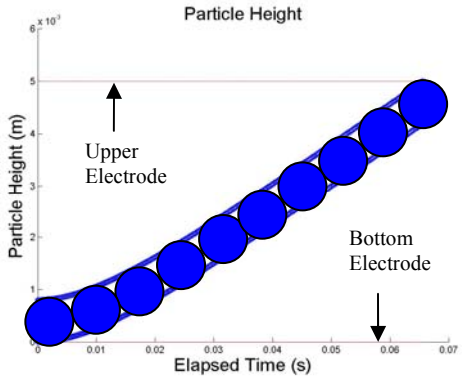

Figure 2: Trajectory of an 800 µm aluminum spherical particle

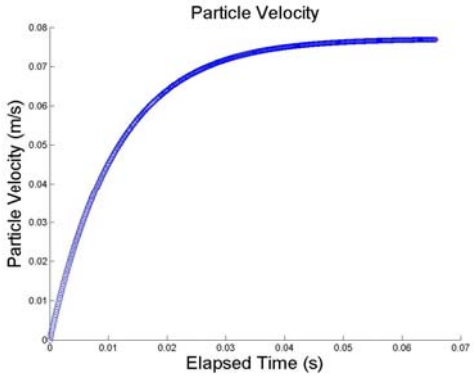

Figure 3: Velocity of an 800 µm aluminum spherical particle

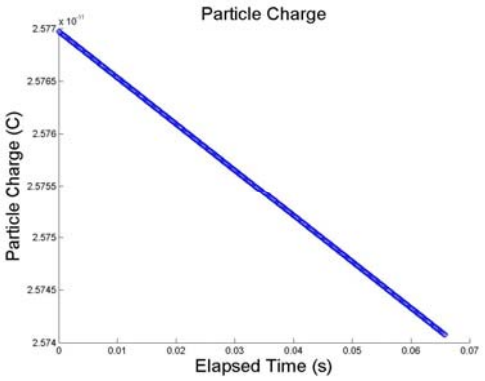

Figure 4: Charge of an 800 µm aluminum spherical particle

We plan to compare the results of this experiment with the simulation to determine the particle's charge and velocity, and the required applied potential to transport the particle.

As of this writing, the experimental apparatus has been just completed. Initial quick tests are showing behavior very close to expectations. Measurements of charge

transfer and observations of particle motions will be obtained.

The second stage of the experimental series will be a modification of the first and will hopefully prove the feasibility of particle extraction for millimeter-sized particles in both air and in vacuum. Figure 5 depicts the experimental setup for this stage. A third electrode with a hole in its center is inserted between the two electrodes from the previous stage. The lower gap is filled with the insulating liquid and the upper gap is in vacuum. Potentials applied to the electrodes will create uniform electric fields in both gaps. A conducting particle resting on the bottom electrode will become charged as described in stage 1. If strong enough electric fields are generated in the lower electrode gap, the particle will be transported through the liquid and to the liquid vacuum interface. If the fields in the upper gap are strong enough, the particle should then be extracted through the liquid surface and accelerated to the top electrode. We have developed a simulation to predict the particles trajectory in the liquid, through the liquid surface, and in the vacuum. Figures 6 through 8 are plots of the particle's trajectory, charge, and velocity, respectively, initially using an 800 µm aluminum spherical particle, silicone oil, a lower electrode gap of 0.5 cm, an upper electrode gap of 0.2 cm, with separate potentials across the lower and upper gaps.

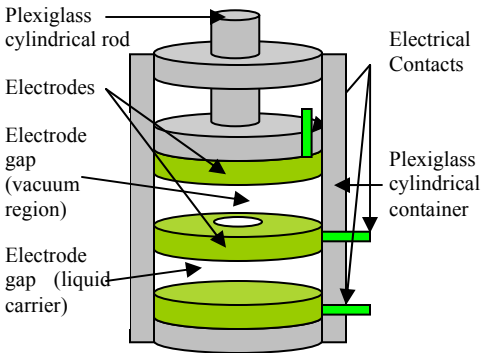

Figure 5: Experimental setup for stage 2.

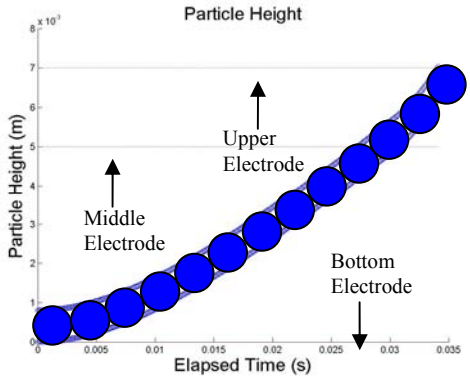

Figure 6: Trajectory of an 800 µm aluminum spherical particle

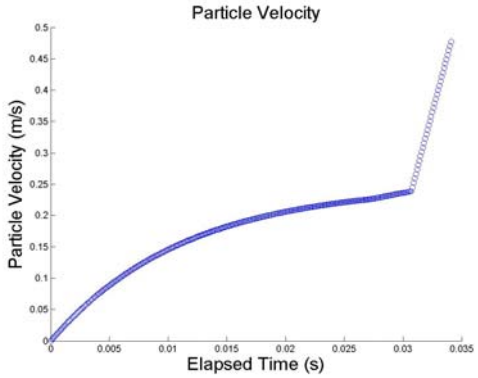

Figure 7: Velocity of an 800 µm aluminum spherical particle

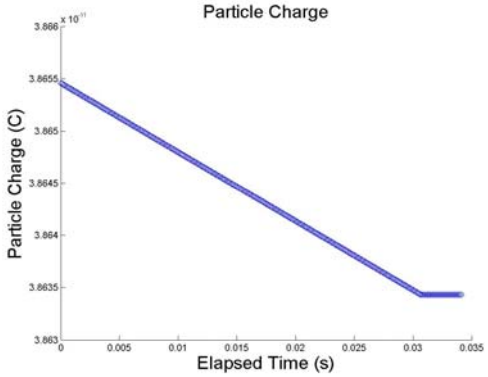

Figure 8: Charge of an 800 µm aluminum spherical particle

For the vacuum experiments we have recently configured the chamber shown in Figure 9. We are using a diffusion pump and expect to get an ultimate pressure down around 10^{-7} Torr.

The final stage will be very similar to the second but will be a scaled down to investigate the feasibility of extracting

Figure 9: Vacuum chamber for particle extraction experiments

micro- and nano-sized particles. We will initially use the Figure 5 test apparatus, but are also hoping to use a MEMS accelerating gate structure being developed for another project. These MEMS gates are conducting grid structures that can be placed over a flat surface to apply an electric field to that surface. The advantage of the MEMS gate over, say, a metal screen is that they allow micron-scale or closer surface proximities, thus enabling the application of strong electric fields at modest voltages. These MEMS gates are currently being developed at the University of Michigan to be integrated with nano-structured surfaces such as cubic boron nitride and carbon nano-tubes to permit "tip-less" electron emission for low-power field emission cathodes (FEC). A reversed bias on the MEMS gate could be used to provide the electric fields (~1E6 V/cm) needed to extract the nano-particles using modest bias voltages (< 300 V).

The MEMS gate consists of a conductive layer placed over a dielectric spacer with channels arrayed throughout the structure to permit passage of nano-particles or electrons. Use of micro-fabrication techniques enables the dielectric spacer to be made very thin, with the latest iteration of the MEMS gate having a dielectric thickness of 2 μm. By placing the conductive layer closer to the emission material; electric fields are concentrated and the bias voltage needed to achieve emission is reduced. Numerical simulations indicates that an approximate 1:1 ratio between the dielectric thickness and the channel diameter produces uniform field lines, so nano-particles used with the current iteration of the MEMS gate must have diameters on the order of hundreds of nanometers or less.

Gate layers are supported in a bulk silicon square with 1-cm sides. Ten viewing windows are etched in the bulk silicon to expose the emission channels, with each viewing window containing about $4*10^4$ emission channels, thus providing 12.6% transparency. The top surface of the MEMS gate is a gold layer to facilitate wire bonds to the gate, and open regions are present that enable the gate to be clamped down upon the emission interface. Note that the current iteration of the MEMS gate is a prototype design that has not undergone optimization. More advanced micro-fabrication techniques would be employed in the future following device characterization and integrated testing. Optimizations include reducing the gap to decrease required extraction voltages and increasing the transparency. A stacked gate design is also under consideration to decouple the extraction and acceleration stages[14]. Figure 10 shows an older version of the MEMS gate design with 12 viewing windows instead of the current ten[15].

Figure 10: First-generation MEMS gate design showing the viewing windows etched into the bulk silicon. Each viewing window contains about $4*10^4$ emission channels. The current MEMS gate is a second-generation design.

After demonstrating the ability to extract particles from a liquid into vacuum

using electric fields, the experiment will be repeated on a small scale with the use of nano-particles and the MEMS gate. Figure 11 shows the intended test setup, with an external power supply biasing the source plate positive and the collection plate negative with respect to the MEMS gate. Nano-particles experiencing charge exchange with the source plate would drift towards the fluid-vacuum interface, where they would be extracted by the electric field set up between the MEMS gate and the source plate. After extraction, the nano-particles would be accelerated up to and collected by the collection plate. Current sensors will measure the operational current from the power supply and the emission current from the collection plate; the difference between these currents would be the gate current. Issues such as gate integration onto the liquid surface and feeding of the nano-particle solution into the test system are currently being addressed in preparation for the test.

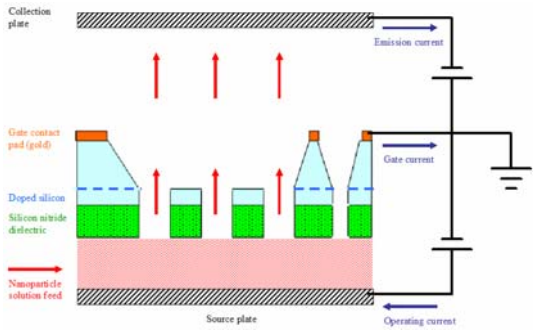

Figure 11: Experimental setup for stage 3

Nano-Particle Transport and Extraction from Liquid Carrier

Ultimately, the details of nano-particle transport in and extraction from a liquid carrier will be very important. For example, for operation in space it will be important that there is a very low vapor pressure at the holes. We also must be able to transport the particles to the surface and then efficiently extract them through the surface tension without significant liquid loss. Initially, we are focusing on a practical detail of whether the liquid should be conducting or insulating. Further theoretical and experimental research will be required to determine which method will work best. Both methods have their own advantages and disadvantages, which will be discussed in this section. A single emitter using an insulating liquid carrier is shown in Figure 12. For this case the particle is charged when it contacts the bottom electrode due to the presence of an electric field. After acquiring charge, it is transported to the liquid/vacuum interface by way of Coulomb's force. This force will continue to extract the particle through the liquid surface, accelerate, and finally eject it.

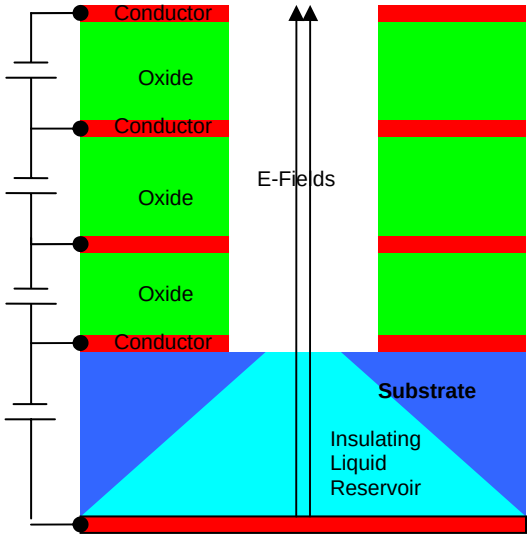

Figure 12: Structure of a single emitter, multi-grid nano-particle thruster using an insulating liquid

The case of a mildly conducting liquid works differently due to the absence of electric fields within the liquid. A single emitter using a mildly conducting liquid is shown in Figure 13. Since there are no significant fields in the liquid, another method must be devised to transport the particles to the liquid surface. Particle transport to the liquid surface could be accomplished by mixing the liquid (by heating, acoustic waves, etc.), which should allow particles to randomly approach the liquid surface. Upon approaching the surface, the (cylindrical) particles will align themselves, as suggested in Figure 14, due to polarization charging. If the electric field can focus on the tip of the particle, there will

Figure 13: Single emitter of nano-particle thruster with conducting liquid.

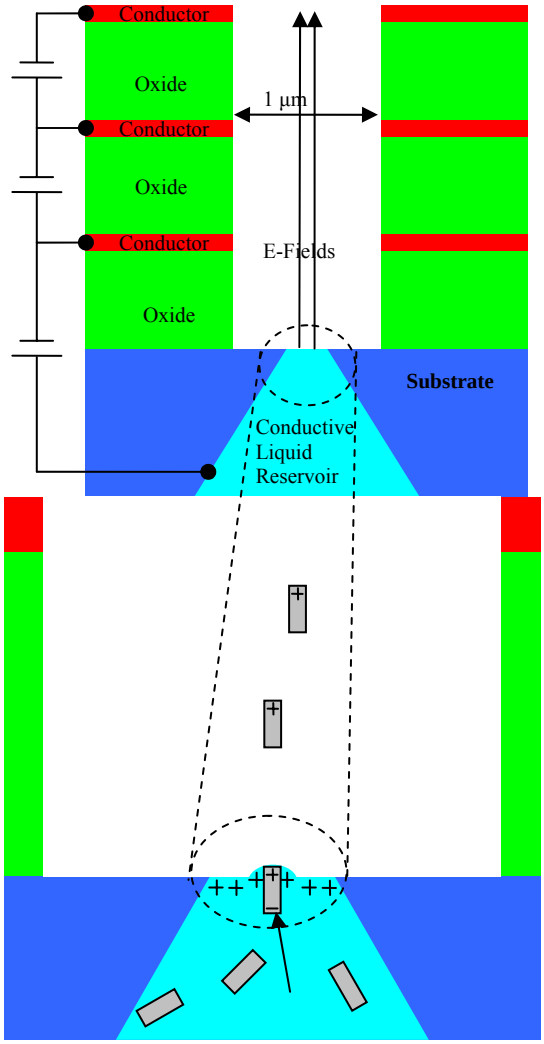

Figure 14: Nano-particles extracted and accelerated.

be preferential charging, and with sufficient charging the particle can be extracted through the surface tension. An estimate of the final charge is given by Equations 1 and 2 replacing ε_l with ε_o. Once charged and extracted, the particle would be accelerated and ejected just as in the insulating liquid case.

Since the behavior of the particles within the liquid is highly dependent on the conductivity of the liquid, there are several advantages and disadvantages of each scenario.

A. Advantages of an Insulating Liquid

- The transport of particles within the liquid to the surface can take advantage of electric fields that can be independently established.
- The movement of new particles into the reservoir may be handled in a similar manner by utilizing localized (pulsed) electric fields as well as other possible methods. This allows particles to be moved within the liquid, rather than moving the liquid itself.
- The formation of Taylor cones or other surface irregularities should be less likely and therefore particle emission should be more uniform though they may not be eliminated without care[19].

B. Advantages of a Conducting Liquid

- The electric fields at the surface of the liquid should be normal to the surface and therefore more in the thrusting direction, which will help to prevent accelerating the particles into the grid structure.

C. Disadvantages of an Insulating Liquid

- The electric fields at the surface of the liquid may have components tangential to the surface, which may accelerate particles into the grid unless the particle is extracted near the center of the hole in the accelerating grids. This is because the particles reach a low terminal velocity within the viscous liquid and may not have the momentum to keep from being accelerated in the horizontal direction and into the grid structure.

D. Disadvantages of a Conducting Liquid

- The surface of the liquid would have charge density, which may induce Taylor cones of some sort.
- The movement of particles would require either moving the liquid along with the particles or some non-electric method (thermal,

ultrasonic) to move just the particles.

Summary

Initial work continues to suggest that our concept is viable and offers a new paradigm shift in terms of the propulsion system. It may offer substantially better overall performance on the one hand while providing system designers greater flexibility.

Publications and Presentations

Presented at the International Electric Propulsion Conference (IEPC) at Princeton, NY on November 3, 2005.

References

1. Behan, Niall, "Nanomedicin and Drug delivery at the University of Limerick," The University of Limerick. http://www.ul.ie/elements/Issue4/behan.htm
2. Calero, J. "The electrohydrostatics of a Conductive Liquid Meniscus," IEEE 1988, p 1547-1551.
3. Chesta, E., Nicolini, D., Robertson, D. and Saccoccia, G., "Experimental Studies Related to Field Emission Thruster Operation: Emission Impact On Solar Cell Performances And Neutralization Electron Backstreming Phenomena," IEPC-2003-102, Proceedings of the International Electric Propulsion Conference, Toulouse, France, March 17-20, 20033 Choi, Changrag. "Dynamic Motion of a Conductive Particle in Viscouse Fluid Under DC Electric Field," IEEE Transactions on industry Applications, vol 37, No 3, May/June 2001.
4. Gallimore, A. "Micro Electric Propulsion Proposal," The University of Michigan, November 2003.
5. J.R. Brophy, J.E. Polk, V.K. Rawlin, Ion engine service life validation by analysis and testing, AIAA Paper 96-2715, JUly 1996.
6. Khayari, A. "The Charge Acquired by a Spherical Ball Bouncing on an Electrode: Comparison Between Theory and Experiment;" 2000 Conference on Electrical Insulatoin and Dielectric Phenomena.
7. Marcuccio, S. "Attitude and Orbit Control of Small Satellites and Constellations with FEEP Thrusters," Electric Rocket Propulsion Society, 1997.
8. Marcuccio, S. "FEEP Microthruster Technology Status and Potential Applications," International Astronautical Federation, 1997.
9. Marcuccio, S. "FEEP Thrusters," Nov. 1998, http://www.centrospazio.cpr.it/Centrospazio6FEEP.html.
10. M. Fehringer, F. Ruedenauer, W. Steiger, ESTEC Contract 12376/97/NL/PA Tech. Note No. 2, 1997.
11. Najafi, Khalil. Personal Communications, Univeristy of Michigan, 2004.
12. Stark, John. "Micro-Fabrication and Operation Nano Emitters Suitable for a Colloid Thruster Array," University of London, UK, https://escies.org/public/mnt4/S9.1Stark.pdf
13. Chock, R. "Photovoltaic & Space Environment Branch," NASA Glenn Research Center, July 2002, http://powerweb.grc.nasa.gov/pvsee/publications/tropix/Paper/AppA.html
14. Morris, D.P., Gilchrist, B.E., Gallimore, A.D., "Application of Dual Grids to Cold Cathode/ Field Effect Electron Emission, AIAA-2005-3669, 41st Joint Propulsion Conference, Tucson, AZ, July 10-13, 2005.
15. Goldberg, H., Encarnación, P., A., Morris, D., Gilchrist, B., Clarke, R., "Cold-Cathode Electron Field Emission of Boron Nitride Thin Film with a MEMS-Based Gate for Space Applications, AIAA-2004-3499, 40th Joint Propulsion Conference, Ft. Lauderdale, FL, July 11-14, 2004.
16. Tobazeon, R. "Behavior of Spherical and Cylindrical Particles in an Insulating Liquid Subjected to a DC Uniform Field." Laboratoire d'Electrostatique et de Materiaux Dielectriques. BP 166-38042 Grenoble Cedex 9 (France) pp. 415-420.
17. Felici, N. Rev. Gen. Elect., 75, pp. 1145-1160, 1966.
18. Wertz, Larson, "Space Mission Analysis and Design 3rd Ed." 1999
19. Jayasinghe, S., Edirisinghe, M. "Electrically Forced Jets and Microthreads of High Viscosity Dielectric Liquids." Journal of Aersol Science 35, (2004) 233-243.

Appendix C

NIAC Phase I Status Report 2

Scalable Flat-Panel Nano-Particle MEMS/NEMS Propulsion Technology for Space Exploration in the 21st Century – *nanoFET*

Status Report 2 (5th Month)

University of Michigan

Overview

The following is the 5th month status report for the exploration of the *nanoFET* (nano-particle Field-Emission Thruster) propulsion concept. As stated in the 3rd month status report, we are focusing on:

a) More fully assessing the significance of the paradigm shift the *nanoFET* concept represents;
b) Addressing fundamental questions that could be viewed by some as "show stoppers" in the application of the *nanoFET* concept to in-space propulsion.

As part of assessing the significance of the nanoFET paradigm shift, we have further analyzed the possible specific impulse (I_{sp}) range using the nano-particle mode exclusively (as opposed to an ion mode) and have determined that it may be possible to extend the operating range from 100 s up to (a much higher) 10,000 s. This will greatly increase mission flexibility over earlier predictions and broaden the mission categories that are feasible using nanoFET.

We have begun the experimental process and have completed important parts of the first two experiments described in our first status report. First, we were able to demonstrate the transportation of a conducting particle through an insulating liquid by way of electric field. Second, *we have achieved particle extraction from a liquid, which is a significant step towards proving the fundamental feasibility of nano-particle propulsion concept.*

To prepare for future experiments, we have been modifying an existing vacuum chamber. These modifications are almost complete, and we anticipate the first pump down very shortly.

The nanoFET Impact - Mission Analysis

The nanoFET concept derives its benefits from the (1) the ability of operating at very high efficiencies, (2) near continuous variation of specific impulse over an appropriately large range (100 s to 10,000 s), (3) scalability over a large power/thrust range, and (4) the minimization life-limiting factors. If these benefits can be realized, important new benefits for in-space flight may be possible.

Since the previous status report, we have extended and re-examined some of our key assumptions and analysis with the following new results:

- Previously, we suggested that to cover the full 100 s to 10,000 s Isp range, nanoFET would operate in nano-particle mode for 100 to 3,000 s Isp and would operate in an ion mode for the 3000 s to 10,000 s range. *After further analysis, we believe that it may be possible to cover the entire 100 s to 10,000 s range using just nano-particles, eliminating the need for an ion mode.* For the previous assessment, we calculated the expected I_{sp} range using small aluminum cylindrical particles. Recently, we redid these calculations with very high aspect ratio carbon nano-tubes (CNT). Using just three different sizes of CNTs, we can cover the entire 100 s to 10,000 s range. Table 1 illustrates possible I_{sp} ranges obtained with CNTs compared to aluminum particles.

[1] Point of Contact: Prof. Brian Gilchrist, University of Michigan, 1301 Beal Ave, Ann Arbor, MI 48105-2122; Michigan team: A. Gallimore, B. Gilchrist, M. Keidar, T. Liu, L. Musinski, K. Najafi, P. Patel

Particle Comp	Particle Size (length x diameter) nm	Voltage Range (V)	I_{sp} Range (s)
Aluminum	100 x 10	400 – 8500	110 – 510
Aluminum	500 x 2.5	250 – 8500	535 – 3100
CNT	1,000 x 2	160 – 7500	100 – 690
CNT	20,000 x 1	150 – 7500	690 – 4900
CNT	100,000 x 1	1750 – 7100	4900 – 10,000

- The use of near continuously variable I_{sp} thrust increases mission flexibility. For example, a nanoFET thruster will be able to accomplish an orbit transfer with different thrusting times depending on the I_{sp} level, while a constant I_{sp} thruster can only perform the same transfer with a single thrusting time. If it is important to achieve the transfer in a short time, nanoFET can operate at a low I_{sp} (and consume a large amount of propellant). On the other hand, if the thrusting time is not important, then nanoFET can operate at a high I_{sp} and conserve propellant.
- A highly variable I_{sp} system will provide many more options to rescue an emergency situation than a constant I_{sp} system. This added security will be important in many cases, especially manned missions.
- A scalable, variable I_{sp} thruster can potentially decouple the propulsion and satellite designs. Spacecraft engineers would design their spacecrafts without the narrow constraints of available propulsion systems. A spacecraft engineer could use a nanoFET thruster at the power and I_{sp} level optimal for their mission.
- nanoFET could potentially cover almost any NASA, DOD, or commercial mission due to its highly scalable nature.

Experimental Progress

Over the past several months we have been working to experimentally demonstrate the movement and extraction of small conducting particles from an insulating liquid using an electric field. We will first discuss the transport of particles only and then discuss how we have extracted them.

The main goal of this first experiment was to show how a conducting particle submersed in an insulating liquid can be transported from a bottom electrode to an upper electrode by way of an adequately strong electric field. This experiment is similar to the work of Tobazeon[16] and Khayari[6]. Figure 1 is a sketch showing our experimental setup. In this report, we will discuss how a particle is transported through the liquid only at a basic level, but the details can be found in our previous status report. An electric field is created between the electrodes by applying a potential difference between them. A conducting particle resting on the bottom electrode in the presence of this electric field will become charged as described by Felici. Once charged, the particle will experience an electric force pulling it towards the top electrode. If the net force on the particle is directed upwards, the particle will be put into motion and will be transported. It is important to note that the other forces acting on the particle in our experiment are the 1) gravitational force, 2) buoyancy force, and 3) drag force. Once reaching the top electrode, the particle will undergo a charge exchange, acquiring charge of the opposite polarity, and it will be drawn back to the bottom electrode.

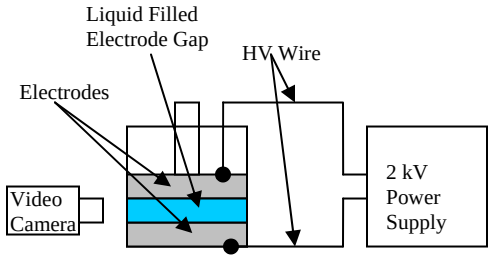

Figure 1: The experimental setup.

It is also important to note that while the particle is being transported from one electrode to another, charge will be lost

to the liquid because the liquid's conductivity is not perfectly zero.

From Figure 1, the experimental apparatus is contained by a hollow acrylic cylinder. Inside the cylinder, the electrodes are made of stainless steel, and the electrode gap is created with nylon spacers. The liquid we chose to use is a silicone oil that has a density of 965 kg/m^3, a viscosity of 100 cSt, and a conductivity of 3.33E-13 S/m. We have used an assortment of millimeter-sized cylindrical and spherical aluminum particles.

The particles oscillated between the electrodes as expected, and the experimental results matched fairly well with the simulation that was discussed in the previous status report. We measured the lift-off voltage and oscillation voltage for different particle sizes, shapes, and electrode gaps. The lift-off voltage is defined as the minimum voltage required to lift the particle off of the bottom electrode, and the oscillation voltage is defined as the minimum voltage required to keep a particle in oscillation between the two electrodes.

In addition to measuring the lift-off and oscillation voltages, it is interesting to discuss other behaviors of the particles. Most of our experiments were performed with cylindrical particles with diameters of 300 µm and lengths ranging from 1 mm to 2.5 mm originally placed horizontally on the bottom electrode. As the voltage between the electrodes was increased, the particles were pulled into a vertical position where they began to oscillate. The speed of the oscillation was easily controlled by varying the applied voltage. Figure 2 is a picture of a cylindrical aluminum particle in mid oscillation.

The goal of the second experiment was to demonstrate particle extraction from a liquid using an electric field. We believe that proving the feasibility of particle extraction is a major step in showing that nano-particle propulsion is, in fact, feasible.

The particle extraction experiment was performed using the same apparatus and experimental setup as the particle oscillation experiment, with a few modifications. The

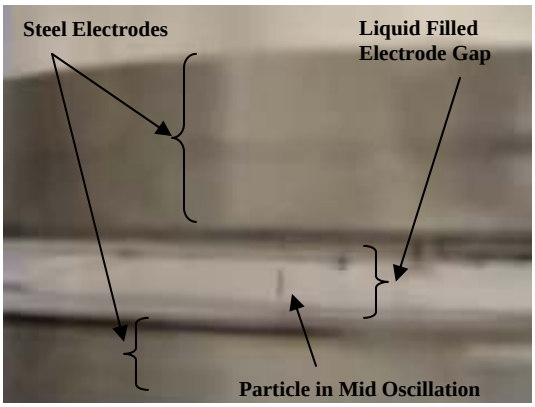

Figure 2: A cylindrical particle in oscillation. The particle is aluminum with dimensions: d = 300 µm, l = 2 mm. Electrode gap is 4 mm.

electrode gap was only filled half-way with the silicone oil, and a larger high voltage power supply was used. Figure 3 show the experimental setup for the particle extraction experiment.

Cylindrical aluminum particles, with a diameter of 300 µm and a length of 2 mm, are initially placed horizontally on the bottom electrode, and the liquid fills the gap

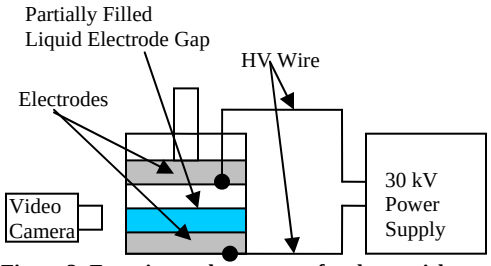

Figure 3: Experimental apparatus for the particle extraction experiment.

about half-way. The total electrode gap is 6.35 mm. It was expected that when the potential between the electrodes was large enough, the particle would be pulled into a vertical position, lifted through the liquid to the surface, and finally be lifted out of the liquid. *For the setup described above, we witnessed particle extraction at a potential just less than 8 kV (for these somewhat large particles).*

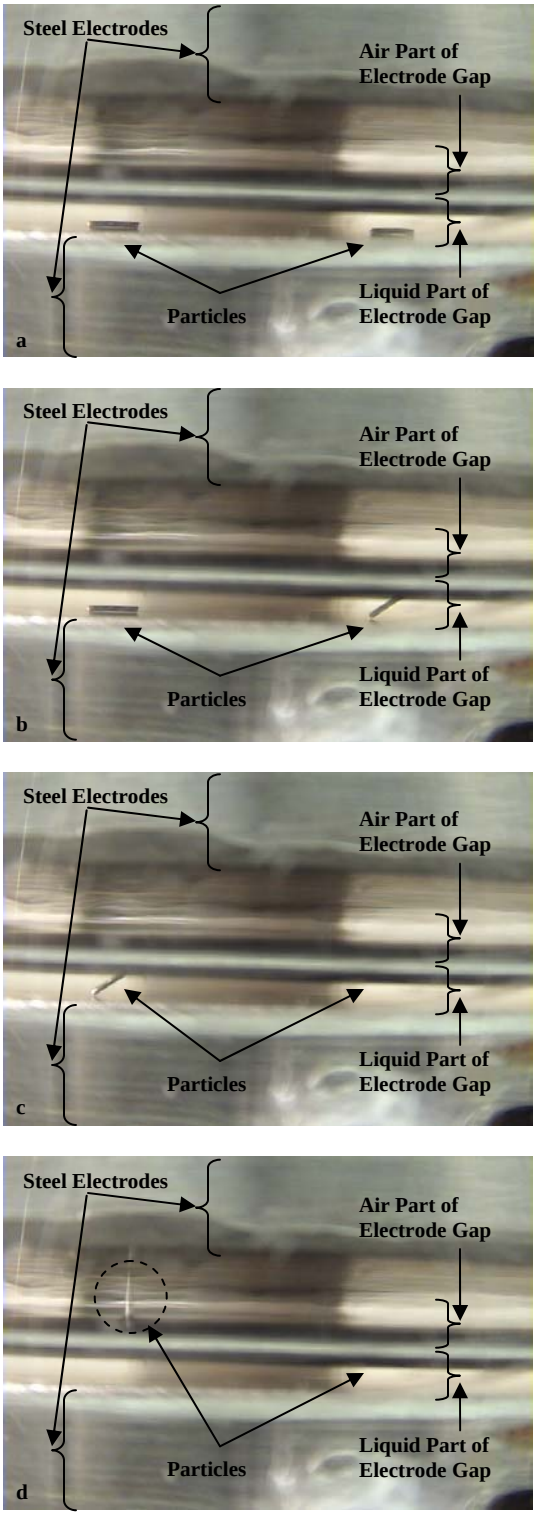

Figure 4: A series of pictures showing particle extraction. a) Two particles resting on bottom electrode. b) Right particle is lifted to the surface. c) Left particle is lifted. d) Left particle is extracted

Figure 4 contains a series of pictures of particles being extracted from the liquid. Picture (a) shows two particles resting on the bottom electrode in a horizontal position before the potential was turn up. After the potential was turned up to about 7.5 kV, the particle on the right was lifted to the liquid surface (b) and caught there because the electric force acting on it was not strong enough to pull it through the surface tension. As the potential was increased to 8 kV, the particle on the left was lifted (c) and pulled through the liquid surface (d), *achieving particle extraction*.

During the particle extraction experiment, we found that at high enough potentials, the liquid formed Taylor cones in a few areas. The formation of these cones does not appear to affect particle extraction, but it is not ideal for nano-particle propulsion. We already have some ideas for minimizing or eliminating the formation of the Taylor cones, and this will be pursed in the next experiments.

What's Next?

Currently we are working to better understand the process of Taylor cone formation so that it can be avoided. The formation of these cones is the result of balancing the electrical force on charge at the liquid surface with the surface tension force. It is easier to understand the formation of Taylor cones on a conducting liquid, so we will discuss this case and then attempt to explain how these cones form on an insulating liquid.

Figure 5a shows a conducting liquid in the presence of an intense electric field before the Taylor cones have been formed. Positive charges migrate to the surface of the liquid as shown. The resulting force on these charges attempts to pull them out of the liquid, and the surface tension force pulls back, trying to hold the charges in the liquid. As a result of balancing these forces, cones begin to protrude from the liquid surface as show in figure 5b.

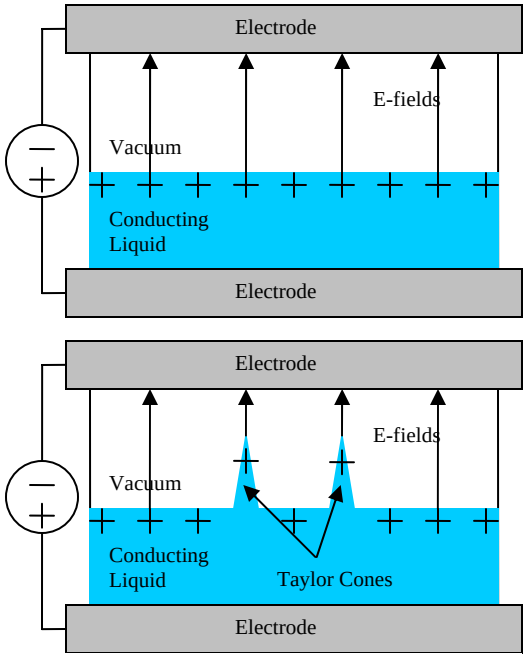

Figure 5: a) An electric field applied to a conducting liquid before Taylor cone formation. b) Taylor cones form from a conducting liquid in the presence of an electric field.

We believe that Taylor Cones are forming from our insulating liquid for the same reason. The silicone oil that we are using is a very good insulator, but it does have a finite conductivity, which will allow some charge to move slowing to the surface and eventually for these cones to form. As we study these cones, we plan to find a method to eliminate their formation.

In addition to studying the formation of Taylor cones, we plan to continue experimenting with particle transport and particle extraction. In fact, we plan to take our experiments down to the nano-scale as described in the previous status report. The gate structure that we will be using is currently being fabricated at the Solid State Electronics Laboratory here at the University of Michigan for another project.

Vacuum Chamber

We have recently completed the assembly of our nanoFET chamber. Figure 6 is a picture of the vacuum chamber. It uses a diffusion pump along with a roughing pump to pump down the cylindrical chamber to an expected 10^{-6} Torr. We expect the pump down time to be less than one hour due to the size of the large diffusion pump and the relative small size of the chamber.

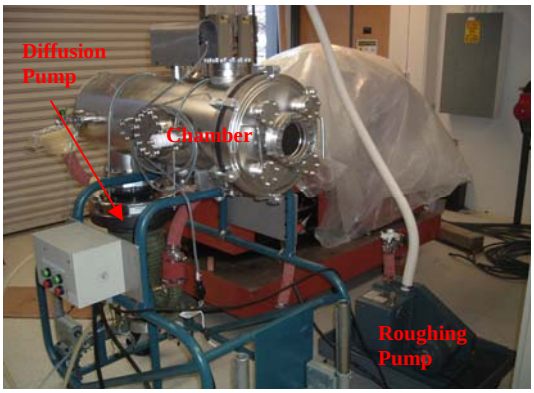

Figure 6: Vacuum Chamber

References

1. Behan, Niall, "Nanomedicin and Drug delivery at the University of Limerick," The University of Limerick. http://www.ul.ie/elements/Issue4/behan.htm
2. Calero, J. "The electrohydrostatics of a Conductive Liquid Meniscus," IEEE 1988, p 1547-1551.
3. Chesta, E., Nicolini, D., Robertson, D. and Saccoccia, G., "Experimental Studies Related to Field Emission Thruster Operation: Emission Impact On Solar Cell Performances And Neutralization Electron Backstreming Phenomena," IEPC-2003-102, Proceedings of the International Electric Propulsion Conference, Toulouse, France, March 17-20, 20033
Choi, Changrag. "Dynamic Motion of a Conductive Particle in Viscouse Fluid Under DC Electric Field," IEEE Transactions on industry Applications, vol 37, No 3, May/June 2001.
4. Gallimore, A. "Micro Electric Propulsion Proposal," The University of Michigan, November 2003.
5. J.R. Brophy, J.E. Polk, V.K. Rawlin, Ion engine service life validation by

analysis and testing, AIAA Paper 96-2715, JUly 1996.
6. Khayari, A. “The Charge Acquired by a Spherical Ball Bouncing on an Electrode: Comparison Between Theory and Experiment;” 2000 Conference on Electrical Insulatoin and Dielectric Phenomena.
7. Marcuccio, S. “Attitude and Orbit Control of Small Satellites and Constellations with FEEP Thrusters,” Electric Rocket Propulsion Society, 1997.
8. Marcuccio, S. “FEEP Microthruster Technology Status and Potential Applications,” International Astronautical Federation, 1997.
9. Marcuccio, S. “FEEP Thrusters,” Nov. 1998, http://www.centrospazio.cpr.it/Centrospazio6FEEP.html.
10. M. Fehringer, F. Ruedenauer, W. Steiger, ESTEC Contract 12376/97/NL/PA Tech. Note No. 2, 1997.
11. Najafi, Khalil. Personal Communications, Univeristy of Michigan, 2004.
12. Stark, John. “Micro-Fabrication and Operation Nano Emitters Suitable for a Colloid Thruster Array,” University of London, UK, https://escies.org/public/mnt4/S9.1Stark.pdf
13. Chock, R. “Photovoltaic & Space Environment Branch,” NASA Glenn Research Center, July 2002, http://powerweb.grc.nasa.gov/pvsee/publications/tropix/Paper/AppA.html
14. Morris, D.P., Gilchrist, B.E., Gallimore, A.D., “Application of Dual Grids to Cold Cathode/ Field Effect Electron Emission, AIAA-2005-3669, 41st Joint Propulsion Conference, Tucson, AZ, July 10-13, 2005.
15. Goldberg, H., Encarnación, P., A., Morris, D., Gilchrist, B., Clarke, R., “Cold-Cathode Electron Field Emission of Boron Nitride Thin Film with a MEMS-Based Gate for Space Applications, AIAA-2004-3499, 40th Joint Propulsion Conference, Ft. Lauderdale, FL, July 11-14, 2004.
16. Tobazeon, R. “Behavior of Spherical and Cylindrical Particles in an Insulating Liquid Subjected to a DC Uniform Field.” Laboratoire d’Electrostatique et de Materiaux Dielectriques. BP 166-38042 Grenoble Cedex 9 (France) pp. 415-420.
17. Felici, N. Rev. Gen. Elect., 75, pp. 1145-1160, 1966.
18. Wertz, Larson, “Space Mission Analysis and Design 3rd Ed.” 1999

Appendix D

IEPC 2005 Paper

Scalable Flat-Panel Nano-Particle MEMS/NEMS Thruster

IEPC-2005-176
Presented at the 29th International Electric Propulsion Conference, Princeton University
October 31 – November 4, 2005

L. Musinski*, T. Liu†, B. Gilchrist‡, A. Gallimore§, M. Keidar**
University of Michigan, Ann Arbor, MI 48109, USA

Abstract

A new electrostatic thruster technology appears feasible using nano-particles with micro- and nano-electromechanical systems (NEMS/MEMS) fabrication technology. MEMS technologies are already being explored as a possible approach to achieve scalability and system simplification by creating higher efficiency "flat panel" thrusters. They also appear to offer a way to eliminate life-limiting physical characteristics present in state-of-the-art ion propulsion by eliminating the need for a discharge chamber and reducing or eliminating charge-exchange (CEX) collision effects in the ion optics region of the thruster. Further, by considering the use of nano-particles as a propellant with *electric field-emission* based MEMS/NEMS thruster concepts, important new performance improvements appear possible. These include (1) operations at high power levels at much lower system-level specific mass, (2) even higher efficiency, (3) a further increase in thrust densities over present-day ion propulsion technologies, and (4) the ability to tune desired thrust characteristics by simply changing nano-particle size and shape. At the University of Michigan, the nano-particle electrostatic propulsion concept is called nanoFET (nano-Field Emission Thruster) and can be thought of as a flat-panel ion thruster that can be designed for variable power and particle sizes.

Nomenclature

A	=	Thruster area	P	=	Power
C_d	=	Coefficient of drag	q	=	Charge
d	=	Diameter of particle	r	=	Particle radius
E_l	=	Applied electric field in liquid	ρ	=	Mass density of particle
ε_l	=	Liquid dielectric constant	ρ_l	=	Mass density of liquid
ε_o	=	Free space dielectric const	n	=	# density of particles
F_c	=	Coulomb force	T	=	Thrust
F_d	=	Drag force	τ	=	Relaxation time constant
g	=	Earth's gravitational constant	v	=	Particle velocity
γ	=	Surface tension	V_o	=	Voltage
I_{sp}	=	Specific impulse			
l	=	Particle length			
m	=	Particle mass			

* Graduate Student, Electrical Engineering, louisdm@umich.edu
† Graduate Student, Aerospace Engineering, liutm@umich.edu
‡ Professor, Electrical Engineering and Space Science, gilchrst@umich.edu
§ Professor, Aerospace Engineering, rasta@umich.edu
** Professor, Aerospace Engineering, keidar@umich.edu

I. Concept Overview

Figure 1 is a simplified systems sketch of the flat-panel MEMS/NEMS based thruster concept that uses both nano-particles and ions as propellant. Figure 2 shows a present-day ion thruster block-diagram for comparison. The ion thruster must create plasma using a gas (e.g. Xe) in a chamber and allow the ions to escape across an accelerating grid structure. There are several practical limitations: (1) the ionization process represents an important life-limiting factor, (2) an important fraction of the propellant is never ionized, and (3) the plasma interacts with the walls and the grid, thus generating waste heat and limiting lifetime[5].

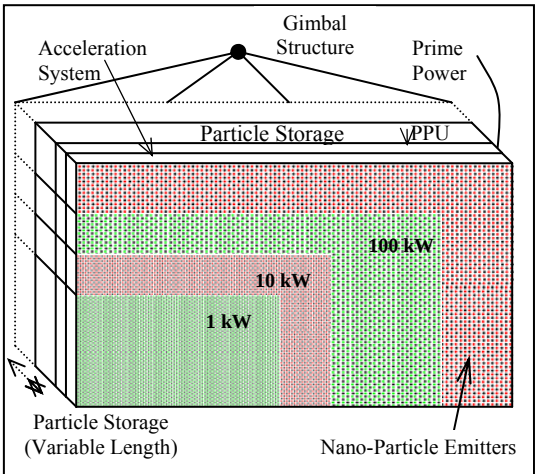

Figure 1: Concept sketch of a flat-panel nano-particle and ion MEMS/NEMS thruster.

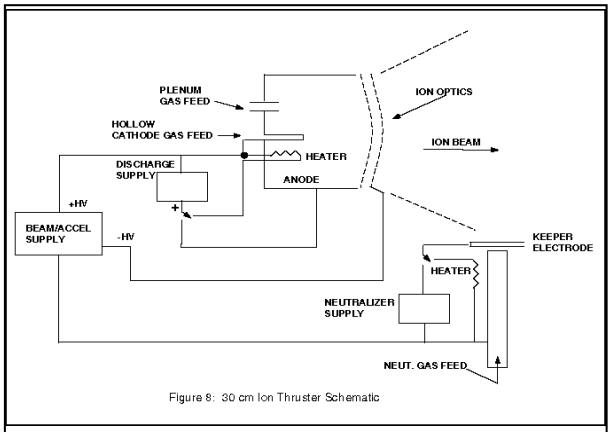

Figure 2: Block diagram of a present-day ion thruster system[13].

In contrast, at the core of the flat-panel thruster, we propose to use millions of MEMS/NEMS based micron-size vias, similar to what is shown in Figure 3, that have a multi-layer grid to establish critical electric-field levels to extract and accelerate either ions using field emission from a conducting liquid (e.g. indium) or, in a different section of the thruster, charged conducting nano-particles (Figure 4) from the surface of either an insulating or mildly conducting liquid used to transport the particles. These nano-particles will range in size from below 0.1 nm to over 100 nm.

The concept of utilizing field emission and electrostatic acceleration of ions is well known as Field Emission Electric Propulsion (FEEP). FEEP thrusters can produce specific impulses above 10,000 seconds at electrical efficiencies exceeding 90% using melted metal liquid propellant such as indium[3,13]. However, FEEPs use needle-like emitters that require footprints many of times wider than the needle tips. Thus, their potential for being scaled-up to say multi-kW power levels is doubtful. Our concept proposes to use highly scalable MEMS/NEMS technologies applied to both nano-particle and ion propulsion and is referred to as nano-Field Emission Thruster (nanoFET).

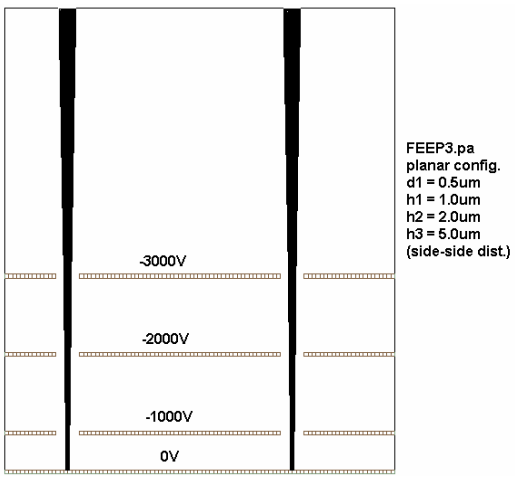

Figure 3: Two small vias shown extracting and accelerating either nano-particle or ions (likely separate vias for each kind).

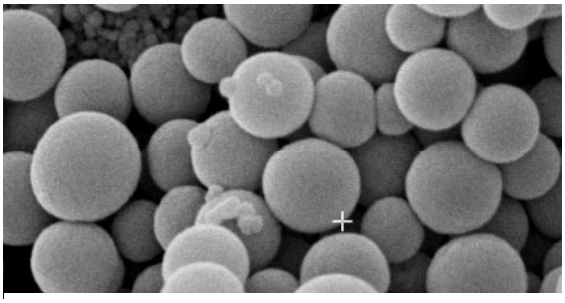

Figure 4: Example of a collection of unsorted nano-particles in the 100 nm diameter range[1].

As will be shown more quantitatively in a later section, the use of nano-particles in our nanoFET will allow for the ability to tune the I_{sp} and thrust over a very broad range at high efficiency. When little thrust with a high specific impulse is required, ions should be emitted. As thrust requirements go up, small nano-particles can be used to achieve slightly higher thrust and lower I_{sp}, and the larger nano-particles can be used for very high thrust and low I_{sp}. The range of thrust will be principally limited by the size, shape, and density of the particles, as well as the potential that they fall through.

The use of nano-particles should be contrasted with the formation of small droplets (colloid thruster). It is known that with the right emission current and temperature, charge extraction in FEEPs can produce instabilities that sometimes result in the formation of charged microscopic droplets (colloids)[5]. While these droplets could in principle be used to accomplish the same goal as our nano-particles, it is difficult to control their size and a distribution is expected. *Our nanoFET propulsion concept avoids the conditions that generate colloids and allows us to tune the nano-particle size independently of other factors.* Other benefits of our nanoFET approach include the use of multiple grids for high-finesse control of ion/nano-particle extraction and acceleration processes, robust material selection for field emission surfaces to ensure long life, and the use of separate ion and nano-particle emission zones to span the 100-10,000 s I_{sp} range. The multiple-grid design ensures that a large accelerating potential can be applied without exceeding the breakdown potential between adjacent grids. A two-dimensional ion trajectory simulation through multiple nanoFET grids (Figure 3) shows that ions/nano-particles experience steady acceleration through each grid and that the use of multiple grids helps to collimate the beam, thus minimizing spreading due to space-charge effects. Thus, by reducing beam divergence and by better coupling the grid potentials to the charged particles, our multi-grid approach improves the efficiency and likely lifetime of micron-scale field emission accelerators both at high I_{sp} with ions and at lower I_{sp} with charged nano-particles.

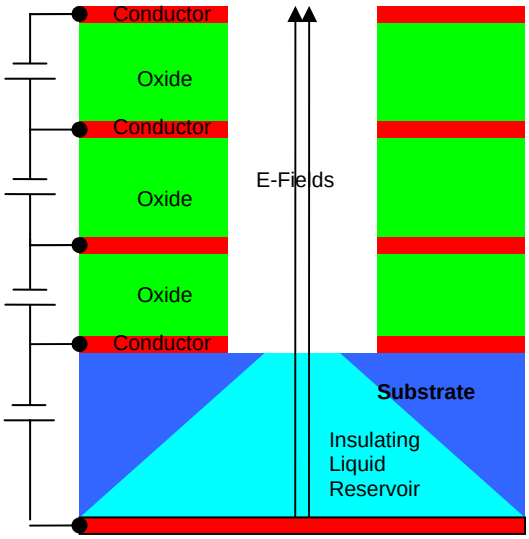

Figure 5: Structure of a single emitter, multi-grid nano-particle thruster using an insulating liquid

We envision the design of nanoFET as an extension to colloid thrusters, but emitting charged conducting nano-particles of known size and charge-to-mass ratios instead of charged liquid droplets which necessarily will have a distribution of sizes and charge-to-mass. Figure 5 depicts a model of a single emitter from the nano-particle thruster using an insulating liquid reservoir. These nano-spheres and cylinders would be fed into a liquid-filled reservoir and subjected to an electric field created by the acceleration grid. Particles that come into contact with the bottom electrode would become charged and pulled to the liquid surface by the electric field. If the electrostatic Coulomb force can cause nano-particles to break through the surface tension, field focusing should allow the particle to lift out of the liquid. Once extracted, the positively charged nano-particle would be accelerated by the electric field and ejected. It is also possible to consider with the same configuration a slightly conducting liquid where nano-particles arrive at the surface and are preferentially charged relative to the surrounding surface and therefore extracted in to the vacuum and ion optics region.

Note that neutralization of the charged particles is required. However, the concept of using MEMS-based technology to manufacture arrays of small vias with biased grids (just like nanoFET) to extract electrons is well known[5]. These are often called FEACs - Field Emission Array Cathodes. It is also possible to bias a separate section of the grid with opposite polarity and emit both positive and negatively charged particles, eliminating the need for a neutralizer when operating in the nano-particle mode.

II. The Physics Behind Nano-Particle Propulsion

A. Defining Thrust

Without getting into the details of extraction and acceleration of nano-particles, it is possible to understand how particle charge and mass both affect thruster performance. It is interesting to recast well-known propulsion equations to show the dependence on both the particle's mass and charge. First, thrust can be derived as

$$T = 2(q*n)*V_o*A, \tag{1}$$

where q is the charge of the nano-particle, n is the number density of particles, V_o is the potential difference applied across the accelerating grid(s), and A is the thruster area. The power is governed by

$$P = n*A*\left(\frac{2}{m}\right)^{\frac{1}{2}}(qV_o)^{\frac{3}{2}}, \tag{2}$$

where m is the mass of the particle. Now, dividing the thrust by the power, we obtain the specific thrust.

$$\frac{T}{P} = \left(\frac{2m}{qV_o}\right)^{\frac{1}{2}}. \tag{3}$$

The specific impulse is

$$I_{sp} = \frac{1}{g}\left(\frac{2qV_o}{m}\right)^{\frac{1}{2}}, \tag{4}$$

where *g* is the Earth's gravitational constant.

Note that the thrust-to-power ratio is *inversely proportional* to the square root of the charge-to-mass ratio of the particle while the I_{sp} is directly proportional to the same square root quantity. The importance of the charge-to-mass ratio lies at the foundation of some critical advantages of nano-particle propulsion over colloid thrusters and will be discussed in a later section.

B. Behavior of Nano-Particles in the Liquid Reservoir

Understanding the behavior of conducting particles in a liquid subjected to an electric field is of great importance to nano-particle propulsion technology. Most investigations of this topic have consisted of millimeter-sized spheres and cylinders placed in an insulating liquid between parallel planar electrodes with a potential difference applied between them[17]. Under the influence of an electric field, the particles become charged and bounce back and forth between the electrodes due to the Coulomb force, exchanging charge at every collision.

It is important to note that the following discussion only applies to the case when the liquid carrier is insulating. The easiest way to see how the particles are set into motion is to look at the forces acting on them, which are the Coulomb force and drag force:

$$F_c = qE \qquad (5) \qquad\qquad F_d = C_d\frac{\pi}{8}d^2\rho_l v^2. \qquad (6)^{16}$$

Here, q is the charge on the particle, v is the particle velocity, C_d is the coefficient of drag, and d is the particle diameter. Note that gravitational and buoyancy forces are neglected in zero gravity. To determine the equation governing the particle's motion, simply apply Newton's force equation to obtain

$$m\frac{d^2z}{dt^2} = F_c - F_d. \tag{7}$$

The particles' trajectories can be realized by numerically solving this equation.

It is possible to determine the charge acquired by a particle in contact with an electrode in the presence of an electric field by calculating the electric field intensity at the surface of the particle and applying Gauss's law. Felici predicted the charge acquired by spherical and cylindrical particles to go as[17]

$$q_{sph} = 4\pi r^2 \varepsilon_\ell \frac{\pi^2}{6} E \qquad (8) \qquad\qquad q_{cyl} = \frac{\pi \ell^2 \varepsilon_\ell E}{\ln\left(\frac{2\ell}{r}\right) - 1}, \qquad (9)$$

where r is the nano-particle radius, ℓ is the cylinder length, E is the electric field in the liquid, and ε_l is the dielectric constant of the liquid.

Once the particle begins to move away from one electrode, it will begin to lose charge to the liquid at a rate determined by the liquid conductivity (~$3.33*10^{-13}$ S/m for silicone oil). The charge loss will go as

$$q(t) = q_o e^{-t/\tau} \qquad (10)$$

where $\tau = \varepsilon_l/\sigma$ and is termed the electrical relaxation time constant. Therefore, in order to emit charged nano-particles, the electrical charge relaxation time should be large compared to the time it takes the nano-particles to be transported through the liquid to the surface.

Once the particles reach the liquid surface, the surface tension force will resist particle extraction. Surface tension is of great importance because it becomes a dominant force for particles at the micron scale and smaller. This is because it decreases linearly with the scale of the particle while all other forces decrease by a higher power. For example, the gravitational force is proportional to the volume of the particle and therefore decreases as a power of three. Similarly, the drag force is dependent on the surface area of a particle so it decreases as a power of two.

We are concerned with the ability to utilize an electric field to extract a charged nano-particle through the surface of a liquid. To approximate the minimum field strength and particle charge required for particle extraction, it is necessary to ensure that the Coulomb force is greater than the surface tension force, which is given as

$$F_s = \gamma \ell_{eff} \qquad (11)$$

where γ is the surface tension of the liquid and ℓ_{eff} is the effective radius of the particle. Setting the Coulomb force equal to the surface tension force and solving for the minimum required electric field for particle extraction, we obtain the following expressions for the spherical and cylindrical cases:

$$E_{sph,\min} = \sqrt{\frac{3\gamma \ell_{eff}}{2\pi^3 r^2 \varepsilon_\ell}} \qquad (12) \qquad\qquad E_{cyl,\min} = \sqrt{\frac{\gamma \ell_{eff}\left(\ln\left(\frac{2\ell}{r}\right) - 1\right)}{\pi \ell^2 \varepsilon_\ell}}. \qquad (13)$$

Returning to the thrust equations at the beginning of this section, we can see that the specific charge (charge-to-mass ratio) is very important in determining the thrusting performance. One advantage of nano-particle propulsion is the ability to control this parameter accurately as well as change it depending on the thrusting needs. The specific charge of spherical and cylindrical particles can be calculated to be

$$\left(\frac{q}{m}\right)_{sph} = \varepsilon_\ell \frac{\pi^2}{2r\rho} E \qquad (14) \qquad\qquad \left(\frac{q}{m}\right)_{cyl} = \varepsilon_\ell \frac{\ell}{\left(\ln\left(\frac{2\ell}{r}\right) - 1\right) r^2 \rho} E. \qquad (15)$$

Note that the specific charge of a spherical particle is dependent on the particle radius, density, and the applied electric field, and for the cylindrical particle the specific charge is dependent on the same variables with the addition of the particle length. This additional control parameter will allow for greater tunability. We will be considering both spherical and cylindrical particles as propellant sources. The cylindrical particles offer a greater specific charge range but may introduce other problems such as becoming entangled with others within the liquid reservoir (e.g. a carbon nanotube).

III. New Propulsion Levels of Performance Using Nano-Particles

Nano-particle propulsion provides important performance improvements over state-of-the-art ion, colloid, and possibly other thrusters in terms of thrust efficiency, specific impulse, specific thrust, thrust density, scalability, lifetime concerns, complexity of design, and specific mass.

A. Thrust Efficiency

Colloid thrusters are one approach to achieve similar claims as described here for nano-particles in a liquid carrier. However, nano-particles give greater control of specific charge of each particle. Further, the use of nano-particles should decrease the losses associated with Taylor cone formation.

A comparison of efficiency with other state of the art electrostatic thrusters is shown in Figure 6. The graph suggests that substantial improvements at both the low I_{sp} and high I_{sp} modes should be possible. Both nano-particle and ion emission modes of operation are shown.

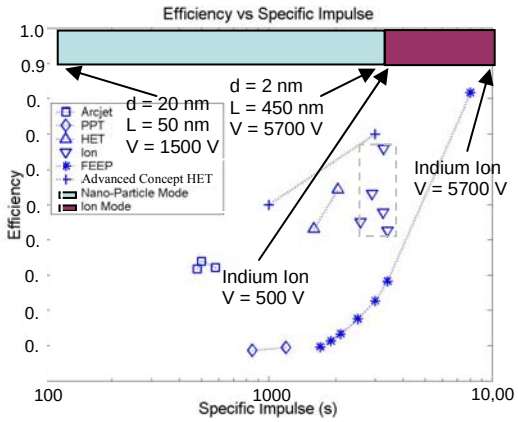

Figure 6: Improved efficiency for entire Isp range using nano-particles and ions[18]

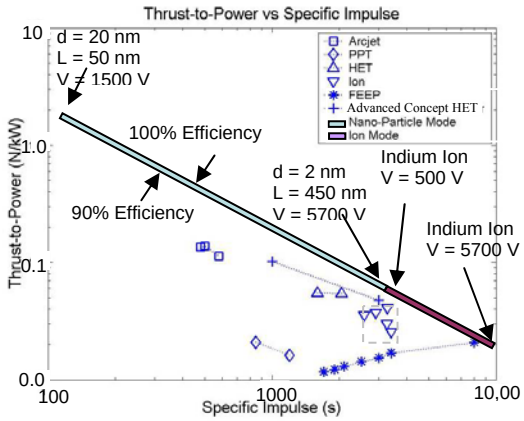

Figure 7: Highly scalable specific impulse and thrust-to-power using nano-particles and ions[18]

B. Specific Impulse and Specific Thrust Range

A significant improvement in the specific thrust and specific impulse range is possible if the specific charge of the particles can be adjusted and controlled. Figure 7 compares the expected specific thrust and I_{sp} when using cylindrical nano-particles with a length ranging from 20 nm to 270 nm, the radius ranging from 1 nm to 10 nm, and the accelerating potential ranging from 1500 to 9000 V to other state-of-the-art thrusters.

C. Thrust Density

State-of-the-art ion thrusters must operate substantially below the space-charge limit to assure proper ion-optic operation which would otherwise significantly increase sputtering damage and therefore decrease life-time. The ion thruster architecture is such that a slow moving ion plasma is drawn across a small gap. For nano-particles, we predict that a different analysis is needed. Isolated emitters operate independently of each other and the condition of importance is whether the amount of charge in the micron-sized hole is close to the charge determined by the capacitance across the gap (gate-to-propellant via). Further, even if nanoFET does approach an equivalent space-charge limit, since the charge may be contained in a fewer number of particles, it should be possible to operate much closer to this limit without degradation.

D. Thruster Lifetime

The lifetime of ion thrusters is limited due to erosion from charge exchange (CEX) collisions in the ion optics region and the discharge plasma source. The CEX collision occurs when a high energy ion collides with a low energy neutral and results in a low energy ion and a high energy neutral. The resulting ion strikes the conducting grid causing erosion. Both of these problems are eliminated when using nano-particle technology. Since only ions or charged nano-particles exist in the NEMS/MEMS grid structures there would be no charge exchange and because no plasma is generated, there would be no discharge plasma source.

E. Improved Specific Mass

While engine life is a critical constraint in many mission planning scenarios, a related and equally constraining thruster characteristic is specific mass. High thruster specific mass increases the mass of a space vehicle. This increase in vehicle mass can increase the needed "burn time" the thrusters must provide to accelerate the spacecraft to the required ΔV and places constraints on the spacecraft trajectory. For example, a heavy spacecraft would have to avoid certain orbits around moons in the Jovian system to minimize the risk of being captured or pulled in by the planetary body. Thus, increased system specific mass reduces the mission envelope the spacecraft can operate in.

Nano-particle technology addresses the specific mass through a number of design features. Ultra-long life could reduce the number of thrusters needed for a given mission. While individual conventional thrusters may be sufficiently light for a variety of missions, their insufficient lifespan means that multiple thrusters will be needed for a given "power slot" to accomplish the mission. For example, a 100 kW spacecraft will actually need eight 25-kW ion thrusters if the life of each engine is only half that required to fulfill the mission. In the example above, only four of the long-lived nano-particle thrusters would be needed. Moreover, the potentially higher thrust density of the thruster reduces the size of each thruster; i.e., one 100-kW thruster has less mass than four 25-kW conventional thrusters.

F. Simple Design

The "flat panel" concept (Figure 5) means that the propellant management system and power-processing unit are integrated right on the thruster, which reduces mass and integration complexity. Lastly, the "flat panel" thruster is smaller than conventional ion thrusters and will not need the magnets, grids, and discharge channel walls that account for the bulk of the mass of the latter.

IV. Conducting vs. Insulating Liquid Carrier

Further theoretical and experimental research will be required to determine which method of liquid carrier will work best: conducting or insulating. Both methods have their own advantages and disadvantages, which will be discussed in this section. The case of an insulating liquid carrier (Figure 5) was discussed in a previous section, where the particle is charged when it is in contact with the bottom electrode due to the presence of an electric field. Once the particle is charged, it would be transported to the liquid/vacuum interface by way of Coulomb's force. This force would continue to extract the particle through the liquid surface, accelerate, and finally eject it.

The case of a mildly conducting liquid would work much differently due to the absence of electric fields within the liquid (Figures 8). Since there are no significant fields in the liquid, another method must be devised to transport the particles to the liquid surface where they would be charged. Current ideas involve mixing the liquid (by heating, acoustic waves, etc.), which should allow particles to randomly approach the liquid surface. Upon approaching the surface, the (cylindrical) particles will align themselves, as suggested in Figure 9, due to polarization charging. If the electric field can focus on the tip of the particle, there will be preferential charging, and with sufficient charging the particle can be extracted through the

Figure 8: Single emitter of nano-particle thruster with conducting liquid.

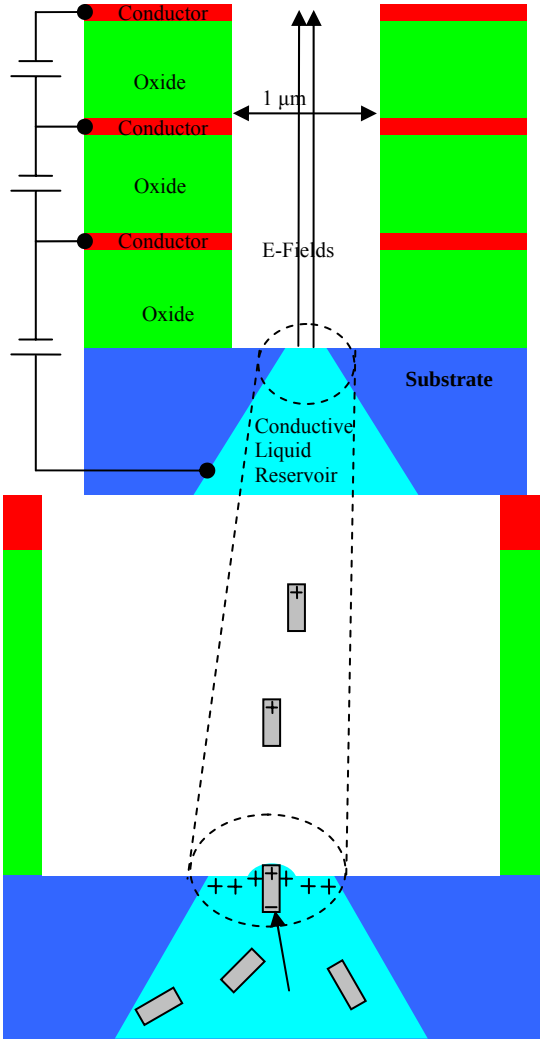

Figure 9: Nano-particles extracted and accelerated.

surface tension. An estimate of charge is given by equations 8 and 9 replacing ε_l with ε_o. Once charged and extracted, the particle would be accelerated and ejected just as in the insulating liquid case.

Since the behavior of the particles within the liquid is highly dependent on the conductivity of the liquid, there are several advantages and disadvantages of each scenario.

A. Advantages of an Insulating Liquid

- The transport of particles within the liquid to the surface can take advantage of electric fields that can be independently established.
- The movement of new particles into the reservoir may be handled in a similar manner by utilizing localized (pulsed) electric fields as well as other possible methods. This allows particles to be moved within the liquid, rather than moving the liquid itself.
- The formation of Taylor cones or other surface irregularities should be less likely and therefore particle emission should be more uniform.

B. Advantages of a Conducting Liquid

- The electric fields at the surface of the liquid should be normal to the surface and therefore more in the thrusting direction, which will help to prevent accelerating the particles into the grid structure.

C. Disadvantages of an Insulating Liquid

- The electric fields at the surface of the liquid may have components tangential to the surface, which may accelerate particles into the grid unless the particle is extracted near the center of the hole in the accelerating grids. This is because the particles reach a low terminal velocity within the viscous liquid and may not have the momentum to keep from being accelerated in the horizontal direction and into the grid structure.

D. Disadvantages of a Conducting Liquid

- The surface of the liquid would have charge density, which may induce Taylor cones of some sort.
- The movement of particles would require either moving the liquid along with the particles or some non-electric method (thermal, ultrasonic) to move just the particles.

V. Future Experiments

We are developing a series of initial experiments to better understand nano-particle propulsion. The objectives of these initial experiments are to 1) determine the behavior of particles in insulating and conducting liquids subjected to an electric field, 2) prove the feasibility of extracting particles from a liquid by way of electric field, and 3) identify appropriate liquid and nano-particle characteristics for in-space operation. Some experiments will be scaled-up, but we are also proceeding to develop micro-structure experiments.

Figure 10: First-generation MEMS gate design showing the viewing windows etched into the bulk silicon. Each viewing window contains tens of thousands of emission channels. The current MEMS gate is a second-generation design.

The micro-structure experiments will allow micro- and nano-sized particles and use a MEMS accelerating gate structure. MEMS gates are conducting grid structures that can be placed over a flat surface to apply an electric field to that surface. The advantage of the MEMS gate over metal screens is that they allow micron-scale or closer surface proximities, thus allowing the application of similarly strong electric fields as metal screens at modest voltages. These MEMS gates are currently being developed at the University of Michigan to be integrated with nano-structured surfaces such as cubic boron nitride and carbon nano-tubes for "tip-less" electron field-emission cathodes (FEC) and are being adopted for initial nanoFET experiments. Such FEC would be usable as a neutralizer for the nanoFET system to maintain charge balance during thruster

operation. A reversed bias on the MEMS gate could be used to provide the electric fields (~1E6 V/cm) needed to extract the nano-particles using modest bias voltages (< 300 V).

The MEMS gate consists of a conductive layer placed over a dielectric spacer with channels arrayed throughout the structure to permit passage of nano-particles or electrons. Use of micro-fabrication techniques enables the dielectric spacer to be made very thin, with the latest iteration of the MEMS gate having micron-scale dielectric thickness. By placing the conductive layer closer to the emission material; electric fields are concentrated and the bias voltage needed to achieve emission is reduced. Numerical simulations indicates that an approximate 1:1 ratio between the dielectric thickness and the channel diameter produces uniform field lines, so nano-particles used with the current iteration of the MEMS gate must have diameters on the order of hundreds of nanometers or less.

Gate layers are supported in a bulk silicon square with 1-cm sides. Ten viewing windows are etched in the bulk silicon to expose the emission channels, with each viewing window containing tens of thousands of emission channels. The top surface of the MEMS gate is a metal layer to facilitate wire bonds to the gate, and open regions are present that enable the gate to be clamped down upon the emission interface. Note that the present iteration of the MEMS gate is a prototype design that is undergoing optimization. More advanced micro-fabrication techniques will be employed in the future following device characterization and integrated testing. Optimizations include reducing the gap to decrease required extraction voltages and increasing the transparency. A stacked gate design is also under consideration to decouple the extraction and acceleration stages[14]. Figure 12 shows an older version of the MEMS gate design with 12 viewing windows instead of the current ten[15].

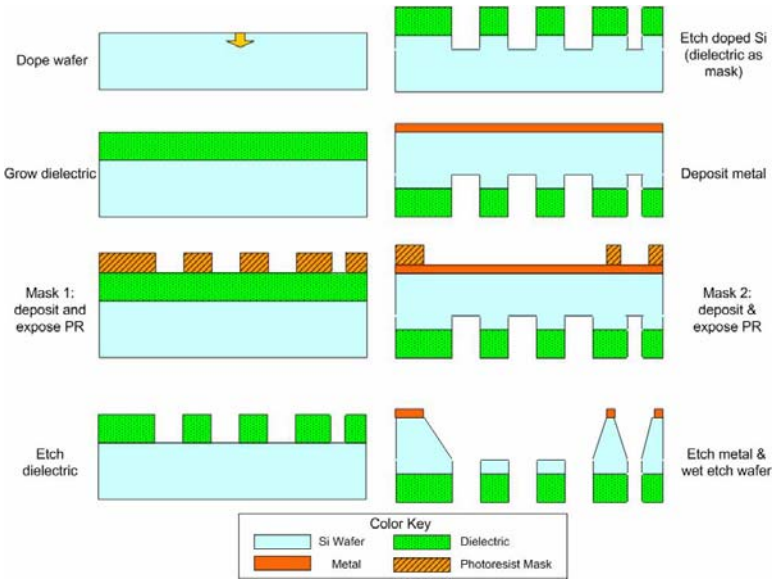

Figure 11: Gate fabrication process

The MEMS gates are fabricated via optical lithography and doped silicon wafers to minimize voltage drops within the gate. Micro-fabrication techniques used in the process are outlined below and are also shown in Figure 13.

1. One side of the silicon wafer is subjected to boron ion implantation to create a sub-micron thick region of highly doped silicon. This highly doped layer serves as the conductive gate layer and also as the etch stop for the final wet etch process. By using ion implantation rather than depositing a separate layer, a thin conductive layer can be formed to reduce gate current collection while still retaining sufficient structural robustness to resist rupture during gate handling and integration.
2. Low-stress silicon nitride of micron-scale thickness is grown on top of the highly doped silicon layer to serve as the dielectric spacer. The silicon nitride provides a slight tensile stress to keep the gate layers from peeling away from the bulk silicon. With a dielectric constant above 1E7 V/cm, silicon nitride is able to withstand the electric field strengths required for both nano-particle extraction and field emission.
3. Contact lithography is used to pattern the emission channels and backside scribe lanes. Spaced microns apart center-to-center, the emission channels are created using highly anisotropic reactive ion etch (RIE). The scribe lanes are also formed via RIE.
4. On the unprocessed side of the silicon wafer, a metal layer is deposited to form a surface that facilitates wire bonding to the MEMS gate. Good conductivity exists between the wire bond surface and the heavily doped gate layer due to the low resistivity of the bulk silicon.

5. Optical lithography is used to pattern the viewing windows and the front-side scribe lanes on the gold layer. A dissolved wafer process using ethylene diamine pyrocatechol (EDP) etches the viewing windows in the bulk silicon to expose the emission channels. With scribe lanes on both sides of the wafer, the gate structures are separated from each other as the final step of the EDP bath. This self-dicing prevents the particulate contamination and potential rupturing of the gate layers that could result from mechanical dicing.

To improve yield for the MEMS gates, test chips are included in the fabrication run to monitor each process step. These test chips would verify the presence of emission channels and the conductive ion-implanted layer following fabrication, and the test chips would also provide an indication of spatial variability during the fabrication process.

VI. Degrees of Freedom

The design of the nano-particle propulsion system leaves many degrees of freedom to obtain the ideal propulsion characteristics. There are three areas of the system that must be considered: the nano-particles, liquid in the reservoir, and the emitter.

The ability to choose the size, shape, and composition of the nano-particles gives rise to multiple options. As discussed before, we have the option to control the specific charge simply by determining the size and shape. This allows the thrust to power ratio to be varied easily. Other choices include the conductivity and density of the particles.

The choice of liquid will determine how the particles behave before and during extraction. Some important liquid characteristics are surface tension, viscosity, conductivity, polarity, permittivity, temperature effects, and behavior in a vacuum. For example, the surface tension will need to be strong enough to keep the liquid in the reservoir while weak enough to allow the particle to be extracted.

The size of the emitter opening and the gap between the grids offer more degrees of freedom. Note that the breakdown of the dielectric is around 300 $V/\mu m$[9].

VII. Conclusion

The investigation of the fundamentals of a MEMS/NEMS based flat-panel electric thruster along with the understanding of feasibility for nano-particle electric propulsion should provide important information on the prospects for an improved reliability and highly scalable propulsion system capable of operating over a large range of thrust and I_{sp}. Using MEMS/NEMS based field emission, it should be possible to improve lifetime by eliminating an ion thruster's discharge chamber and issues associated with CEX erosion in the ion optics region. Finally, it offers many degrees of freedom that allow it to be tweaked for the needs of various missions.

We are proceeding to investigate several fundamental questions about the nanoFET concept. Scaled experiments are being developed to validate the basic concepts for both emission and transport of the nano-particles.

VIII. Acknowledgments

Special thanks to Kimberly Appel and Robert Hower at the University of Michigan's Solid State Electronics Laboratory for their help in designing the MEMS gate fabrication process.

IX. References

1. Behan, Niall, "Nanomedicin and Drug delivery at the University of Limerick," The University of Limerick. http://www.ul.ie/elements/Issue4/behan.htm
2. Calero, J. "The electrohydrostatics of a Conductive Liquid Meniscus," IEEE 1988, p 1547-1551.
3. Chesta, E., Nicolini, D., Robertson, D. and Saccoccia, G., "Experimental Studies Related to Field Emission Thruster Operation: Emission Impact On Solar Cell Performances And Neutralization Electron Backstreming Phenomena," IEPC-2003-102, Proceedings of the International Electric Propulsion Conference, Toulouse, France, March 17-20, 20033 Choi, Changrag. "Dynamic Motion of a Conductive Particle in Viscouse Fluid Under DC Electric Field," IEEE Transactions on industry Applications, vol 37, No 3, May/June 2001.
4. Gallimore, A. "Micro Electric Propulsion Proposal," The University of Michigan, November 2003.
5. J.R. Brophy, J.E. Polk, V.K. Rawlin, Ion engine service life validation by analysis and testing, AIAA Paper 96-2715, JUly 1996.
6. Khayari, A. "The Charge Acquired by a Spherical Ball Bouncing on an Electrode: Comparison Between Theory and Experiment;" 2000 Conference on Electrical Insulatoin and Dielectric Phenomena.
7. Marcuccio, S. "Attitude and Orbit Control of Small Satellites and Constellations with FEEP Thrusters," Electric Rocket Propulsion Society, 1997.
8. Marcuccio, S. "FEEP Microthruster Technology Status and Potential Applications," International Astronautical Federation, 1997.
9. Marcuccio, S. "FEEP Thrusters," Nov. 1998, http://www.centrospazio.cpr.it/Centrospazio6FEEP.html.
10. M. Fehringer, F. Ruedenauer, W. Steiger, ESTEC Contract 12376/97/NL/PA Tech. Note No. 2, 1997.
11. Najafi, Khalil. Personal Communications, Univeristy of Michigan, 2004.
12. Stark, John. "Micro-Fabrication and Operation Nano Emitters Suitable for a Colloid Thruster Array," University of London, UK, https://escies.org/public/mnt4/S9.1Stark.pdf
13. Chock, R. "Photovoltaic & Space Environment Branch," NASA Glenn Research Center, July 2002, http://powerweb.grc.nasa.gov/pvsee/publications/tropix/Paper/AppA.html
14. Morris, D.P., Gilchrist, B.E., Gallimore, A.D., "Application of Dual Grids to Cold Cathode/ Field Effect Electron Emission, AIAA-2005-3669, 41st Joint Propulsion Conference, Tucson, AZ, July 10-13, 2005.
15. Goldberg, H., Encarnación, P., A., Morris, D., Gilchrist, B., Clarke, R., "Cold-Cathode Electron Field Emission of Boron Nitride Thin Film with a MEMS-Based Gate for Space Applications, AIAA-2004-3499, 40th Joint Propulsion Conference, Ft. Lauderdale, FL, July 11-14, 2004.
16. Tobazeon, R. "Behavior of Spherical and Cylindrical Particles in an Insulating Liquid Subjected to a DC Uniform Field." Laboratoire d'Electrostatique et de Materiaux Dielectriques. BP 166-38042 Grenoble Cedex 9 (France) pp. 415-420.
17. Felici, N. Rev. Gen. Elect., 75, pp. 1145-1160, 1966.
18. Wertz, Larson, "Space Mission Analysis and Design 3rd Ed." 1999